Renewable and Sustainable Energy Reviews 24 (2013) 223–270

Contents lists available at SciVerse ScienceDirect

Renewable and Sustainable Energy Reviews

journal homepage: www.elsevier.com/locate/rser

Topologies and control strategies of multi-functional grid-connected inverters for power quality enhancement: A comprehensive review

Zheng Zeng *, Huan Yang [1], Rongxiang Zhao [2], Chong Cheng [3]

College of Electrical Engineering, Zhejiang University, 310027 Hangzhou, Zhejiang Province, China

ARTICLE INFO

Article history:
Received 20 March 2012
Received in revised form
11 March 2013
Accepted 15 March 2013
Available online 18 April 2013

Keywords:
Multi-functional grid-connected inverter
Topologies and control strategies
Auxiliary services
Power quality enhancement
Distributed generation system and micro-grid
Review

ABSTRACT

Grid-connected inverters are key components of distributed generation systems (DGSs) and micro-grids (MGs), because they are effective interfaces for renewable and sustainable distributed energy resources (DERs). Recently, multi-functional grid-connected inverters (MFGCIs) have attracted more and more attention for their benefits on auxiliary services on power quality enhancement in DGSs and MGs. These kinds of converters can not only achieve the power generation of DERs, but also can perform as power quality conditioners at their grid-connected points. It should be noted that these functionalities are optimally organized in the same device, which can significantly enhance the cost-effective feature of the grid-connected inverter, as well as can decrease the investment and bulk compared with multiple devices with independent functionalities. MFGCIs are especially suitable for DGSs and MGs application due to their good performances and benefits. Topologies and control strategies of MFGCIs are comprehensively reviewed in this paper. Additionally, detailed explanation, comparison, and discussion on MFGCIs are achieved. Furthermore, some future research fields on MFGCIs are well summarized.

Contents

1. Introduction

Several blackouts caused by chain failures [1], as well as the electric grid splits because of the extreme weather [2,3] threaten the security and stability of traditional electric power systems. In addition, the continuous consumption of fossil fuels is leading to energy crisis and increasing environmental pollution problems. Therefore, the “green” and “low carbon” power becomes the urgent need of traditional electric power systems [4,5]. Facing to these issues, distributed generation systems (DGSs) gradually return to the stage [6–8]. Numerous studies show that DGSs can not only connect renewable energy sources (RESs), such as wind, solar and so on, to utility grid, but also can improve the stability of traditional electric power systems in some sense. In order to make better use of RESs, micro-grids (MGs) considered as special DGSs have been widely discussed and demonstrated, and are given great expectations. A micro-grid is a local power supply system, which integrates RESs, energy storage devices, local loads, communication devices, protection units, and the control center [9–14]. Recently, DGSs and MGs are very active and encouraging research fields.

* Corresponding author. Tel.: +86 13567123512.
E-mail addresses: zengerzheng@zju.edu.cn (Z. Zeng), yanghuan@zju.edu.cn (H. Yang), rongxiang@zju.edu.cn (R. Zhao), chengchong@zju.edu.cn (C. Cheng).
[1] Tel.: +86 13588846066.
[2] Tel.: +86 13906508946.
[3] Tel.: +86 15957136558.

1364-0321/$ - see front matter © 2013 Elsevier Ltd. All rights reserved.
http://dx.doi.org/10.1016/j.rser.2013.03.033

In DGSs and MGs, the grid-connected inverters (GCIs) are essential interfaces to connect RESs and energy storage devices to utility grid [15,16]. To reduce the investment, operation and maintenance cost, man-hour, as well as the bulk, and enhance the cost-effective feature of the GCIs in DGSs and MGs, the multi-functional grid-connected inverters (MFGCIs) are proposed in [17–26]. The so-called MFGCIs can connect RESs and storage devices to utility grid, and simultaneously enhance the power quality at their points of common coupling (PCCs). Compared with the multiple devices with different functionalities, the MFGCIs can greatly save capital investment and system space, because the different functionalities of multiple devices are integrated in the same equipment. So MFGCIs are good choices for DGSs and MGs application and are paid common attention.

In this paper, a comprehensive review on the topologies and control strategies of MFGCIs is achieved. Meanwhile, from the views of single-phase and three-phase utility grid, detailed explanation, comparison, and discussion of the MFGCIs are summarized. Besides, some future frameworks on MFGCIs are presented. The paper is organized as follows. In Section 2, some important outlines on GCIs are briefly introduced. The power quality of DGSs and MGs, as well as some possible response strategies to enhance the power quality are described in Section 3. In Sections 4 and 5, the available topologies and control strategies of MFGCIs are comprehensively reviewed for single-phase and three-phase utility application, respectively. A detailed analysis and comparison of the available MFGCIs are investigated in Section 6. In addition, some interesting research points are presented. Some conclusions are drawn in Section 7.

2. Some outlines on grid-connected inverters

MFGCIs are special GCIs, so a brief introduce on conventional GCIs is quite necessary [27–29]. GCIs are key components in DGSs and MGs, and act as effective interfaces to connect distributed RESs or micro-sources, such as photovoltaic (PV) arrays, wind turbines (WTs), micro-gas turbines, energy storage devices and so on, to utility grid, as shown in Fig. 1. It is worth nothing to note that the high efficiency and low cost are two important issues of GCIs. In general, GCIs can be classified as single-stage and multiple-stage. Because the more stages reduce the efficiency of a GCI much more, a multiple-stage GCI mainly has two stages. A typical two-stage GCI is comprised of a DC/DC stage and a DC/AC stage, as depicted in Fig. 1. The DC/DC stage is usually used to realize maximum power point tracking (MPPT) for WT or PV applications, or bidirectional power flow control for energy storage application [30–32]; whereas, the DC/AC stage is used to control the power and current injected into utility grid. Accordingly, a single-stage GCI just has the DC/AC stage, which must complete all the functionalities of a two-stage one had. However, a single-stage GCI uses few electronic components, and has smaller bulk, higher efficiency, lower cost, as well as higher reliability, compared with a two-stage one. On the contrary, a two-stage GCI has a simpler control algorithm since different functionalities are separated in two independent stages. Besides, the low dc voltage of the micro-source can be flexibly boosted by the DC/DC stage to meet the requirement of the DC/AC stage, which is another advantage of a two-stage GCI compared with a single-stage one.

Single-stage and two-stage GCIs have advantages and disadvantages of each other, so it is hard to say which ones are better. They are all implemented in different suitable occasions. Generally, small-capacity-scale grid-connected systems are more like to use two-stage GCIs due to their flexible feature; however, big-capacity-scale systems mainly use single-stage GCIs for their high efficiency and reliability. Some engineering examples are illustrated as follows:

1. For PV application, as demonstrated in Fig. 2, the two-stage GCIs are mainly employed in single-phase utility grid and their capacities are usual small; however, the single-stage GCIs are mainly utilized in three-phase utility and their capacities are relatively bigger.
2. For WT application, the grid side converter of doubly fed induction generator (DFIG) can be regarded as a single-stage GCI, as indicated in Fig. 3. However, for small-capacity-scale direct-driven permanent magnet synchronous generators (PMSG) WT application, the two-stage GCI configuration shown

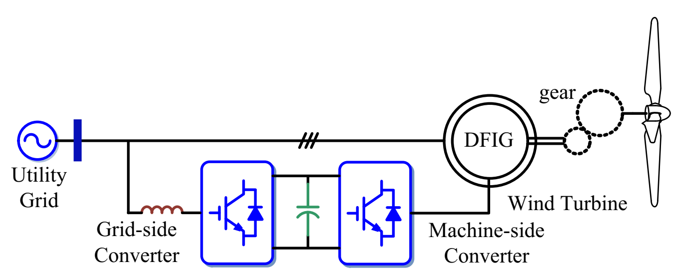


Fig. 3. Grid-connected system of DFIG.

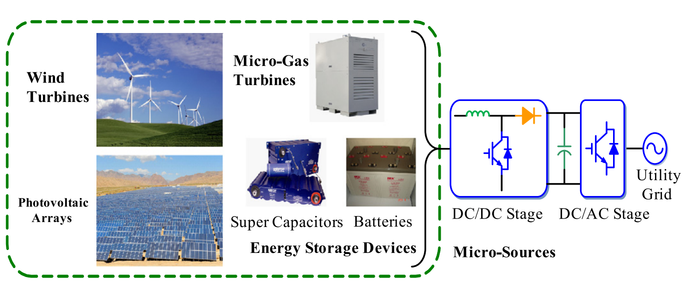


Fig. 1. Typical configuration of a grid-connected system with micro-sources.

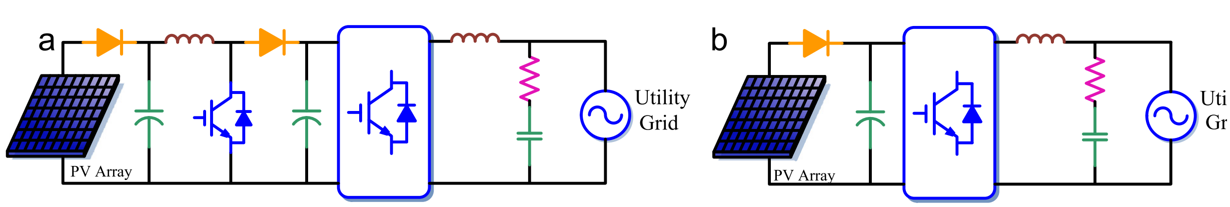


Fig. 2. Configuration of different PV application circumstances. (a) Two-stage structure and (b) single-stage structure.

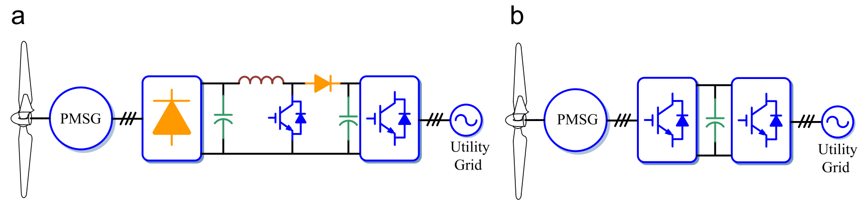


Fig. 4. Generation systems of direct-driven PMSG. (a) Two-stage structure and (b) single-stage structure.

in Fig. 4(a) is a good choice as well. The DC/DC stage is fed by the diode rectifier and tracks the maximum power point of the WT, while the DC/AC stage connects to utility. However, for a large-capacity-scale PMSG WT system, the single-stage GCI is the best choice, as exhibited in Fig. 4(b).

3. For energy storage application, the single-stage and two-stage GCIs are also suitable for different circumstances, as displayed in Fig. 5. The energy storage cells with high enough dc voltage can be directly fed by a single-stage PWM converter. Otherwise, a DC/DC stage with step-up feature is necessary to match the output voltage of cells and the input voltage of the DC/AC stage.

According to previously mentioned topologies of GCIs for RESs application, it can be seen that either two-stage or single-stage GCI has a DC/AC stage. The DC/AC stage is the absolutely indispensable part of a GCI to convert the dc energy of RESs into the ac energy and interface into utility. In this paper, as shown in the following parts, the common DC/AC stages of the GCIs are focused, and it is found that the DC/AC stages of GCIs can be carried out some advanced and auxiliary functionalities to enhance the power quality at their PCCs.

3. Power quality of distributed generation systems and micro-grids

Due to the numerous power electronic devices, nonlinear, unbalance and reactive local loads, the power quality at the PCCs of DGSs and MGs maybe rather bad [33–37]. However, the power quality of DGSs and MGs is very important issue for the stable and economical operation of GCIs. On one hand, price of the electricity sold to utility will be determined by its quality in a competitive electricity market in the near future. So the power quality of DGSs and MGs will directly relate to the price of sold electricity, and affect their economic benefits [38–40]. On the other hand, the power quality at PCC will seriously influence the stability of GCIs [41–43]. Because the GCIs are mainly connected to the secondary side of the transformers, the nonlinear loads will cause the distortion of PCC voltage. This distorted voltage will directly worsen the voltage and current control loops of a GCI, and lead to distortion of its grid-connected current. In some severe cases, it even leads to the unplanned trip off of the GCI. Besides, from the electric power system point of view, poor power quality may result in additional loss and overheat of power equipment, boring noises as well torque oscillations of electric machines, the faults of sensitive loads, and the interference of communication network [44].

Available researches on the power quality of DGSs and MGs mainly focus on the comprehensive assessment of power quality, advanced control strategies of GCIs in non-ideal voltage conditions, and power quality management. Literature [33] has analyzed the sources of power quality problem in MGs, and has exploited this new research field. In [35,36] the resonance phenomenon in a PV plant has been studied to explain the undesired trip off of GCIs, which shows the significant necessary of power quality enhancement in DGSs and MGs. In comprehensive power quality assessment field, literature [39] gives some useful

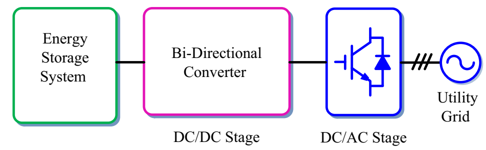


Fig. 5. Grid-connected system of energy storage device.

approaches to form a quantitative comprehensive indicator including many different power quality indicators. Unfortunately, the comprehensive assessment can just provide a judgment of the existing power quality, which may be used as a reference for DGSs and MGs to manage their power quality. However, the bad power quality will not be enhanced if there has no effective response to be taken. Facing to the bad power quality of DGSs and MGs, there are two response strategies, in general. One strategy is effective ride-through approaches of GCIs to adapt the poor power quality [41–43]. Literature [41] has studied the operation strategy of GCIs in unbalance and distorted voltage conditions to enhance the quality of grid-connected current. Obviously, this is a passive response strategy, which cannot fundamentally change the existing bad power quality of DGSs and MGs. Another strategy is employing active and/or passive power quality conditioners to manage the bad power quality of DGSs and MGs. Among them, harmonic filters and capacitors are typical passive ones, which are good choices due to their advantages of low cost and easy maintenance. However, the active power quality conditioners, such as active power filter (APF) [45–48], dynamic voltage regulator (DVR) [49–51], power factor correction (PFC) [52,53], unified power quality conditioner (UPQC) and so on [54,55], gain more and more applications because of their good performance and flexibility. It is worth nothing to note that all these power quality conditioners will cause new extra capital investment in a DGS or MG, and need additional space, maintenance cost, and man-hours; besides, they also may decrease the stability and reliability of the DGS or MG.

Fortunately, active power quality conditioners have the same essential DC/AC stage of GCIs, as shown in Fig. 6 and mentioned before, thus these DC/AC stages can be multiplexed [47–55]. Therefore, there just a little modification in software is needed to change the conventional GCIs into MFGCIs, in such a way that the DC/AC stage of a GCI can be utilized to realize the functionalities of the GCI and the power quality conditioners, as well as, can greatly reduce the cost and bulk, and increase the cost-effective features of the system, compared with multiple devices with different individually independent functionalities.

4. Multi-functional grid-connected inverters in single-phase system

MFGCI topologies in single-phase system usually have small capacities and aim to small-scale RESs application. Available MFGCIs in single-phase are mainly employed for PV application, and attach APF and/or DVR functionalities.

A kind of MFGCI configuration using single-phase full-bridge topology is given in [56–58], as illustrated in Fig. 7, whose

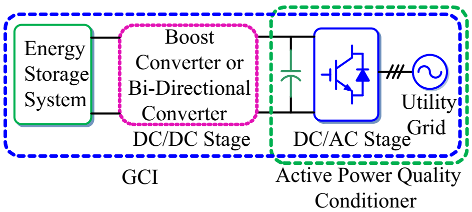


Fig. 6. Basic components of an active power quality conditioner compared with a GCI.

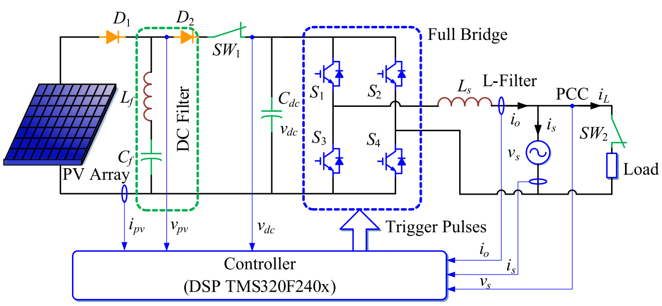


Fig. 7. Typical configuration of a single-phase full-bridge MFGCI.

Table 1
Parameters of the typical single-phase full-bridge MFGCI.

Dc source	PV array, the voltage of dc-link is $V_{pv}=250$ V
Capacity	≤1.5 kVA
Utility voltage	110 V/60 Hz
Switching frequency	20 kHz
Passive components	$L_f=2$ mH, $C_f=880$ μF, $C_{dc}=940$ μF, $L_s=5$ mH
Power electronic devices	IGBT (Toshiba: GT15Q101, 1200 V/15 A)
Control strategy	PI control, SPWM modulation
Extra functions	APF, RPI

important system parameters are listed in Table 1. The whole system consists of PV array, dc filter, dc switch SW_1, buffer capacitor C_{dc}, single-phase full-bridge converter, filter inductor L_s, utility, local load, load switch SW_2, and the controller.

This configuration can act as the interface of PV and APF at the same time. According to the reference directions of current in Fig. 7, either the utility or the GCI can supplies the load after load switch SW_2 is closed. If the capacity of load is small, the surplus power of PV, after supplied to load, will feed to utility. On the contrary, if the capacity of load is so large that the PV can just supply part power to it, the rest power of load will be provided by utility. Note that if the local load is a rectifier or other nonlinear load, the output current of the GCI can be regulated by the controller, which can compensate the harmonic components of load current. Therefore, the grid-connected current i_s will be ensured as the pure active current component. This condition is named as real power injection (RPI) operation mode. Visibly, the GCI also can act as an APF.

According to the topology in Fig. 7, literature [56] gives the control strategy as indicated in Fig. 8. This MFGCI has two operation modes, namely, maximum generation power tracking and APF. The reference voltage of dc-link $v_{c,ref}$ is set according to the operation mode to satisfy the requirement of APF functionality in APF mode; however, the v_{ref} is directly determined by MPPT in maximum generation mode. Note that, G_{vf} is the filter of feedback loop. The output of dc voltage regulator G_{vci} forms the amplitude of the reference current I_m, which multiplies the unit-quantity synchronous signal of the utility voltage v_s to form the instantaneous reference current $i_{s,ref}$. The reference current summing the load current i_L yields the output current reference $i_{o,ref}$ of the

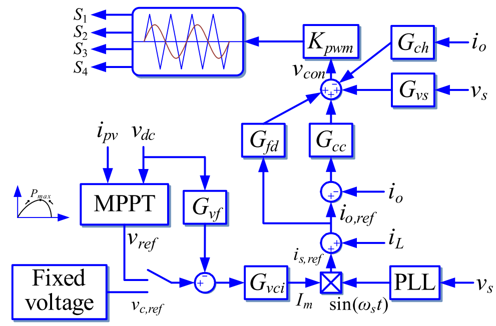


Fig. 8. Control strategy of the MFGCI configuration in [56].

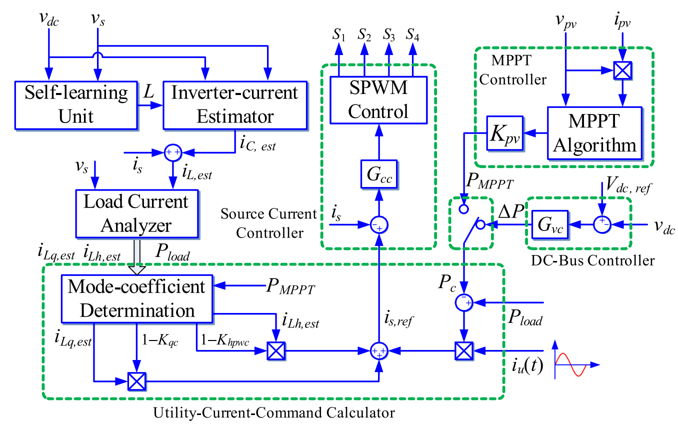


Fig. 9. Control strategy of the MFGCI configuration in [57].

Table 2
Parameters of the single-phase full-bridge MFGCI presented by Wu et al.

Dc source	PV array (SOLAREX MAGA SX-60)
Capacity	1 kW
Utility voltage	110 V/60 Hz
Passive components	$L_s=5$ mH, $C_s=5$ μF, $C_f=0.1$ μF, $L_r=1.7$ mH, $C_r=5.6$ nF, $C_{dc}=470$ μF, $C_1=C_2=470$ μF
Switching frequency	19.45 kHz
Control strategy	PI control, SPWM
Extra functions	APF, PFC

MFGCI. This reference current and the feedback current i_o, associated with the current regulator G_{cc}, the fed-forward controller G_{vs}, the feed-forward controller G_{fd}, and the compensation controller G_{ch}, form the modulation signal v_{con}. With the help of sinusoidal pulse width modulation (SPWM) coefficient K_{PWM}, the trigger pulses of insulated gate bipolar transistors (IGBTs) S_1–S_4 can be obtained.

Facing to the single-phase full-bridge topology as shown in Fig. 7, literature [57] also gives a control strategy, whose configuration is depicted in Fig. 9. In this strategy, there are two operation modes as well, namely, maximum power generation tracking and APF. In daytime, the MFGCI acts as a solar generator and track the maximum power generation to convert solar irradiation energy to electric energy. In day night, because the solar irradiation is zero, the MFGCI acts as an APF to improve the power quality at PCC. As demonstrated in Fig. 9, the control strategy mainly consists of a self-learning unit, an inverter-current estimator, a load current analyzer, a utility-current-command calculator, a MPPT controller, and a dc-bus controller. Where, the MPPT controller takes disturbance and observation (D&O) approach [59–61], since it is simple and easy to implement

on a digital signal processor (DSP) control board. By the means of self-learning unit, the pseudo-linear inductance $L|i_{est}(t)$ can be estimated, then the inverter-current $i_{o,est}$ can be formed by the current estimator. Therefore, the current senor for inverter current can be cancelled. Furthermore, due to the sampled utility current i_s, the load current $i_{L,est}$ can be obtained. Besides, the extended instantaneous power theory is used to calculate the total power of the load P_{load}, as well as the reactive and harmonic current, $i_{Lq,est}$ and $i_{Lh,est}$, respectively. Notation that reactive and harmonic current limiters are employed to prevent the total reference output current of the MFGCI exceeding its rated one, which can generate two compensation coefficients, namely K_{qc} and K_{hpwc}. In order to control the voltage of dc-bus, the reference active power P_c can be formed by voltage deviation regulator ΔP or MPPT controller P_{MPPT} in APF or MPPT modes, respectively. Then, the P_c subtracting load power P_{load} yields the reference grid-connected power. And it multiplies the unit-amplitude-voltage synchronous signal i_u, which yields the active part of the reference current. To achieve harmonic and reactive current compensation of the MFGCI, it is important to analyze the estimated harmonic and reactive current, $i_{Lh,est}$ and $i_{Lq,est}$. It should be noted that the rated apparent power of the MFGCI is the limited. So the total apparent power of extra compensation power and the conventional active power for RPI may exceed the rated apparent capacity of the MFGCI. The simplest approach to solve this issue is to limit the amplitude of the compensation current. In Fig. 9, coefficients $1-K_{hpwc}$ and $1-K_{qc}$ are employed to yield the limited harmonic and reactive compensation reference current. The synthetic reference current $i_{s,ref}$ and grid-connected current i_s are utilized in the current regulator G_{cc} to generate the trigger pulses of IGBTs S_1–S_4 by SPWM modulation.

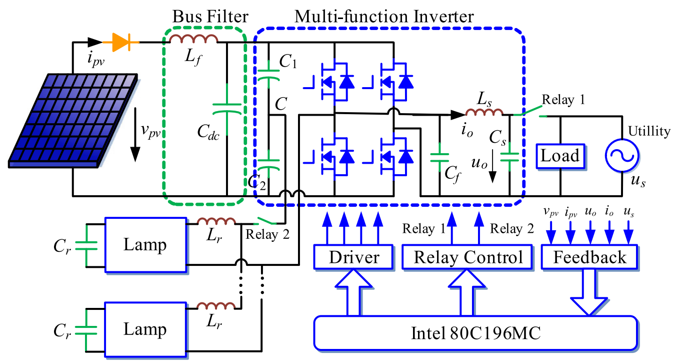


Fig. 10. Configuration of the MFGCI investigated by Wu et al.

Wu et al. have also described a MFGCI configuration for street lighting application as introduced in Fig. 10, whose parameters are described in Table 2 [62]. At daytime, the PV array is interfaced to utility by the MFGCI. At night, the lamps attached at the dc-link can be fed by utility and the MFGCI acts as an APF to compensate the harmonic and reactive current. To decrease the cost, the whole

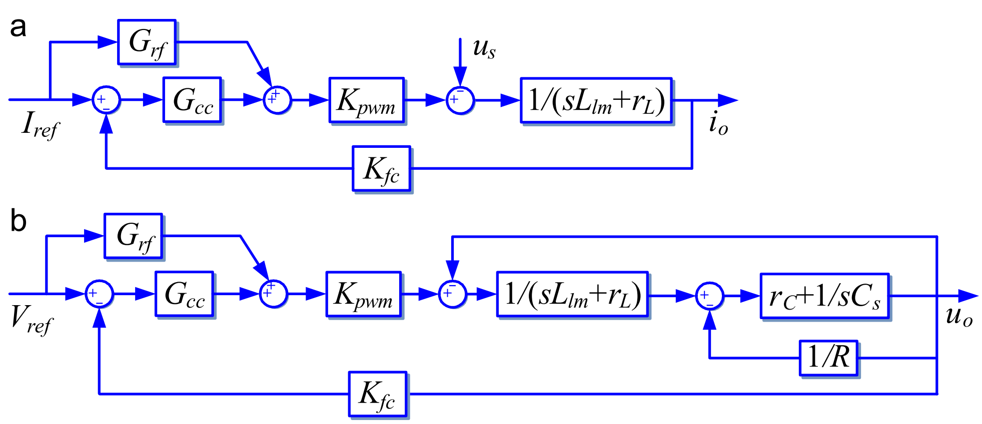


Fig. 11. Schematic control diagram of the MFGCI presented by Wu et al. (a) Control principle under grid-connected mode and (b) control principle under islanded mode.

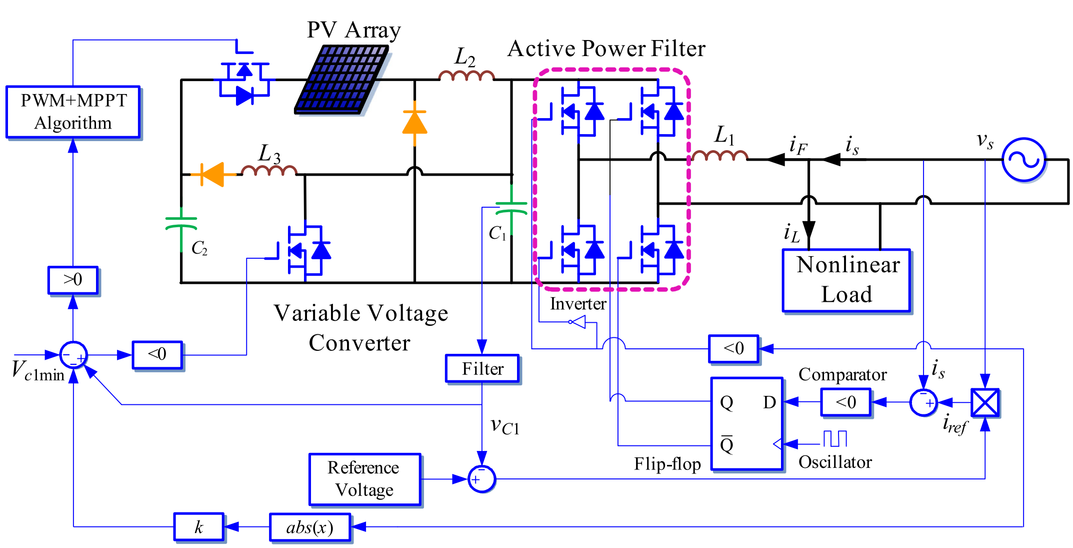


Fig. 12. Configuration of the MFGCI investigated by Sladic et al.

system is controlled by a micro-computer unit (MCU) Intel 80C196MC.

It should be noted that the MFGCI can work in grid-connected and islanded modes at daytime. The control schematic diagram of the MFGCI in two different modes is given in Fig. 11(a) and (b). Under grid-connected mode, the MFGCI supplies the solar energy to local load firstly, and the load can absorb the rest power from utility; of cause, the surplus power of PV can be fed to utility as well. Therefore, the main mission of the controller in grid-connected mode is to control the current of the MFGCI and interface the solar energy to utility as much as possible, as shown in Fig. 11(a). It can be found that a feed-forward controller G_{rf} and a PI controller G_{cc} are employed to achieve the performance of the system, where K_{fc} is the feedback gain. On the other hand, the MFGCI can also act as an uninterrupted power source (UPS) in islanded mode to feed the local load when the utility is fault. As indicated in Fig. 11(b), the controller ensures the MFGCI to be a voltage-controlled source in such condition.

Table 3
Parameters of the MFGCI presented by Sladic et al.

Dc source	Voltage of PV array 150–500 V
Passive components	L_1=8 mH, L_2=1 mH, L_3=1 mH, C_1=10 μF, C_2=2 mF
Switching frequency	15 kHz
Control strategy	Hysteresis modulation
Extra functions	APF

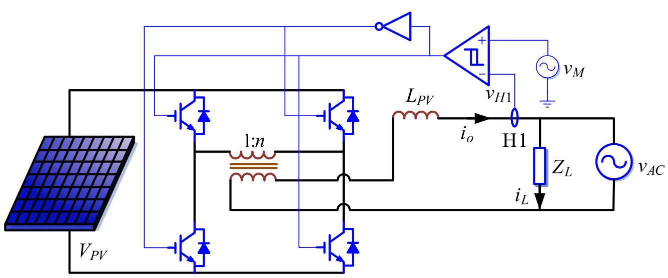


Fig. 13. MFGCI configuration presented by Calleja and Jimenez.

Sladic et al. have investigated a MFGCI configuration as depicted in Fig. 12, whose parameters are presented in Table 3 [63]. Unlike a conventional GCI, a novel variable voltage converter is embedded in the dc side to adapt large dc voltage range of PV arrays [64]. Besides, an analog controller is implemented to generate the trigger pulses of IGBTs.

Calleja and Jimenez also give a MFGCI configuration as shown in Fig. 13, whose parameters is described in Table 4 [65]. Fig. 14 demonstrates its control scheme. From Fig. 14(a) it can be seen that three Hall Effect sensors H1, H2, and H3, are employed to obtain the current signals for MPPT controller and power quality conditioning. It should be noted that D&O method is utilized for MPPT. Fig. 14(b) illustrates the block diagram of the circuit for harmonic and reactive current detection by the means of adaptive interfacing cancelling algorithm, where v_R is the amplitude of the sinusoidal reference signal. According to Fig. 14(b), the transfer function between v_{H3} and v_{QD} can be expressed as

$$G(s) = \frac{s^5 + 2s^3\omega^2 + s\omega^4}{s^5 + 2s^3\omega^2 + s\omega^4 - k\omega^4} \quad (1)$$

where $k = G_1G_2v_R/\tau$, and τ is the integral time constant.

Seo et al. also have presented a single-phase single-stage MFGCI configuration and its control strategy, as shown in Fig. 15, whose important parameters are available in Table 5 [66]. From the configuration, it can be seen that, the reference current is composed of two parts. One part $I_{mppt,ref}$ is from the result of MPPT.

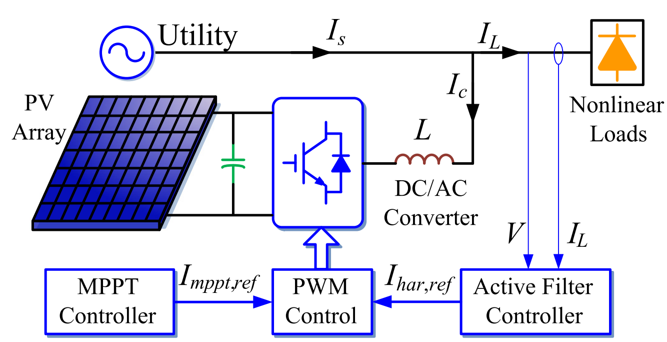


Fig. 15. Single-phase full-bridge MFGCI configuration presented by Seo et al.

Table 4
Parameters of the MFGCI presented by Calleja and Jimenez.

Dc source	PV array, v_{pv}=150 V
Capacity	1 kW
Passive components	Transformer ratio 1:2, L_{PV}=35 mH
Switching frequency	14.2 kHz
Control strategy	Hysteresis modulation, hysteresis B=200 mA
Extra functions	APF and RPI

Table 5
Parameters of the single-phase full-bridge MFGCI proposed by Seo et al.

Dc-source	PV array, the voltage of dc-bus, V_{pv}=600 V
Capacity	3 kVA
Voltage of utility grid	220 V/60 Hz
Switching frequency	20 kHz
Control strategy	PI Controller, SPWM modulation
Extra function	APF

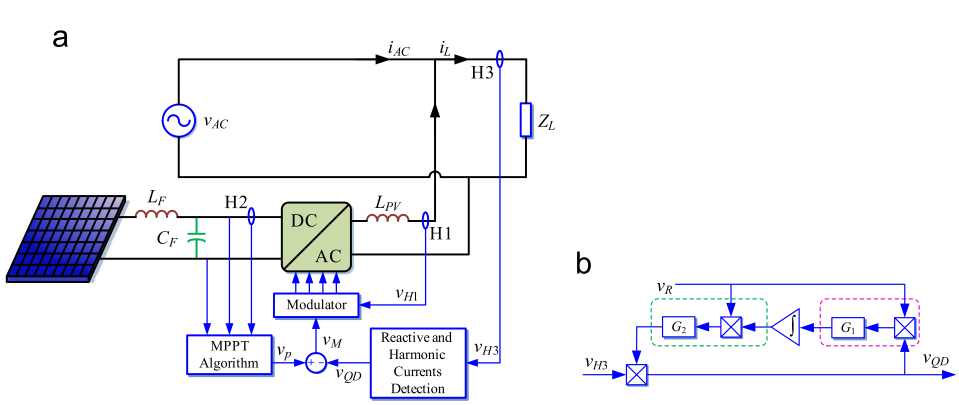


Fig. 14. Control scheme of the MFGCI proposed by Calleja and Jimenez. (a) Schematic diagram of control strategy and (b) structure of the adaptive filter.

The other part $I_{har,ref}$ is from the APF controller. Therefore, the MFGCI can also be used as APF in day night, which can increase the using hours of the MFGCI compared to conventional GCIs. Simultaneously, the trigger pulses are generated by SPWM modulation.

According to the MFGCI previously mentioned configuration, Fig. 16 gives the detailed control structure. The phase-locked loop (PLL) is employed to obtain the phase of utility θ_{PLL}. Meanwhile, the sampled load current is defined as $I_{load,a}$, namely equivalent load current of phase-a in virtual three-phase system. Then the equivalent current of virtual phase-b and c can be yielded by 120° and 240° phase-shift. According to the transformation from abc frame to $\alpha\beta$ frame, namely Clarke transformation as shown in (2) and its inverse transformation is $\boldsymbol{C}_{\alpha\beta/abc}=\boldsymbol{C}_{abc/\alpha\beta}^{-1}=\boldsymbol{C}_{abc/\alpha\beta}^{T}$, the equivalent current in $\alpha\beta$ frame can be expressed as $I_{load\alpha}$ and $I_{load\beta}$. As a result, the load current in dq frame can be formed based on the transformation in (3) whose inverse transformation meets $\boldsymbol{C}_{dq/\alpha\beta}=\boldsymbol{C}_{\alpha\beta/dq}^{-1}=\boldsymbol{C}_{\alpha\beta/dq}^{T}$, as well the ones filtered by low pass filter (LPF) can be written as I_{lpfd} and I_{lpfq}. As a consequence, the fundamental component of the load current $I_{ref\alpha}$ can be yielded with the aid of inverse transformations. The deviation between $I_{load\alpha}$ and $I_{ref\alpha}$ is the harmonic component of the load $I_{har,ref}$. On the other hand, the reference voltage of the dc bus can be determined by the MPPT controller associated with D&O approach. Due to the dc bus voltage regulator, the maximum current amplitude of the inverter is ensured as I_{max}, which multiplies the sinusoidal waveform $\sin\theta_{PLL}$ to form the reference current $I_{mppt,ref}$. It is worth nothing to note that this part of reference current is the pure active power component. To compensate the harmonic current of the load, the detected current component $I_{har,ref}$ should be added into $I_{mppt,ref}$ to yield the total reference current I_{ref}. With the output current regulator, the trigger pulses of the full-bridge can be obtained by SPWM generator.

$$\boldsymbol{C}_{abc/\alpha\beta}=\sqrt{\frac{2}{3}}\begin{bmatrix}1 & -1/2 & -1/2\\ 0 & \sqrt{3}/2 & -\sqrt{3}/2\end{bmatrix} \tag{2}$$

Table 6
Parameters of the single phase full bridge topology by Wu et al.

DC-source	PV array, voltage of dc-bus V_{dc}=400 V
Capacity	1 kVA
Voltage of utility grid	220 V/60 Hz
Switching frequency	25 kHz
Control strategy	PI controller, SPWM modulation
Extra function	APF

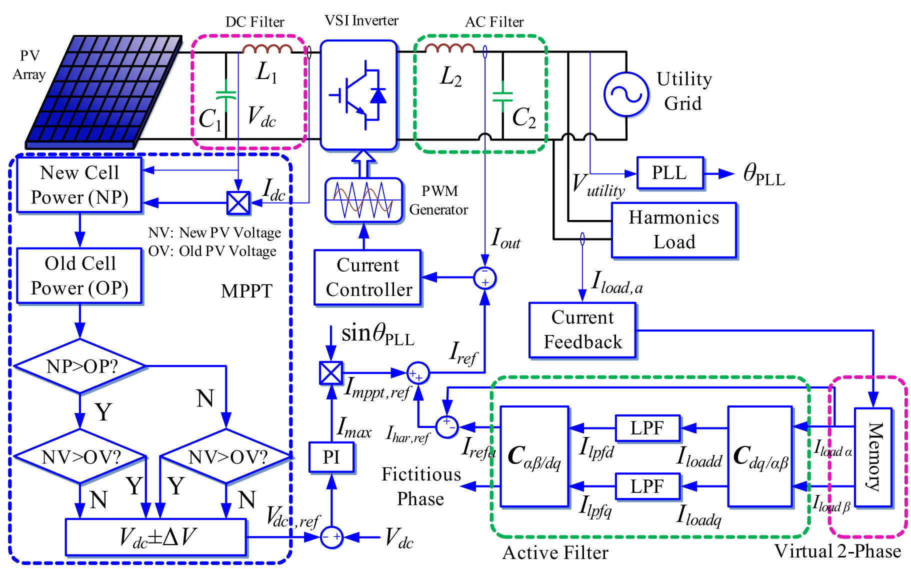


Fig. 16. Control strategy of the MFGCI configuration presented by Seo et al.

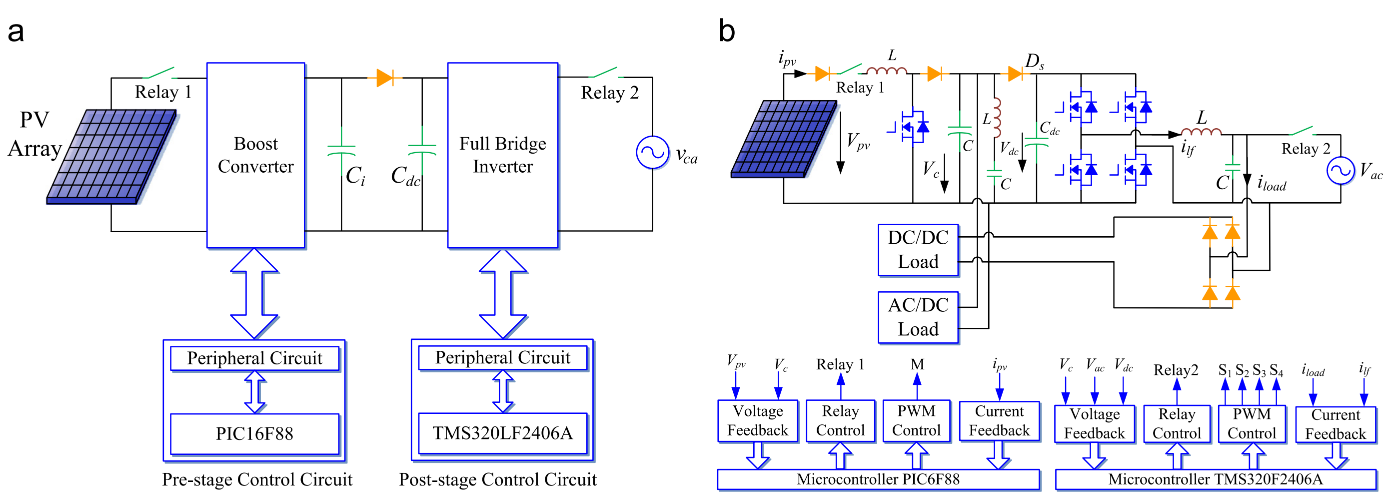


Fig. 17. The MFGCI configuration proposed by Wu et al. (a) Overall view of the MFGCI and (b) detailed block diagram.

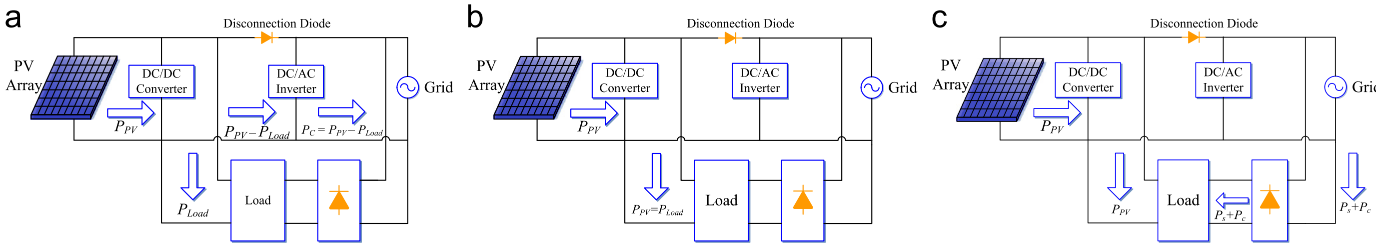


Fig. 18. Power flow of the MFGCI configuration operates under (a) the grid-connection mode, (b) direct supply mode, and (c) APF mode.

Table 7
DC voltages of the system in different operation modes.

Operation modes	Voltage
Grid-connected mode	V_c>400 V, V_{dc}=450 V
Direct supply mode	V_c<311 V, V_{dc}=450 V
APF mode	V_c=311 V–400 V

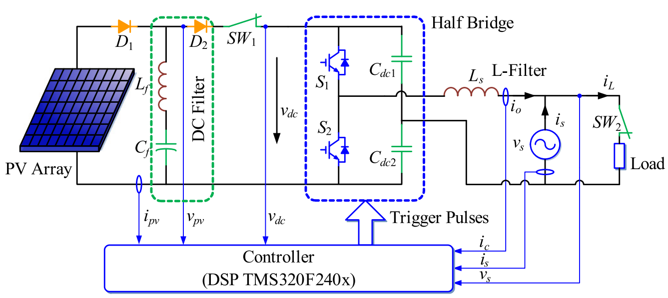


Fig. 19. Single-phase half-bridge MFGCI configuration presented by Wu et al.

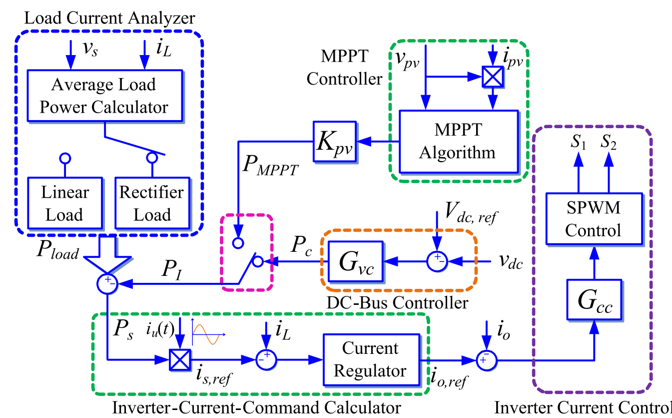


Fig. 20. Control strategy of the MFGCI given by Wu et al.

Table 8
Controller coefficients under different operation modes.

Coefficients	FAPF	PAPF mode			RPI mode
		Linear loads ASA $i_{c,ref}(t)>I_{sw}$	Rectifier loads ACA $i_{c,ref}(t)\leq I_{sw}$		
K_{ACA}	0	0	0	1	0
K_{ASA}	1	$(I_{sw}-I_{R,pv})$/Icp	1		1
K_{pv}	1	1	1		0

$$C_{\alpha\beta/dq}=\begin{bmatrix}\cos\theta_{PLL} & \sin\theta_{PLL}\\ -\sin\theta_{PLL} & \cos\theta_{PLL}\end{bmatrix} \quad (3)$$

Wu et al. have described a single-phase two-stage MFGCI structure as demonstrated in Fig. 17, whose parameters are listed in Table 6 [67]. Metal-oxide-semiconductor field-effect transistor (MOSFET) is employed due to its fast switching frequency. It can be found that different CPUs are employed for DC/DC and DC/AC stages. The DC/DC stage is a typical boost circuit and a microcontroller PIC6F88 is implemented; on the contrary, the TMS320F2406A DSP is used in the DC/AC stage. Note that there is a single-phase diode rectifier connected at the output terminal of the MFGCI to act as a nonlinear load. Meanwhile, the load is also connected at the dc-bus of the MFGCI for reliability improvement.

There are three operation modes of this MFGCI according to the output power of the PV array, namely grid-connected mode, direct supply mode, and APF mode. When the solar irradiation is high, the output power of the PV array supplies load firstly, and the surplus power is fed to utility by the MFGCI, as depicted in Fig. 18(a). When the solar irradiation is middle, the PV array just supplies load and there is no ac power fed to utility grid. That is to say, the whole system operates in direct supply mode, as shown in Fig. 18(b). As shown in Fig. 18(c), when the solar irradiation is low, the output power of the PV array cannot satisfy the demand of load, the shortage power is supplied by utility and the MFGCI acts as APF to compensate the harmonic current of nonlinear load. Table 7 shows the different voltage levels of the boost circuit V_c and dc-bus V_{dc} in different operation modes.

On the basis of Fig. 7, Wu et al. give a further work. As indicated in Fig. 19, the half-bridge topology is employed to replace the full-bridge in Fig. 7, which have the same functionalities of the before mentioned one [68,69]. Although this half-bridge circuit can decrease the cost of IGBTs, the voltage balance of the two series capacitors is hard. It should be noted that, this MFGCI also has three operation modes. When the solar isolation is high, it works under RPI mode to convert the solar energy efficiently. When the solar isolation is middle, it acts as a partial APF (PAPF). When the solar isolation is low, it operates under full APF mode (FAPF).

The control strategy of the half-bridge MFGCI is shown in Fig. 20. From this detailed block diagram, it can be seen that the control strategy contains a MPPT controller, an inverter-current-command calculator, a dc-bus controller, and an inverter current controller. Some detailed outlines are similar as the control strategy mentioned in Fig. 8. The load type and its power P_{load} can be detected by load current analyzer. According to the type of load, the MFGCI can work under APF mode or MPPT mode, while the MPPT controller employs D&O approach. The power P_l determined by its operation mode and the load power P_{load} yield the reference active power P_s. The reference power multiplies the unit-amplitude-voltage synchronous signal $i_u(t)$, which derives the reference current $i_{s,ref}$ for RPI implementation. With load current i_L feedback and inverter-current-command calculator, it is available to generate the reference current of the MFGCI $i_{o,ref}$. There are two different algorithms for current regulator application to prevent the reference current exceeding the rated one of the MFGCI, namely amplitude clamping algorithm (ACA) and amplitude-scaling

algorithm (ASA). The reference current can be expressed as

$$i_{o,ref} = \frac{\sqrt{2}(P_{MPPT}+P_{ACA}K_{ACA})}{V_{S,rms}}i_u(t) + \left[i_L(t) - \frac{\sqrt{2}P_{load}}{V_{S,rms}}i_u(t)\right] \times K_{PV}(1-K_{ACA})K_{ASA} + (I_{sw}-I_{R,pv})K_{ACA} = i_{c,p}(t) + i_c'(t) \quad (4)$$

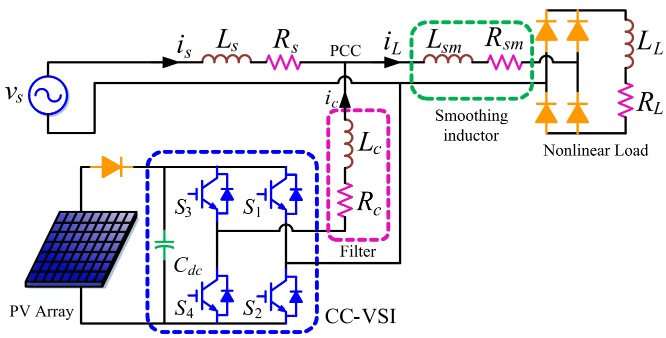


Fig. 21. Single-phase MFGCI configuration presented by Patidar et al.

Table 9
Parameters of the single phase full bridge topology by Patidar et al.

Dc-source	15 series and 1 parallel, BPSOLAR BP280 PV array
Capacity	Approximate 1.2 kVA
Voltage of utility grid	230 V/60 Hz
Switching frequency	25 kHz
Passive components	L_c=3 mH, R_c=0.1 Ω, L_L=25 mH, R_L=7.5 Ω
Control strategy	PI control, hysteresis modulation
Extra function	APF

where $i_{c,p}(t)$ denotes the active component of the inverter current, while $i_c'(t)$ represents its reactive and harmonic components. $i_L(t)$ is the current of the load, while P_{load} is load power. P_{MPPT} is the output power of MPPT controller, and P_{ACA} is the injected power using ACA algorithm. I_{sw} is the rated current of the MFGCI. $I_{R,pv}$ stands for the active part of the output current of the PV array. It should be noted that K_{pv}, K_{ACA}, and K_{ASA} are controller coefficients, which are determined by different algorithms and operation modes as illustrated in Table 8. The amplitude of reference current is limited by the ACA or ASA algorithm in current regulator block, when the reference current exceeds the rated current of the MFGCI. In summary, the MFGCI can transfer among three different modes seamlessly.

Patidar et al. have studied a single-phase MFGCI solution, as demonstrated in Fig. 21, whose important parameters are shown in Table 9 [70]. Fig. 22 gives the detailed block diagram of its control strategy. Obviously, this system is a typical current-controlled voltage source inverter (CC-VSI) and consists of the PV array, an H-bridge, a local load, and the filter inductor L_c. Due to the twice order line-frequency voltage fluctuations of dc-bus, a large buffer capacitor is useful. Meanwhile, the filter inductor is employed to suppress the harmonic current around the switching frequency.

From the control strategy, a TMS320F2812 DSP is utilized as the controller board, where the MPPT controller employs look-up table method that saves much CPU time and storage space; nevertheless, it may deviates from the actual maximum power point in some bad cases. Because of the sampled voltage and current of PV array, I_{pv} and I_{pv}, and the calculated maximum output power of PV P_{pv}, the reference voltage of PV array $V_{dc,ref}$ can be obtained by the MPPT controller. Due to the dc-bus voltage controller, the

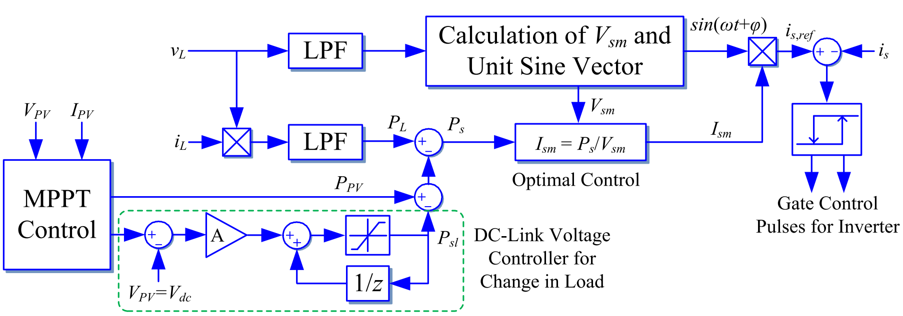


Fig. 22. Control strategy of the single-phase MFGCI proposed by Patidar et al.

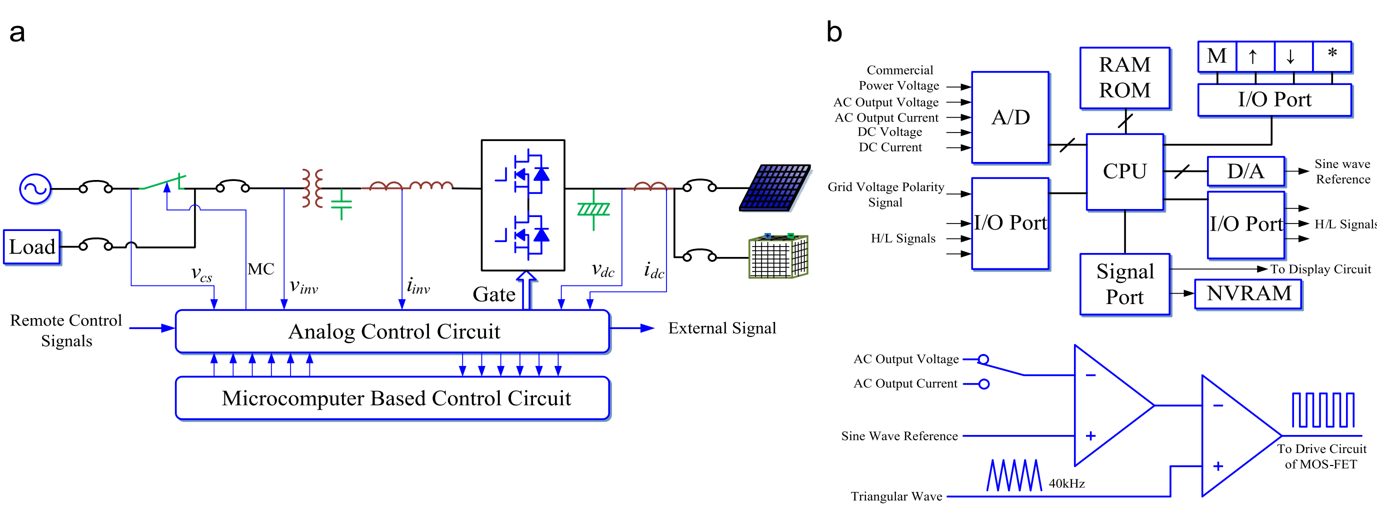


Fig. 23. Brief topology and control strategy of the MFGCI presented by Hirachi, etc. (a) Overview of the MFGCI and (b) control strategy of the MFGCI.

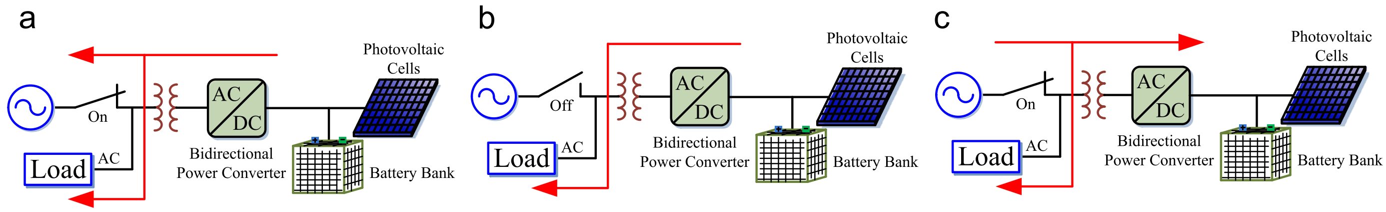


Fig. 24. Three operation models of solar photovoltaic power generation conditioner with bidirectional power converter. (a) On clear sky day (utility interactive operation), (b) on cloudy sky day or power failure (stand alone operation) and (c) during late-night (rectifier operation).

reference power P_{sl} is achieved, meanwhile the average active power of load P_L subtracting P_{sl} derives the grid-connected reference power. With the help of optimal control, it is easy to form the amplitude of the grid-connected current $I_{sm}=P_s/V_{sm}$, and it multiplies the unit-amplitude-voltage synchronous signal to yield the instantaneous reference current $i_{s,ref}$. Then, the trigger pulses of the IGBTs are achieved by the grid-connected current feedback and current regulator associated with hysteresis modulation.

According to the topologies mentioned before, these MFGCI using full-bridge or half-bridge in single-phase have three visible drawbacks:

- Firstly, due to the large fluctuations of solar irradiation, these MFGCI topologies can solely operate under grid-connected mode. If they work under islanded mode and the output power of the PV array is larger than the rated power of the local load, the terminal voltage of the load will be bigger than the rated one. On the contrary, when the output power of the PV array is smaller than the local load, the terminal voltage of load will be smaller than the rated one. In summary, the system is hard to stably work at its nominal point in islanded mode.
- Secondly, the previously mentioned MFGCIs mainly employ L-filter, which need a big inductor and the performance is bad. Furthermore, the cost and bulk of the filter inductor will increase if the inductance is bigger.
- At last, there is no electric isolation, the dc component injects into utility will affect other devices. Especially, the dc component may lead to the saturation of transformer due to the dc bias magnetic.

The single-stage single-phase MFGCI topology presented by Hirachi et al. in Fig. 23, can overcome the drawbacks above, whose parameters are listed in Table 10 [71]. In this topology, the diodes D_1 and D_2 in Fig. 7 can be cancelled because of the energy storage device embedded in the dc-link side. In addition, a LC-filter is implemented to replace the L-filter, and an isolation transformer is attached in the ac side. It should be noted that there are three operation modes. In sunny days, the bi-directional converter feeds the energy of PV array to local load and utility, as shown in Fig. 24 (a). In cloudy day or the interruption of utility, the system work under islanded mode, and the battery supplies power to load, as shown in Fig. 24(b). At day night, the converter acts as a PWM rectifier and charges the battery, as shown in Fig. 24(c).

From Fig. 24, it can be found that the system can stably work under islanded mode. It can be seen that the system is a simple micro-grid. When the grid switch is close, the whole system works under grid-connected mode. The output power of PV array supplies the local load firstly. Then, the surplus PV power feeds to the battery and utility; on the contrary, the shortage power is supplied by utility and the battery. When the grid switch is open, the system works under islanded mode. The battery can absorbs (or supplies) the surplus (or shortage) power of the PV array, which can keep the terminal voltage of the load at its nominal level. As mentioned before, the system can also be modified as an APF to feed harmonic current to local nonlinear load.

Table 10
Parameters of the single-phase full-bridge MFGCI studied by Hirachi et al.

Dc-source	PV array, battery, voltage of dc-bus is 200 V
Capacity	3 kVA
Voltage of utility grid	110 V/60 Hz
Switching frequency	40 kHz
Power electronic device	MOSFET
Control strategy	PI control, SPWM modulation
Extra function	UPS

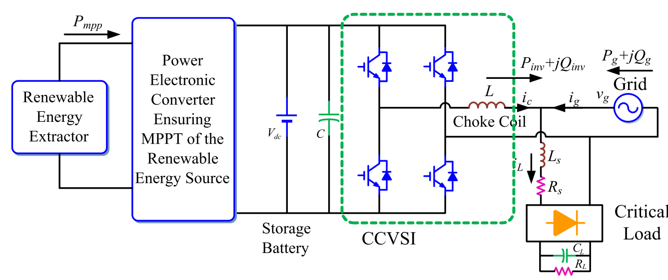


Fig. 25. Configuration of the MFGCI presented by Dasgupta et al.

Table 11
Parameters of the MFGCI presented by Dasgupta et al.

Dc source	$V_{dc}=100$ V
Utility voltage	50 V
Sampling frequency	10 kHz
Control strategy	Lyapunov based and spatial repetitive control, SPWM modulation
Extra functions	APF

As demonstrated in Fig. 25, Dasgupta et al. have investigated a MFGCI configuration for harmonic and reactive compensation in a micro-grid, whose parameters are illustrated in Table 11 [72]. In this MFGCI, a CC-VSI is implemented as the interface. It should be noted that the battery storage is attached in the dc link, so the system can work under islanded condition freely.

Fig. 26 depicts the control scheme of the MFGCI. It can be seen that the Hilbert transform and extended p–q power theory are utilized to detect the compensation current components. Besides, a Lyapunov-based controller and spatial repetitive controller are embodied for excellent dynamic and steady performances on current tracking.

Chiang et al. have studied a MFGCI as shown in Fig. 27, whose parameters are described in Table 12 [73]. From the control part of the configuration, it can be found that a novel MPPT algorithm is utilized to attain high performance, which has considered the dynamic model of the PV array and the state-averaged mode of the DC/DC converter. Besides, the charging and discharging control of the batteries are clearly separated, as well as these modes can be

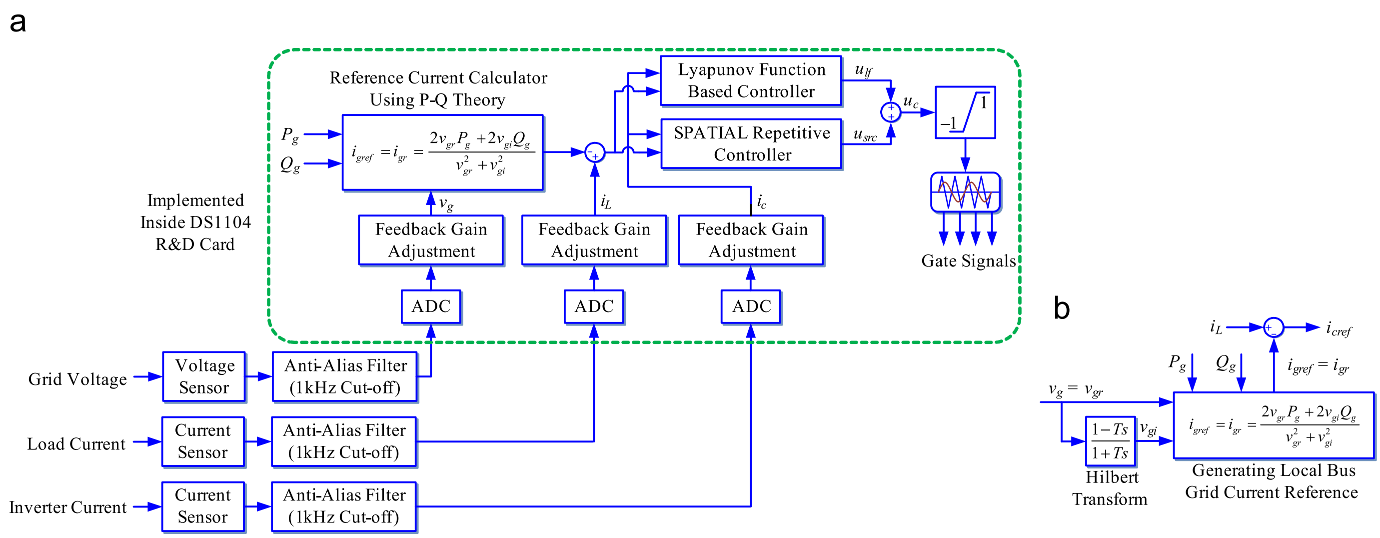


Fig. 26. Control strategy of the MFGCI proposed by Dasgupta et al. (a) Block diagram in detail and (b) the subsystem of the control scheme to generate reference current.

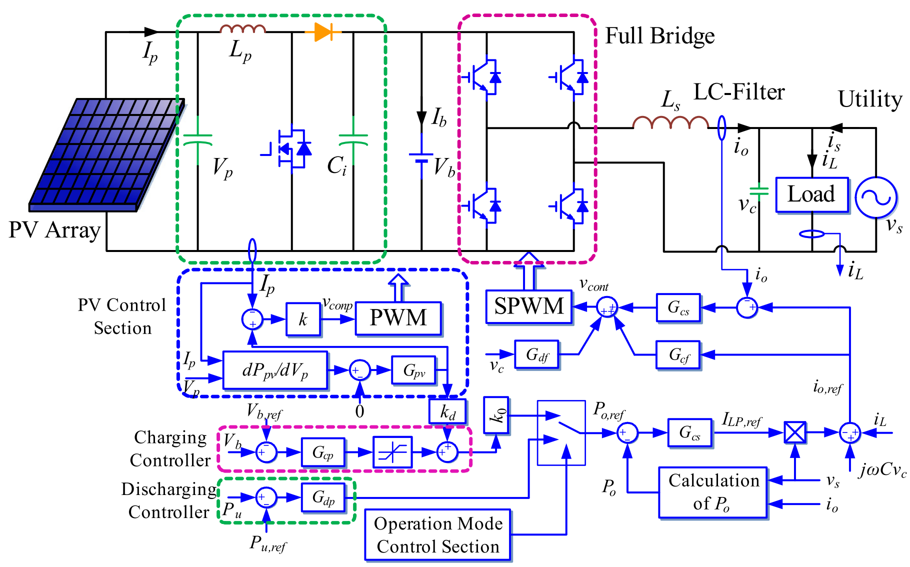


Fig. 27. Architecture of the MFGCI investigated by Chiang et al.

Table 12
Parameters of the single-phase full-bridge MFGCI presented by Chiang et al.

Dc source	PV array, 7 × 6 (each with open voltage V_{oc}=14 V, short current I_{sc}=1.2 A) batteries 12 V/15 Ah × 14
Capacity	Approximately 600 W
Utility voltage	110 V/60 Hz
Passive components	L_p=0.3 mH, C_i=200 μF
Power electronic components	MOSFET 450 V/13 A (boost converter), IGBT 600 V/50 A (inverter)
Control strategy	PI control, SPWM
Extra functions	APF, UPS

easily transferred with the help of the operation modes control section.

Bojoi et al. also survey a MFGCI configuration as illustrated in Fig. 28, whose important parameters are presented in Table 13 [74,75]. Additionally, its control strategy is given in Fig. 29.

Fig. 29 shows the detailed control diagram of the MFGCI configuration presented by Bojoi et al. It can be seen that this control strategy consists of reference current generator, current regulator, and SPWM modulation, where a filter algorithm associated with the instantaneous power theory, named as sinusoidal signal integrator (SSI), is employed to detect the harmonic and reactive current of the load. Furthermore, a repetitive controller and a PI controller are implemented to accurately track the reference current.

Cirrincione et al. have also investigated a MFGCI configuration as shown in Fig. 30 and Table 14 [76]. Simultaneously, Fig. 31 gives its control principle with two neural adaptive filters to extract the compensation current of local loads and compute the fundamental component of the utility voltage. Besides, a proportional-resonant (PR) controller is utilized to achieve excellent performance.

Macken et al. have studied the single-phase single-stage MFGCI system as displayed in Fig. 32, whose parameters are listed in Table 15. Whereas, there may have multiple MFGCIs in a DGS or MG, thus they have presented an agent-based communication approach to coordinate the MFGCIs as described in [77]. In general, to prevent the output current of the MFGCI exceeding its rated one, its apparent power for auxiliary services cannot be too much. Fortunately, a DGS or MG always has integrated many GCIs. If they can work as MFGCIs coordinately, the total apparent power may be large enough to deal with the possible power quality issues.

The MFGCI configurations mentioned before are all used as power quality conditioners in parallel, which can just enhance the power quality issues caused by harmonic and reactive current. Hosseini et al. present a novel single-stage MFGCI topology in series, which can act as a DVR and compensate the voltage swell and sag of utility [78]. Important parameters of the MFGCI configuration are described in Table 16.

As shown in Fig. 33, this topology is made up of two independent boost circuits. The desired voltage v_o can be achieved at its output terminal if a proper control strategy is carried out. When the voltage of utility is swell, sag, and/or interruption, this topology can compensate it effectively. In addition, this topology can also compensate the reactive voltage at the terminal of load, which can confirms unit factor operation of utility. It should be noted that the filter components L_{dc}, L_f, and C_f pay important role to suppress the fluctuations of the dc-link and inhibit the failure of

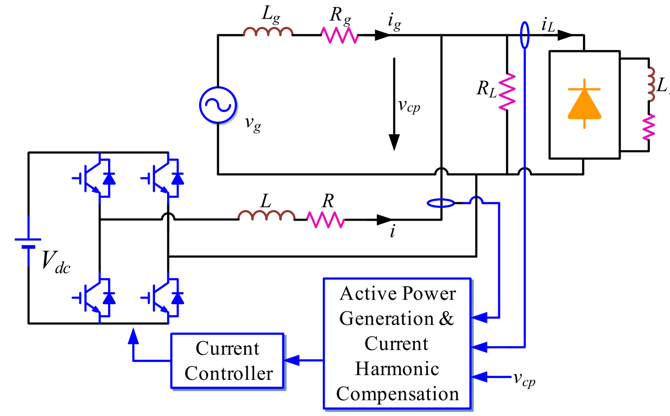


Fig. 30. Schematic diagram of the MFGCI investigated by Cirrincione et al.

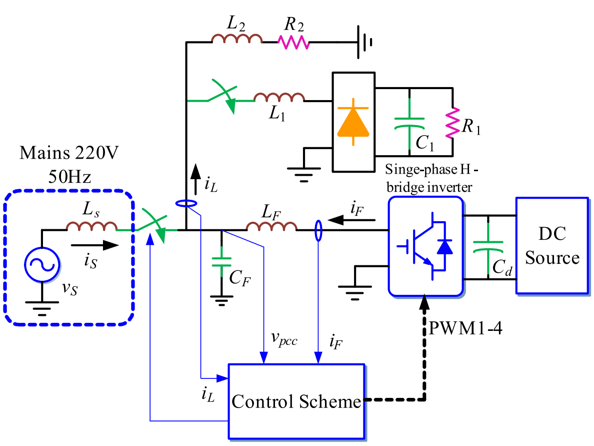


Fig. 28. The MFGCI configuration presented by Bojoi et al.

Table 13
Parameters of the single-phase full-bridge topology by Bojoi et al.

Dc-source	Micro-source, V_{dc}=400 V
Capacity	4 kVA
Voltage of utility grid	220 V/50 Hz
Switching frequency	10 kHz
Passive components	L_F=0.7 mH, C_F=7.5 μH, C_F=2.2 mF, R_2=25 Ω, L_2=30 mH, L_1=0.9 mH, C_1=1 mF, R_1=50 Ω
Control strategy	Repetitive control and PI control, SPWM modulation
Extra functions	APF, reactive compensation

Table 14
Parameters of the single-phase full-bridge MFGCI presented by Cirrincione et al.

Dc source	PV array, V_{dc}=250 V
Utility voltage	130 V/50 Hz
Passive components	L_g=20 mH, R_g=1 Ω, L=4 mH, R=0.2 Ω
Switching frequency	15 kHz
Control strategy	PR control, SPWM
Extra functions	APF

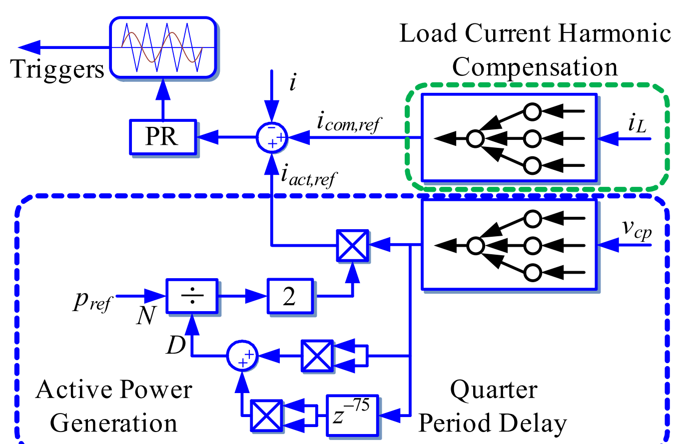


Fig. 31. Control diagram of the MFGCI presented by Cirrincione et al.

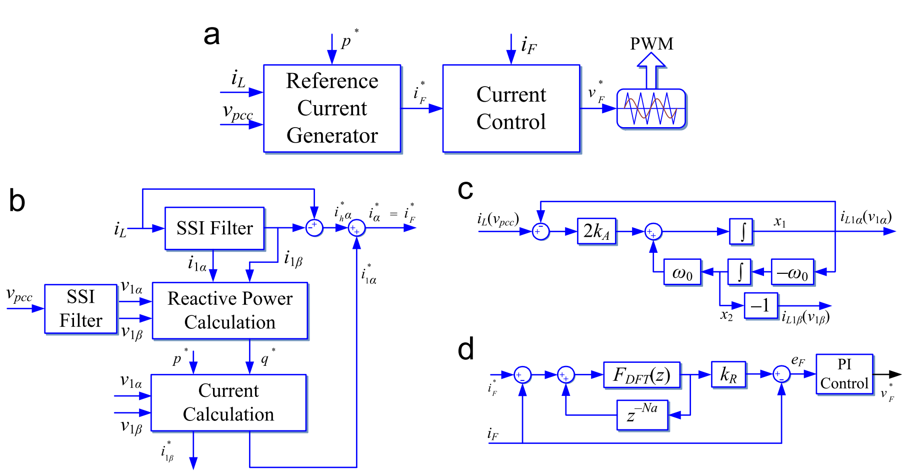


Fig. 29. Block diagram of the MFGCI proposed by Bojoi et al. (a) Overview block diagram, (b) reference current generation algorithm, (c) model of the SSI filter and (d) current regulator.

the MPPT. In the presented topology, each boost circuit is driven by a modulation signal with 180° phase-shift and dc bias. The deviation of these two modulation signals yields a sinusoidal waveform. Therefore, the terminal voltage of this topology can be controlled by the modulation signals directly. As shown in Fig. 33(a) and (b), the controller of the boost circuit consists of an outer current loop, and an inner voltage loop, respectively. If the desired output voltage of this topology can be expressed as $v_{oref}=\sqrt{2}V\sin(\omega t)$, then the reference voltage of two boost circuits can be written as

(1) when $\sin(\omega t)>0$, take

$$\begin{cases} v_{o1ref}=v_{o2}+v_{oref}=v_{o2}+\sqrt{2}V\sin(\omega t) \\ v_{o2ref}=v_{dc}-V\sin(\omega t)/\sqrt{2} \end{cases} \quad (5)$$

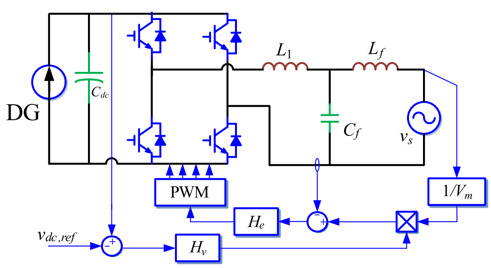


Fig. 32. Configuration of the MFGCI studied by Macken et al.

Table 15
Parameters of the single-phase full-bridge MFGCI presented by Macken et al.

Dc source	PV array
Capacity	1 kW
Utility voltage	110 V/50 Hz
Passive components	$L_1=5$ mH, $C_f=4$ μF, $L_f=2.5$ mH; diode rectifier $L=150$ mH, $R=35\ \Omega$
Switching frequency	10 kHz
Control strategy	PI control, SPWM
Extra functions	APF

Table 16
Parameters of the single-phase MFGCI proposed by Hosseini et al.

Dc-source	PV array
Capacity	$P_L=2$–2.4 kW($R_L=20$–$25\ \Omega$)
Voltage of utility grid	220 V/50 Hz
Switching frequency	20 kHz
Passive components	$L_1=L_2=0.2$ mH, $C_f=1000$ μF, $C_1=C_2=20$ μF, $L_f=2.5$ mH, $L_{dc}=1$ mH
Control strategy	PI control, SPWM modulation
Extra functions	DVR and PFC

(2) when $\sin(\omega t)<0$, set

$$\begin{cases} v_{o1ref}=v_{dc}+V\sin(\omega t)/\sqrt{2} \\ v_{o2ref}=v_{o1}-v_{oref}=v_{o2}-\sqrt{2}V\sin(\omega t) \end{cases} \quad (6)$$

Fig. 34 shows the control block of the boost circuit, and Fig. 34(a) give the algorithm to generate the reference voltage. The reference voltage of dc-bus V_{pref} is achieved by MPPT controller. And the reference maximum output power P_{MMP} is obtained by dc voltage regulator. In addition, the reference phase φ_0 can be accurately calculated. To improve the dynamic performance on power tracking, a close-loop control of P_{INV} is added for the phase compensation. Then, the amplitude of the reference voltage $|v_L|$ can be derived according to different operation modes. Furthermore, by the means of the outer voltage loop and inner current loop, as shown in Fig. 34(b) and (c), the controlled duty cycle of the boost circuits can be achieved.

Because the impedance of utility grid is small, to compensate utility voltage using a parallel converter is unwise, in general. Otherwise, there may be a very large current flow across utility, that is to say, the capacity of the parallel converter must be very large. However, in the view point of the PV GCI, this kind of solution may be suitable, because the capacity of the PV inverter is usually large enough to supply the full capacity of local load. Therefore, a properly large reactive current can change the voltage of load terminal, if a large inductor L_s is introduced in utility side. Mastromauro et al. present this kind of MFGCI as demonstrated in Fig. 35 [79,80], whose parameters are listed in Table 17. It should be noted that the harmonic current is so large, and can cause the distortion voltage on utility inductor. Fortunately, it also can be compensated by the PV GCI.

The control block of this MFGCI is depicted in Fig. 36(a), which consists of an outer voltage loop and an inner current loop. Furthermore, the outer voltage loop employs repetitive controller in Fig. 36(b), which can accurately tracks fundamental and harmonic voltage and effectively compensates the voltage swell, sag, and distortion. Besides, the inner current loop implements PI controller, which has a fast dynamic performance.

According to the MFGCI systems in Fig. 35, literature [81] gives a reference generation algorithm based on droop control, which is indicated in Fig. 37. It can be seen that the reference voltage is formed by the reactive and active power droop loops, where the normal values of reactive and active power are $Q^*=0$ and $P^*=P_{MPPT}$, respectively, and Q_G and P_c are the actually output reactive and active power of the inverter. The detailed block diagram of the droop control can be found in Fig. 38, where m_i, m_p, and n_p are control coefficients. The decoupling strategy of active and reactive power can be expressed as

$$\begin{cases} P'=(P_c-P^*)\sin\theta-(Q_G-Q^*)\cos\theta \\ Q'=(P_c-P^*)\cos\theta+(Q_G-Q^*)\sin\theta \end{cases} \quad (7)$$

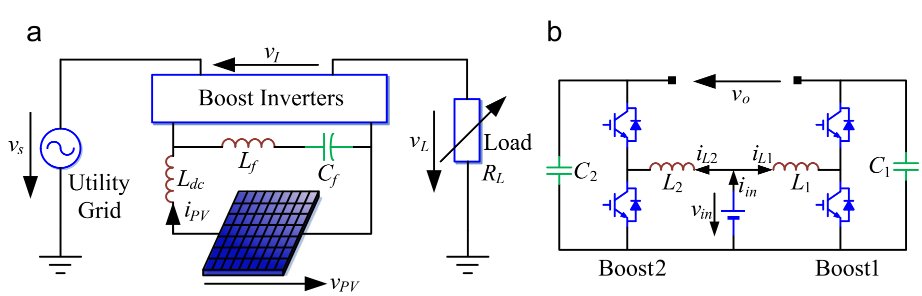


Fig. 33. Single-phase MFGCI presented by Hosseini et al. (a) Schematic configuration and (b) circuit model.

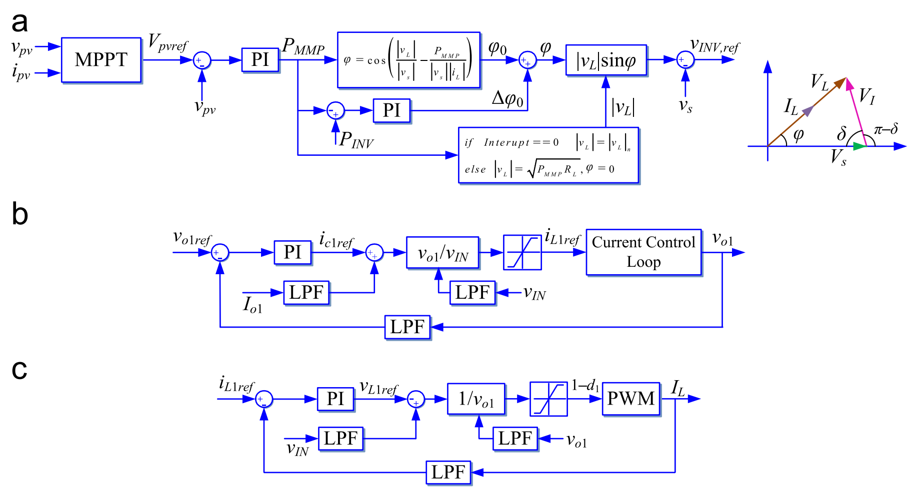


Fig. 34. Control strategies of the boost circuits. (a) Inverter voltage reference controller, (b) voltage control loop and (c) current control loop.

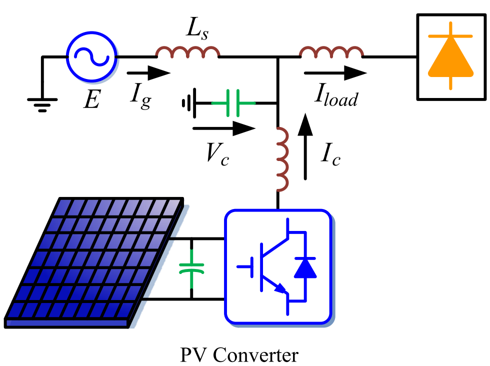


Fig. 35. Block-diagram of the grid-connected PV system with active filter functionality.

Table 17
Parameters of the three phase full bridge topology by Mastromauro et al.

Dc-source	PV array, voltage of dc-bus, V_{dc}=460 V
Capacity	Danfoss VLT 5006 inverter, rated apparent power 7.6 kVA, experimental capacity 1.2 kW
Voltage of utility grid	220 V/50 Hz
Switching frequency	20 kHz
Parameters	LC filter 1.4 mH+5 μF, damping resistance R=1 Ω, inductor in utility grid side L_s=15 mH
Control strategy	Repetitive control, PI control, SPWM modulation
Extra functions	DVR, harmonic voltage compensation

where $\theta = X/R$ is impedance ratio. It should be noted that the stability of the droop controller is directly determined by the control coefficients. It is very important to properly design these coefficients.

Based on the MFGCI presented by Dasgupta et al. as illustrated in Fig. 25, they also give another MFGCI configuration as shown in Fig. 39, whose parameters are listed in Table 18 [82]. It is easy to found that the load is connected between PWM inverter and utility in series. Thus, the voltage satisfy $v_{inv} = v_L - v_g$, in other words, the voltage of load v_L can be controlled by the MFGCI indirectly. Therefore, the MFGCI can greatly enhance the voltage quality of the load.

Fig. 40 shows the control scheme of the MFGCI. According to the phasor diagram in Fig. 39(b), the reference voltage of the load can be calculated as shown in Fig. 40. Then, a spatial controller is utilized to obtain the trigger pulses of the IGBTs.

Lin et al. have investigated a MFGCI as shown in Fig. 41, whose parameters are listed in Table 19. On the basis of the single-phase H-bridge converter, an asymmetrical leg is employed to achieve three-level PWM, which has less voltage harmonic generated on the ac side of the MFGCI compared with a two-level one. An independent cell of this three-level converter is described in Fig. 41(a). According to the cell and its control scheme, it can be applied to three-phase utility as three independent VSIs as shown in Fig. 41(c). However, it can also be applied as a combined inverter as shown in Fig. 41(d), whose three cells share the dc bus fed by energy storage devices and/or RESs. In [83], a single-phase MFGCI is studied, which can act as an UPQC, as shown in Fig. 42.

Geibel et al. also give a single-phase UPQC-based MFGCI as presented in Fig. 43 and have achieved good performance [84].

Kuo et al. have investigated a MFGCI configuration as shown in Fig. 44, whose system parameters are listed in Table 20. In [85], the linear relationship between equivalent conductance and current of PV array is found. As a consequence, a novel MPPT algorithm is presented so as to perform the rapid and accurate power tracking features. Owing to the 3-leg topology, the MFGCI can be applied to single-phase three-wire system.

The control schematic diagram of the MFGCI is depicted in Fig. 44. From the control principle of the line-mode controller in Fig. 45(a), it can be seen that the MFGCI can performs as a conventional GCI or an APF flexibly. The amplitude of the reference current is derived by MPPT controller or APF controller, which multiplies the per-unit signal in phase with utility voltage to generate the instantaneous reference current $i_{ulm,ref}$. It should be noted that the subscript "lm" denotes the line-value, for instance $i_{lm} = i_a - i_b$. Then, the load current i_{Llm} is added to $i_{ulm,ref}$ for output current regulation of the MFGCI. Besides, a phase-lead controller G_{cc}, a feed-forward controller G_{fd}, and a feedback compensator G_{ch} are employed to achieve fast dynamic and accurate steady performance. To against the disturbance from utility voltage, a disturbance immunizing controller G_{vs} is utilized. To balance the currents in phase-a and b, a neural-mode controller is implemented as shown in Fig. 45(b).

All the MFGCI topologies mentioned before employ hard-switching, which may lead to low efficiency of energy conversion. De Souza et al. give a MFGCI topology using soft-switching technology, whose configuration and parameters are demonstrated in Fig. 46 and Table 21, respectively [86–88]. A brief diagram of the topology is

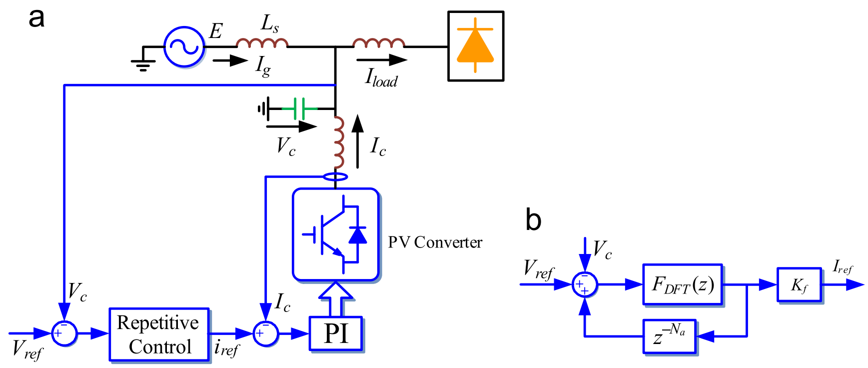


Fig. 36. Full-bridge MFGCI configuration presented by Mastromauro et al. (a) Voltage control of the shunt connected PV converter and (b) repetitive control of voltage loop.

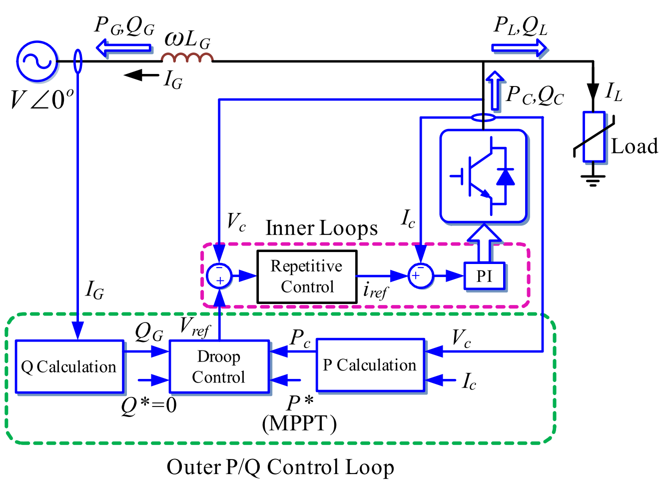


Fig. 37. Block diagram of the grid-connected PV-system power stage and its control scheme.

shown in Fig. 47. It can be found that this topology consists of a half-bridge-zero-voltage DC/DC converter and a cascaded DC/AC converter. Meanwhile, to reduce the electromagnetic capacity and the power loss of the system, the DC/DC stage employs half-bridge zero-voltage switching pulse width modulation (HB ZVS-PWM), as illustrated in Fig. 48. Literature [86–88] show the algorithm to select the optimal parameters of capacitor C_{e1}/C_{e2}, inductor L_r, and the transformer turns ratio.

Fig. 49 gives the block diagram of the DC/AC stage. Similar to the single-phase full-bridge MFGCIs mentioned before, this DC/AC stage can also be implemented as an APF. This topology can not only be an interface to connect PV array to utility, but also can act as an APF to compensate the harmonic and reactive current of the local load. Its operation can be briefly described as follows. The DC/DC converter is employed to boost the output voltage of PV array to be a high enough one to meet the requirement of the DC/AC stage. At the same time, the DC/DC stage also completes the MPPT of PV array. The PV array supplies load firstly, and the surplus power is fed to utility in sunny days; on the contrary, the utility will supply the shortage power of load, when PV array generates not enough power to load in cloudy days. Note that, to ensure the unit power factor of the utility, the MFGCI also can operate as an APF to compensate the harmonic and reactive power of the load. The control strategy of the DC/AC stage mainly consists of an outer dc-bus voltage loop and an inner current loop. The amplitude of grid-connected current is derived by the reference and feedback dc-bus voltage, V_{ref} and k_vV_{dc}, as well as the voltage regulator C_v. The amplitude multiplying the unit-amplitude-voltage synchronous signal yields the reference current. With the help of current regulator C_i and forward back of utility voltage G_{cd}, the trigger pulses of the full-bridge can be obtained by SPWM modulation.

5. Multi-functional grid-connected inverters in three-phase system

As mentioned before, the capacities of the single-phase MFGCIs are low, which are mainly used in residential PV systems. In addition, the harmonic detection approaches of the single-phase MFGCIs are harder than three-phase MFGCIs. It is worth nothing to note that a single-phase MFGCI is a typical unbalance source, which will burden the utility to manage the unbalance issue. Therefore, three-phase MFGCIs have many good performances and are suitable for general application. The available MFGCIs in three-phase system are also some single-stage or two-stage GCIs associated with APF, PFC, DVR and/or UPQC functionalities.

To broaden the application field of the MFGCIs, Wu et al. give a three-phase MFGCI, as shown in Fig. 50, based on the single-phase one in Fig. 7, whose parameters are described in Table 22 [89]. As a consequence, a control strategy is also presented as depicted in Fig. 51. This configuration can accomplish the interface functionality of conventional GCI and the functionality of harmonic and reactive compensation. There are three different operation modes according to the solar irradiation, namely FAPF mode, PAPF mode, and RPI mode. In low irradiation, the MFGCI works under FAPF mode, and there is little active power generated by the PV array. As a result, the MFGCI has enough apparent power to carry out the APF functionality. When the irradiation is middle, the MFGCI works under PAPF mode, namely, it can just supply partial reactive and harmonic current to compensate the local load. When the irradiation is high, the MFGCI works in RPI mode and just generate active power. Literature [89] gives the control strategy as shown in Fig. 52, in which, the detailed harmonic and reactive current detection approach is given as shown in Fig. 53.

As shown in Fig. 52, a three-phase system can be viewed as two single-phase systems. With the aid of the load current analyzer, the average active and reactive power of the two load ports, $\overline{p}_{L1}$, $\overline{q}_{L1}$, $\overline{p}_{L2}$, and $\overline{q}_{L2}$, as well as the reactive and harmonic current, $i_{Lj,h}$ and $i_{Lj,q}$, can be achieved. To prevent the reference current exceeding the rated one of the MFGCI, a limiter is employed to achieve the reactive and harmonic coefficients, $k_{qc1}(k_{qc2})$ and $k_{hpwc1}(k_{hpwc2})$. Then the harmonic and reactive reference current of each phase, $i_{cj,h,ref}$ and $i_{cj,q,ref}$, can be calculated. Similarly, the active reference current $i_{cj,p,ref}$ is available by the means of MPPT and voltage regulator of dc-bus. These three parts constitute the reference current $i_{cj,ref}$. Due to the feedback of output current and the current regulator G_{cc}, the trigger pulses of the three-phase H-bridge can be generated by SPWM modulation.

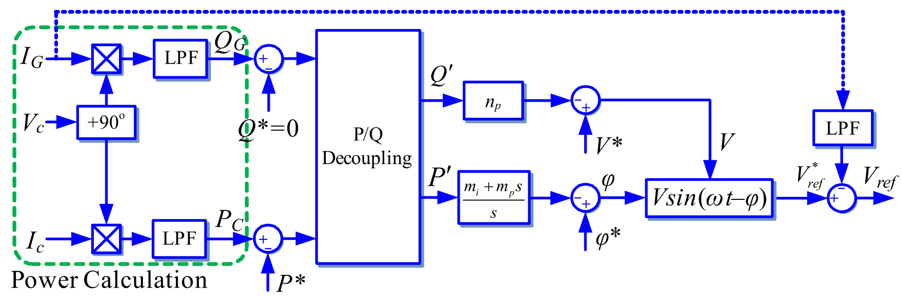


Fig. 38. Block diagram of reference generation algorithm.

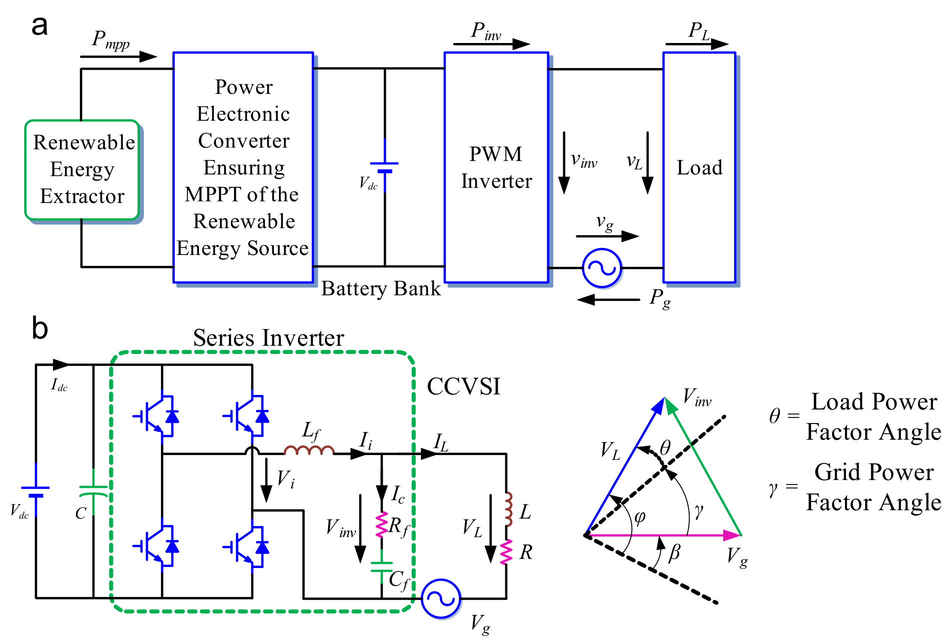


Fig. 39. Configuration of the MFGCI investigated by Dasgupta et al. (a) Schematic diagram and (b) detailed explanation on the phasors diagram of voltages.

Table 18
Parameters of the MFGCI presented by Dasgupta et al.

Dc source	PV array, V_{dc}=270 V
Utility voltage	110 V/50 Hz
Sampling frequency	10 kHz
Passive components	R=150 Ω, L=0.1 H
Control strategy	Spatial repetitive control, SPWM modulation
Extra functions	Harmonic voltage compensation, DVR

Literature [90] founds that the reference current of MFGCI can be simplified as

$$\begin{cases} i_{cu,ref} = (P_{MPPT} - \overline{P}_L)u(t)/[\sqrt{2}V_{rms(uv)}] + i_{Lu} \\ i_{cv,ref} = i_{Lv} \\ i_{cw,ref} = -(P_{MPPT} - \overline{P}_L)u(t)/[\sqrt{2}V_{rms(uv)}] + i_{Lw} \end{cases} \quad (8)$$

where $\overline{P}_L = \overline{p}_{L1} + \overline{p}_{L2}$ is active power of load. $V_{rms(uv)}$ denotes the root-mean-square (RMS) value of line-voltage. $u(t)$ Represents the unit-amplitude-voltage synchronous signal. Furthermore, an algorithm named as fast-zero-phase detection is proposed to generate the unit synchronous signal $u(t)$ to form the reference current.

He et al. also have researched a three-phase H-bridge MFGCI system as illustrated in Fig. 54, whose parameters are listed in Table 23 [91,92]. As known to all, the previously mentioned MFGCIs are mainly CC-VSI as shown in Fig. 54(a) typically. However, if a MFGCI can behave as a voltage-controlled VSI, many good performances can be achieved, such as seamless transfer from grid-connected mode to islanded mode, plug-and-play, supporting the voltage and frequency of the DGSs and/or MGs using droop controller, and power sharing of MFGCIs in islanded mode. Therefore, He et al. give a voltage control scheme for the MFGCI as shown in Fig. 54(b). It should be noted that the sliding discrete Fourier transform (SDFT) is utilized both in voltage control mode or current control mode to detect the harmonic voltage or current for compensation.

Yu et al. also give a MFGCI configuration as depicted in Fig. 55 and Table 24 [93]. It can be found that the derivation regulating of dc voltage derives the reference current in d-axis, as well as the instantaneous reactive theory is implemented to detect the reactive and harmonic current for compensation. The MFGCI can realize active power generation and reactive current compensation simultaneously at daytime. Meanwhile, it can still behave as an APF at night to enhance the power quality of utility.

As previously mentioned, the output power of the PV array and other RESs is random and uncertain. So the whole system may be instable in islanded mode if there is no energy storage device in the MFGCI.

Kim et al. have given a new MFGCI configuration as demonstrated in Fig. 56, whose parameters are given in Table 25 [94]. There is a DC/DC stage adding to the dc-bus of the MFGCI, which can realize MPPT feature. Additionally, due to the extra battery device at dc-bus, the system can stably operate in islanded mode, which can be viewed as an UPS. Besides, the LC-filter brings better performance to suppress switching harmonic current compared with an L-filter.

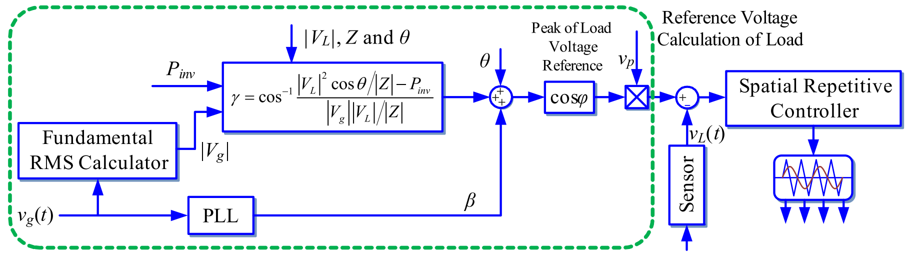


Fig. 40. Control scheme of the MFGCI presented by Dasgupta et al.

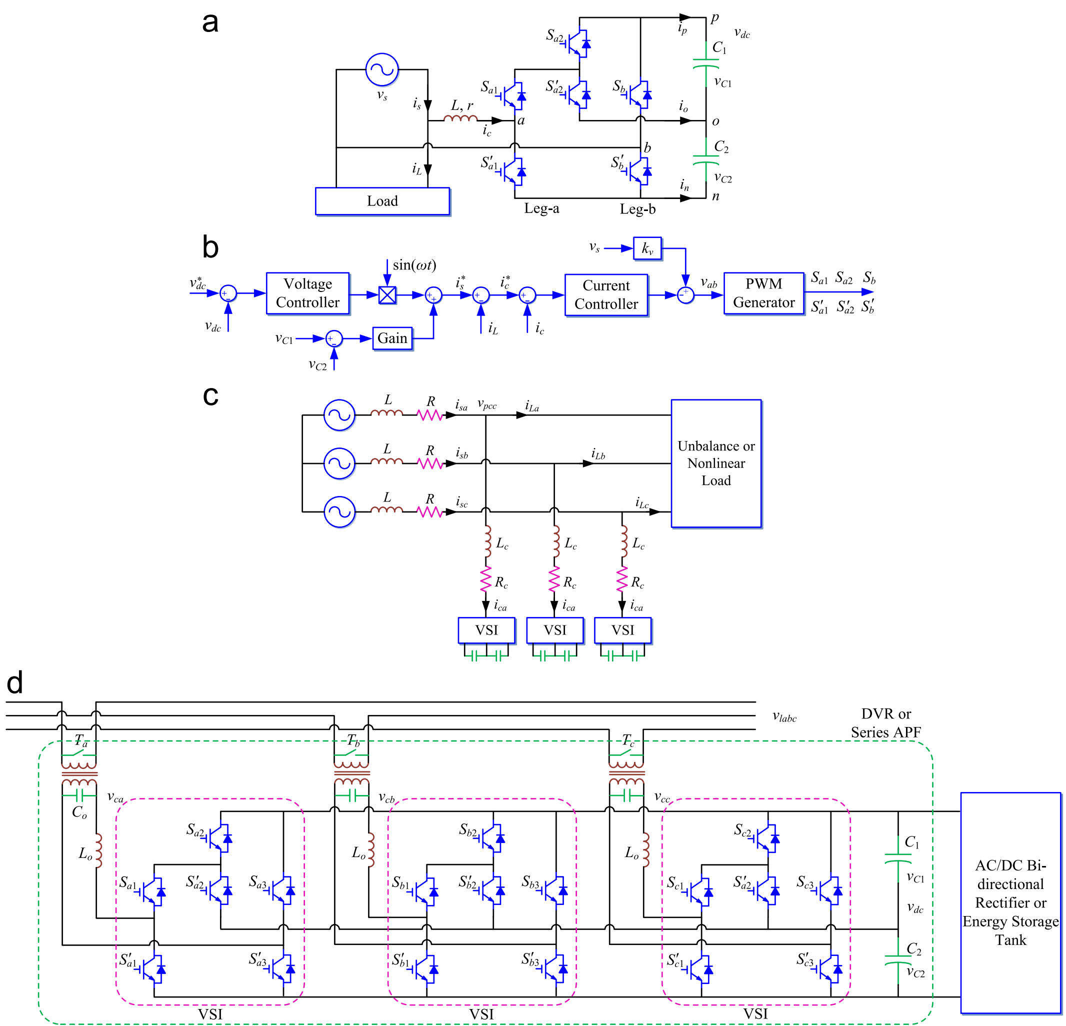


Fig. 41. Topology and its control scheme of the MFGCI cell presented by Lin et al. (a) Topology of the cell, (b) control scheme of the cell, (c) application in three-phase utility: Case 1 and (d) application in three-phase utility: Case 2.

Table 19
Parameters of the MFGCI presented by Lin et al.

Dc source	PV array, the voltage of dc-link is V_{dc}=200 V
Capacity	1.5 kW
Utility voltage	110 V/60 Hz
Passive components	L=2 mH, C_1=C_2=1100 μF, v_{C1}=v_{C2}=100 V
Switching frequency	20 kHz
Control strategy	PI control, SPWM modulation
Extra functions	UPQC

When the grid-connected switch is closed, the PV array supplies the local nonlinear load. The utility will absorbs (or supplies) the surplus (or shortage) active current. On the other hand, when the switch is open, the battery will supply the local load and the MFGCI can act as an UPS.

Fig. 57 shows the control strategy of the MFGCI configuration proposed by Kim et al.. The instantaneous reactive power theory is used to detect the compensation current of load. The sampled three-phase voltage and current can be utilized to calculate the instantaneous power of utility. Then their average active power can be obtained by the means of LPF, which multiplies a coefficient k to derive the amplitude of fundamental active component of load current. The amplitude times the unit-amplitude-voltage synchronous signal, and then it derives the active part of load current. The load current subtracting the detected fundamental one, yields the harmonic and reactive current of load I_C. On the other hand, with the help of MPPT and voltage regulator of dc-bus, it can yield

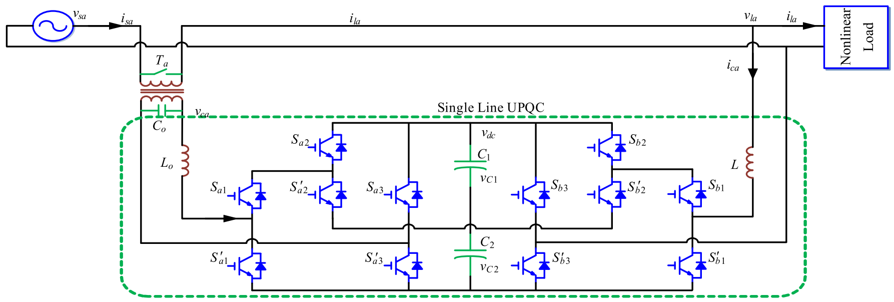


Fig. 42. Single-phase UPQC like MFGCI presented by Lin et al.

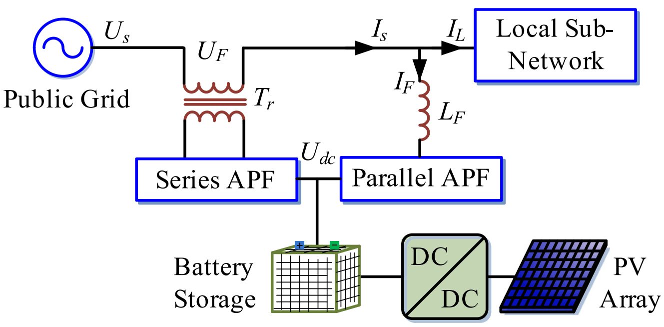


Fig. 43. Configuration of the MFGCI studied by Geibel et al.

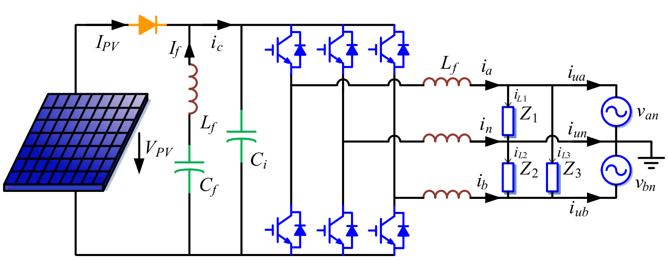


Fig. 44. Configuration of the MFGCI presented by Kuo et al.

Table 20
Parameters of the single-phase full-bridge MFGCI presented by Kuo et al.

Dc source	PV array, V_{PV}=238 V
Capacity	1 kW
Utility voltage	110 V/60 Hz
Passive components	Load: Z_1 rectifier load 100 W, Z_2 resistive load 100 W, Z_3 resistive load 100 W; input filter capacitor C_i=470 μF; LC series filter L_f= 1.66 mH, C_f= 1000 μF; output filter L= 1.2 mH
Power electronic devices	IGBT HG20N60
Switching frequency	18 kHz
Control strategy	PI control, SPWM
Extra functions	APF

the amplitude of grid-connected current I_{ref}. To control the output current of the MFGCI, the current feedback I_{in} and SPWM modulation are employed, too.

Based on their previous work in single-phase system, Dasgupta et al. have researched a MFGCI configuration in three-phase system as shown in Fig. 58, whose parameters are described in Table 26. The control strategy of the MFGCI is illustrated in Fig. 59. To detect the compensation current component, a novel algorithm is proposed in [95,96] as well.

As mentioned before, to suppress the dc bias of GCI that may be inject into utility, the isolation transformer in ac side is necessary sometimes. Cheng et al. give a three-phase MFGCI configuration, as demonstrated in Fig. 60, whose parameters are shown in Table 27 [97]. It can be seen from Fig. 60 that the load and the MFGCI are isolated by isolation transformers in ac side, which will increase the cost and bulk of the system. Compared with Fig. 56, it can also be found that the energy storage device in dc side is cancelled.

Fig. 61 gives the algorithm to calculate the reference current of the MFGCI. It is obvious that the instantaneous power theory is employed to detect the harmonic components of load current. The utility voltage and current in stationary $\alpha\beta$ frame, $u_{\alpha\beta}$ and $i_{\alpha\beta}$, are obtained by the means of sampled PCC voltage and load current. With the help of instantaneous power theory, the fundamental component of load current $i_{\alpha\beta f}$ can be achieved. As a result, the fundamental component of load current in natural *abc* frame i_{babc} can be formed after Clarke transformation. The load current i_{Labc} subtracts i_{babc}, and the result yields the harmonic current i_{habc}. On the other hand, according to the reference power generation of the MFGCI, P and Q, it can generate the normal grid-connected reference current i_{gabc} by the means of (9). The detected harmonic current and the computed grid-connected reference current constitute the total reference current of the MFGCI, as shown in Fig. 60. Note that the transformations $\boldsymbol{T}$ and $\mathbf{C}_{pq}$ in Fig. 61 are (9) and (10), respectively.

$$\begin{cases} i_{\alpha ref} = (u_\alpha P + u_\beta Q)/(u_\alpha^2 + u_\beta^2) \\ i_{\beta ref} = (u_\alpha P - u_\beta Q)/(u_\alpha^2 + u_\beta^2) \end{cases} \quad (9)$$

$$\begin{cases} p = u_\alpha i_\alpha + u_\beta i_\beta \\ q = u_\beta i_\alpha - u_\alpha i_\beta \end{cases} \quad (10)$$

Naderi et al. have studied a MFGCI configuration as illustrated in Fig. 62, whose parameters are listed in Table 28 [98]. From the single-line diagram, it can be found that the step-up transformer is used to reduce the voltage stress of the converter. Besides, the control principle mainly consists of two parts. One is the reference generator, and another is the core controller, which is shown in Fig. 63. From the block diagram of the controller, it is easy to see that the instantaneous reactive power theory is utilized to compute the compensating current components. Besides, hysteresis modulation is implemented so as to achieve fast dynamic performance of the MFGCI.

Mohod et al. have investigated a MFGCI to connect micro-wind generator to utility and compensate the harmonic current of local load, whose parameters are described in Table 29 [99]. The configuration of the MFGCI is shown in Fig. 64, as well as its control strategy is given in Fig. 65. From Fig. 64, it can be seen that the dc-link of the MFGCI is fed by wind generator and storage battery. As a result, the battery can substitute the wind generator and supply the local critical load uninterruptedly when the micro-wind generator is cut off. Specially, the MFGCI can compensate the harmonic current of the local load as well. Therefore, the power quality at the PCC can be greatly enhanced.

To achieve the performances of the MFGCI, its control scheme is demonstrated in Fig. 65. From Fig. 65, it is easy to find that a

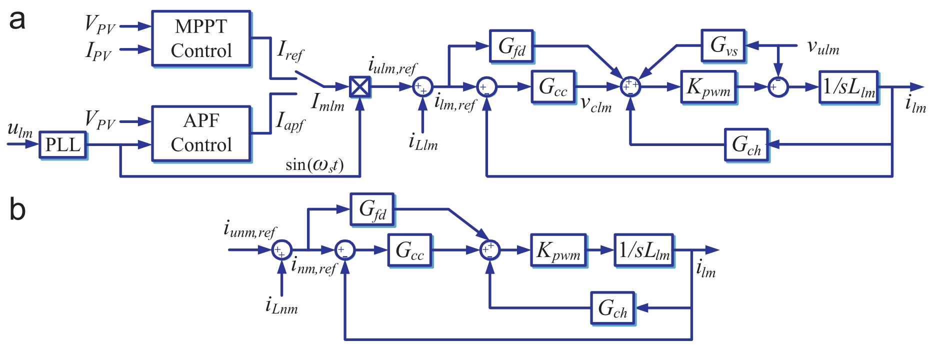


Fig. 45. Control scheme of the MFGCI studied by Kuo et al. (a) Line-mode control diagram and (b) neural-mode control diagram.

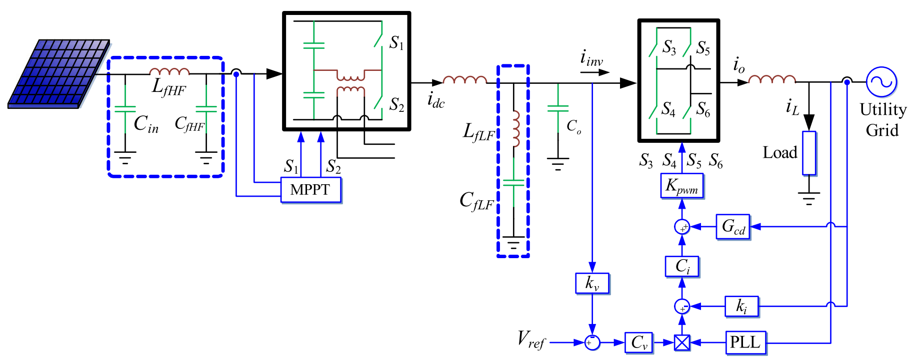


Fig. 46. Single-phase MFGCI with two stages for PV application presented by De Souza et al.

Table 21
Parameters of the single-phase two-stage MFGCI presented by De Souza et al.

Dc-source	PV array
Capacity	1 kVA
Voltage of utility grid	220 V/60 Hz
Passive components	Number of PV array is 20, rated voltage and current of each PV array are 83.5 V and 12 A, respectively, whose short-current (I_s) and open-voltage (V_{oc}) are 12.4 A and 107 V, respectively. Output voltage of DC/DC converter is 400 V, whose switching frequency is 100 kHz. $C_{in}=C_{fHF}=1000$ μF, $C_{e1}=10$ μF, $C_{e2}=5$ μF, $L_{fHF}=50$ μH, $L_r=680$ nH, $C_o=1000$ μF Switching frequency of DC/AC stage is 20 kHz, $C_{fLF}=1000$ μF, $L_{fLF}=1.6$ mH, $L_{o1}=L_{o2}=1.2$ mH
Power electronic devices	MOSFET and IGBT
Control strategy	SPWM modulation
Extra functions	APF

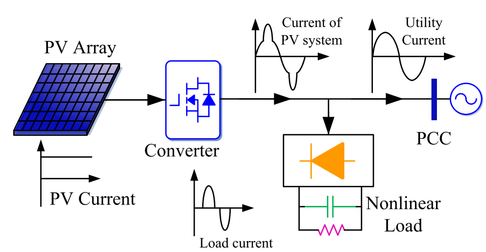


Fig. 47. Schematic configuration of the MFGCI presented by De Souza et al.

DFIG is implemented to catch the wind energy, and a three-phase H-bridge topology is employed to be the energy interface. With the help of dc link voltage PI controller, the amplitude of the reference current i is obtained. The amplitude multiplies the unity-quantity signal u_{sabc} to derive the reference current to inject into utility. By the means of the PI controller and the calculator for compensation current, the trigger pulses of IGBTs can be achieved by hysteresis modulation.

Marei et al. also give a three-phase H-bridge MFGCI configuration, and present a harmonic detection approach to generate its reference current named as multi output adaptive linear (MO-ADALINE), as displayed in Fig. 66 and Table 30 [100,101]. The active and reactive power generation of the MFGCI is controlled by i_d and i_q, respectively. When the MFGCI works under FAPF mode, a fuzzy logic controller (FLC) is employed to control the voltage of dc-bus and enhance the robustness of the system. Meanwhile, MO-ADALINE approach is implemented to detect the compensation component of the load current I_{comp} as shown in Fig. 67. It can be found that, the detected harmonic is feedback to modify the linear weights of neurons. When the algorithm is convergent, the outputs of neurons would be the harmonic current of load exactly. It should be noted that a limiter is carried out to prevent the reference current exceeding the rated one of the MFGCI.

Cheng et al. also depict a MFGCI configuration, as presented in Fig. 68, whose parameters are shown in Table 31 [102]. It can compensate the unbalance current of local load, using a droop control strategy, as shown in Fig. 69. It can be found that the control strategy employs "positive-sequence active power and frequency droop", and "positive-sequence reactive power and voltage amplitude droop" to form reference voltage. In addition, a "negative-sequence reactive power and conductance droop" is utilized to form the negative-sequence reference current. To accomplish these droop controllers, Park transformations in positive- and negative-sequence frames are applied to voltage and current.

Lv et al. have given a MFGCI configuration as demonstrated in Fig. 70, whose parameters are described in Table 32 [103,104]. From the control strategy in Fig. 71, it can be seen that i_d–i_q approach is implemented to detect the compensation current, and the dc-link voltage is control by the means of d-axis current i_d.

To mitigate the unbalance voltage in a DGS using GCI, Mohamed and El Saadany have surveyed a MFGCI system as illustrated in Fig. 72,

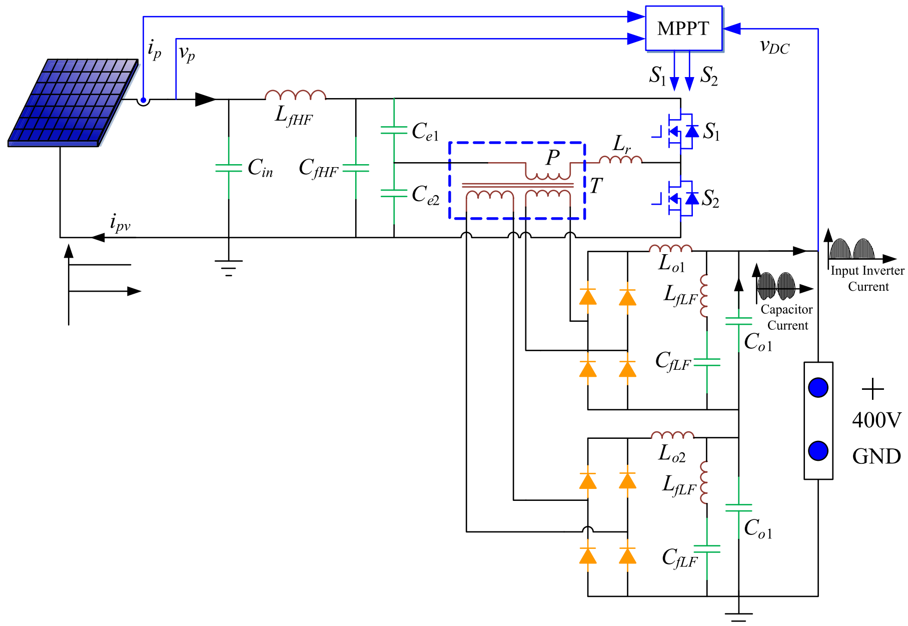


Fig. 48. Block diagram of the half bridge zero-voltage switch DC/DC converter.

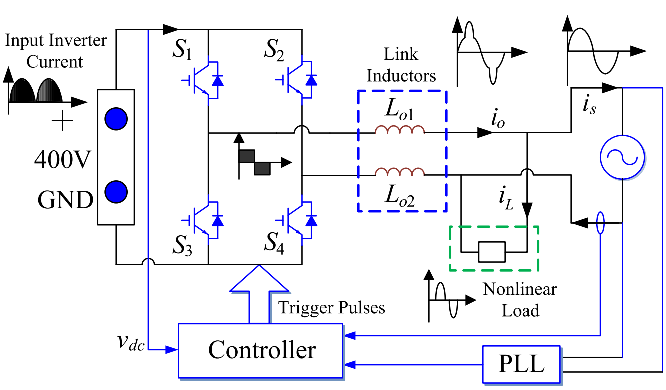


Fig. 49. Block diagram of the inverter stage.

whose parameters are depicted in Table 33 [105]. From the control principle diagram shown in Fig. 72(b), it can be observed that a hybrid linear with variable structure controller (VSC) is implemented to improve its performance. To correct the voltage unbalance at PCC due to sudden loading or capacitor switching, the control approach in Fig. 73 is researched.

In order to mitigate the voltage flickers of the DGSs result from arc furnaces, arc welders, and/or starting of motors using MFGCI, Marei et al. have researched a DGS as shown in Fig. 74 [106]. From the control principle diagram as displayed in Fig. 75, it can be found that Hilbert transform is employed to detect the magnitude of the voltage at PCC.

To control the active and reactive power of a GCI flexibly, M. Saitou and T. Shimizu have investigated a MFGCI system using Hilbert transform, whose important parameters are listed in Table 34 [107]. From the configuration of the MFGCI in Fig. 76, it can be concluded that the Hilbert transform is applied to calculate the instantaneous power and lock the phase of utility easily, which can avoid the complex and time-consuming PLL. The reference reactive power Q_s can be set appropriately to satisfy the requirements for RPI mode or reactive injection in some special operation circumstances.

Chandhaket et al. also give a three-phase MFGCI configuration using soft-switching technology, as demonstrated in Fig. 77 and Table 35 [108,109]. This topology mainly consists of PV array, auxiliary active resonant commutated snubber link (ARCSL), and LCL-filter. There are two operation modes for this MFGCI, as shown in Fig. 78. When the load is small (less than 35 kW), the converter works as a PWM rectifier, and the utility charges the battery using the bi-directional converter. When the load is big (more than 50 kW), the converter acts as a GCI with APF functionality, which can supply peak power and harmonic current to the load. The control strategy of this MFGCI configuration is illustrated in Fig. 79.

From the control diagram depicted in Fig. 79, it can be found that, due to the utility voltage is used to lock phase, the current i_q can determine the power flow of the bi-directional converter. When the load power P_L is bigger than its maximum limitation P_{Lmax}, set $i_q^* > 0$, so the converter will supply power to load. On the contrary, when P_L is less than its minimum limitation P_{Lmin}, set $i_q^* < 0$, thus the bi-directional converter works as a PWM rectifier to charge battery. Especially, when P_L satisfies $P_{Lmin}<P_L<P_{Lmax}$, an optimal operation scheme will be carried out according to the state-of-charge (SOC) of the battery. It should be noted that the instantaneous power theory mentioned before is employed to detect the harmonic current.

Prodanovic et al. have also investigated a MFGCI configuration as presented in Fig. 80 to compensate the harmonic and reactive current of the distributed generation system [110,111]. The basic idea of the MFGCI is to implement the voltage, across the line impedance, to enhance the power quality at PCC according to the configuration in Fig. 80(a). As shown in Fig. 80(b), the Kalman observer is employed to detect the fundamental and harmonic components of current and voltage for compensation. Besides, a power and voltage control sub-system is utilized to generate the reference current for power generation tracking. As shown in Fig. 81, three approaches are available to calculate the reactive power control: (a) to keep the output reactive power of the MFGCI following the desired one, (b) to track the reference voltage, and (c) to limit the voltage in a band range.

The MFGCI configurations mentioned before mainly PV grid-connected systems. However, wind turbine grid-connected systems can also be implanted as MFGCIs [112–114]. A MFGCI configuration using DIFG is studied by Abolhassani et al. as illustrated in Fig. 82 and Table 36. It can suppress the harmonic current of the nonlinear load by the means of harmonic current compensation using the stator of the DFIG, whose control strategy

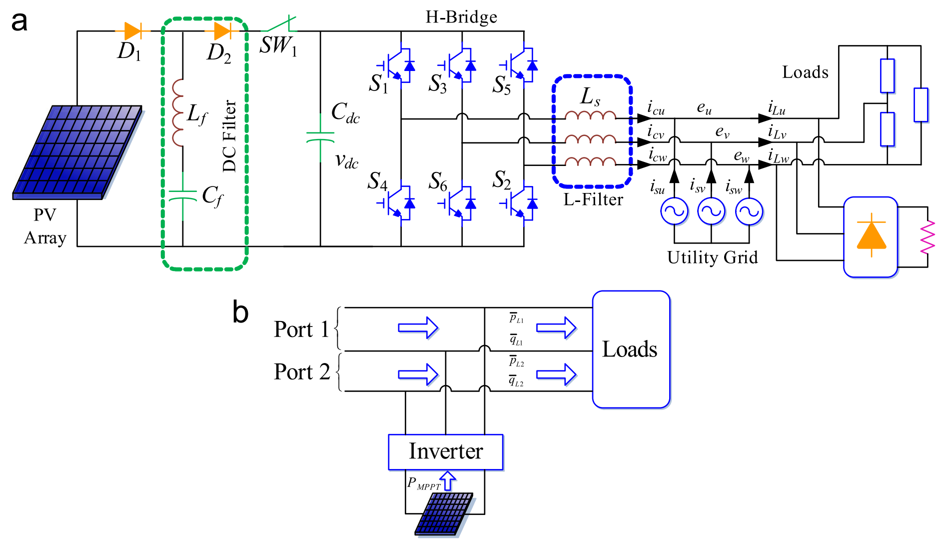


Fig. 50. Three-phase H-bridge MFGCI presented by Wu et al. (a) Detailed configuration of the MFGCI and (b) equivalent two ports model of a three-phase system.

Table 22
Parameters of the three-phase full-bridge MFGCI investigated by Wu et al.

Dc-source	PV array, voltage of dc-bus is 400 V
Capacity	1.1 kW
Voltage of utility grid	110 V/60 Hz
Switching frequency	20 kHz
Passive components	C_{dc}=2200 μF, L_s=5 mH
Control strategy	PI control, SPWM modulation
Extra function	APF

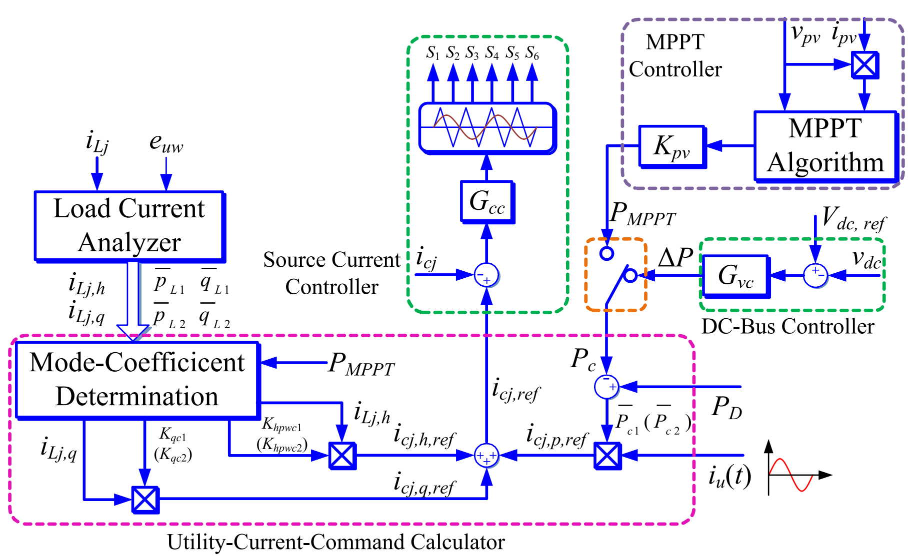


Fig. 51. Control block diagram of proposed inverter system (j=u or w).

is demonstrated in Fig. 83. As the conventional DFIG system, the converter in generator side controls the speed and torque of the DFIG. However, the control of converter in utility side can attach harmonic current compensation functionality. Besides, the reference harmonic current in d- and q-axes, i^{e*}_{qLh} and i^{e*}_{dLh}, are added as well.

The before mentioned MFGCIs are mainly VSIs. However, current-source-inverters (CSIs) and Z-source-inverters (ZSIs) can also be employed as MFGCIs. Gajanayake et al. have investigated a ZSI based MFGCI configuration as shown in Fig. 84, whose parameters are described in Table 37. To maintain the voltage at PCC, the utility current I_g is controlled indirectly. Therefore, the performance is greatly determined by the utility inductor L_g. For a stiff grid with a small utility inductor, perhaps the utility current fully decouples with the voltage at PCC. In other words, the harmonic currents across utility inductor can hardly distort the voltage V_{pcc}.

As shown in Fig. 85, its control strategy consists of a PR controller and a time delay controller, which can satisfy the excellent steady and dynamic performance of the MFGCI. To maintain the power quality at PCC, the reference generator of the controller is a very important component. An improved

reference current generator is proposed by Gajanayake et al., as displayed in Fig. 86 [115]. A moving window RMS calculator is utilized to ensure the generated RMS value of the MFGCI output current is kept free from the ripple components. A PI regulator is implemented to generate the multiplier K_1 so as to exploit the remaining capacity of the MFGCI as much as possible. Besides, it can also prevent the damage to the MFGCI by the unwanted excessive current. It should be noted that a limiter is embedded to avoid the reference current of the MFGCI exceeding its rated one.

As previously mentioned, the MFGCIs mainly implement H-bridge. However, multi-level topology can also be utilized. Tsengenes and Adamidis have studied a MFGCI configuration as shown in Fig. 87, whose parameters are given in Table 38 [116]. The dc source of the MFGCI is comprised of PV arrays in parallel. In addition, a three-level neutral point clamped (NPC) inverter is employed. To compensate the harmonic current of local load, the control strategy presented in Fig. 88 is implemented. It should be noted that the instantaneous reactive theory is utilized to generate the compensating current components.

Note that the MFGCI topologies mentioned before can also be suitable for other RESs application. For the energy storage devices, for instance battery, super capacitor, and superconductivity, their output dc terminals can substitute the dc-link of those topologies. For the ac micro-sources, for instance direct-driven wind turbines, gas turbines, and flywheels, there are diode rectifiers or PWM rectifiers to connect them to the MFGCI topologies.

On the other hand, the topologies previously mentioned mainly take three-phase H-bridge structure. Because there is no neutral line, it can hardly compensate unbalance load current in three-phase four-wire system. To form a neutral line, the split capacitor in dc-bus is a solution. Therefore, the buffer capacitor is split into two parts, and the midpoint of the capacitors is regarded as the neural point. However, the voltages of the two capacitors are hard to balance, which is a very important feature for this kind of structure. To overcome this drawback, some enhanced control strategy should be carried out. In addition, the neural line may flow across big current, which is another disadvantage of this structure. An advanced topology for three-phase four-wire system application is the three-phase four-bridge topology. In this kind of topology, the fourth bridge is employed to control neural line, therefore it will increase the cost of system compared with three-phase H-bridge topology. However, the fourth bridge will greatly enhance the freedom of control strategy.

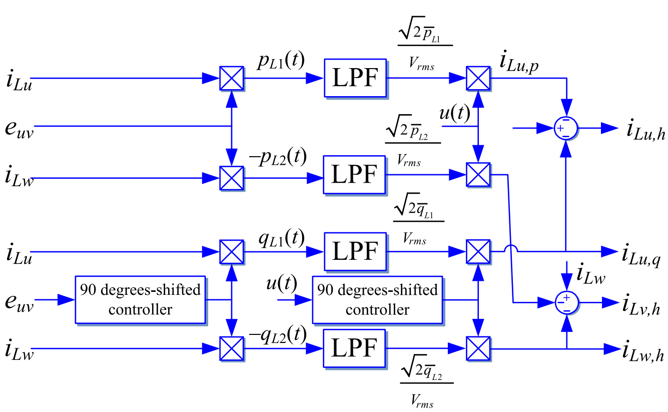


Fig. 52. Detailed block diagram to decompose load currents into real, reactive, and harmonic components.

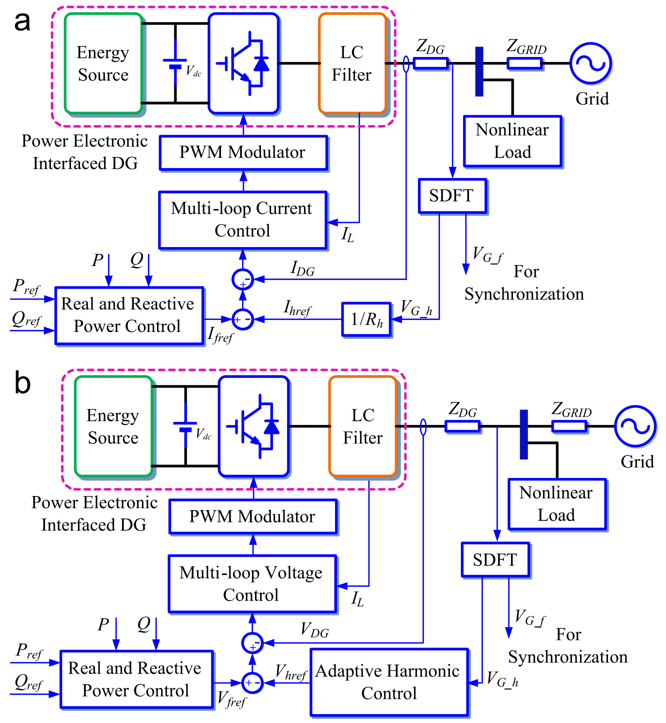


Fig. 54. Configuration of the MFGCI presented by He et al. in different work mode. (a) Current control mode and (b) voltage control mode.

Table 23
System parameters of the MFGCI presented by He et al.

Dc source	DG, V_{dc}=260 V
Capacity	5 kVA
Utility voltage	104 V/60 Hz
Sampling frequency	12 kHz
Passive components	DG impedance: R=1 Ω, L=5 mH
	Grid impedance: R=1 Ω, L=5 mH
	LC filter: L=2.5 mH, C=40 μF
Control strategy	Spatial repetitive control, SPWM modulation
Extra functions	APF

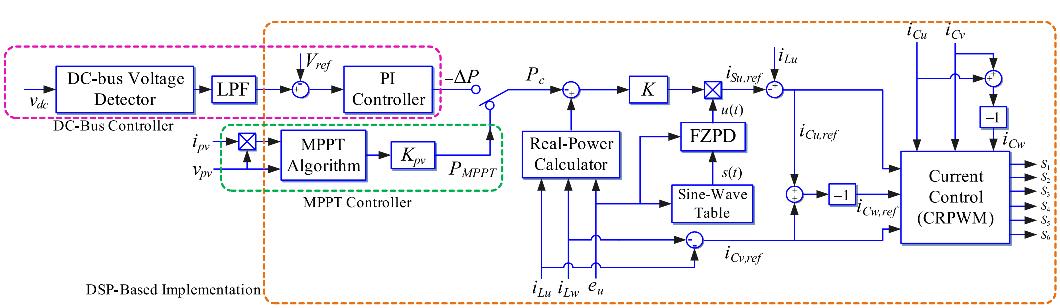


Fig. 53. Control block diagram of the MFGCI in [90].

Sawant et al. investigate a MFGCI configuration to compensate the harmonic and unbalance current of load using three-phase four-bridge topology, as shown in Fig. 89, whose parameters are listed in Table 39 [117]. It can be seen that a back-to-back converter is implemented to connect a direct-driven wind turbine to utility. And the DC/AC converter uses the topology illustrated in Fig. 89(b), which is look forward to act as a MFGCI.

The control strategy of the MFGCI presented by Sawant et al. can be described as shown in Fig. 90. There are two algorithms to generate reference current in *pqr* frame, namely "reference power control method (RPCM)" and "reference current control method (RCCM)", whose freedoms are 3 and 4, respectively. Meanwhile, a 3D-SVPWM modulation is employed to generate the trigger pulses. In addition, Sawant et al. also gives a MFGCI configuration using split capacitor as shown in Fig. 91 [118].

Wang et al. have presented a MFGCI configuration for compensation of voltage dig and unbalance using a three-phase four-leg topology as demonstrated in Fig. 92 and Table 40 [119,120]. From Fig. 92, it can be seen that the sensitive loads attached at PCC may be greatly affected by the unbalance voltage of utility. Thanks to the inductors L_{sabc}, the voltage at PCC can be can be regulated by the MFGCI in some certain. To achieve this functionality, the control principle of the MFGCI is presented as depicted in Fig. 93(a). It can be found that a complex control algorithm is employed in

Table 25
Parameters of the three-phase H-bridge MFGCI proposed by Kim et al.

Dc-source	PV array, battery, voltage of dc-bus 260 V
Voltage of utility grid	110 V/60 Hz
Switching frequency	20 kHz
Passive components	C_{dc}=3500 μF, L_f=7 mH
Control strategy	Hysteresis modulation
Extra functions	PFC and UPS

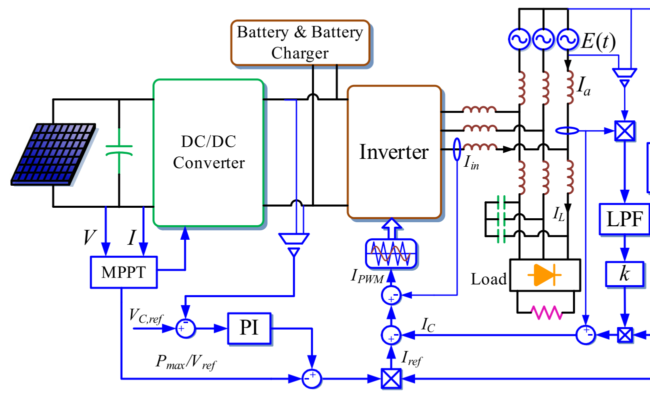


Fig. 57. Block diagram of photovoltaic system control.

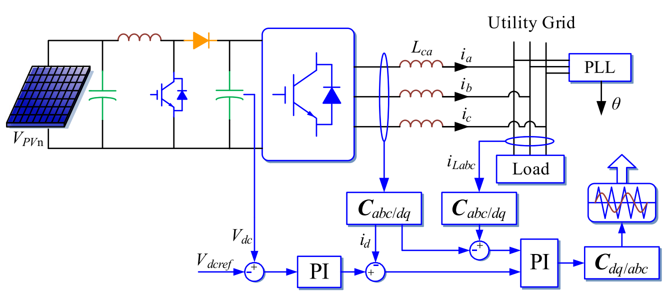


Fig. 55. Schematic diagram of the MFGCI system presented by Yu et al.

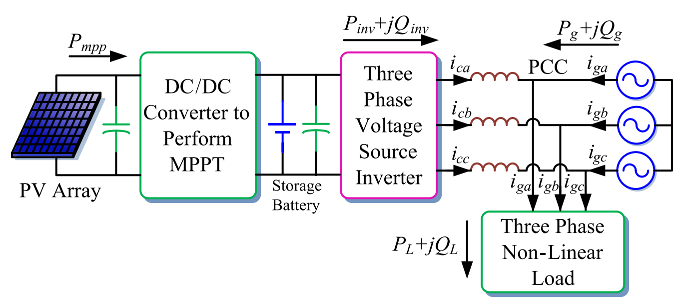


Fig. 58. Schematic diagram of the MFGCI presented by Dasgupta et al.

Table 24
Parameters of the MFGCI presented by Yu et al.

Dc source	DG, v_{dc}=800 V
Utility voltage	380 V
Capacity	10 kW
Control strategy	PI control, SPWM modulation
Extra functions	APF and RPI

Table 26
System parameters of the MFGCI presented by Dasgupta et al.

Dc source	DC source, V_{dc}=200 V
Capacity	75 W
Utility voltage	Approximately 40 V
Passive components	L=2.5 mH, R=1 Ω, C_{dc}=180 μF
Control strategy	Lyapunov control, SPWM modulation
Extra functions	APF

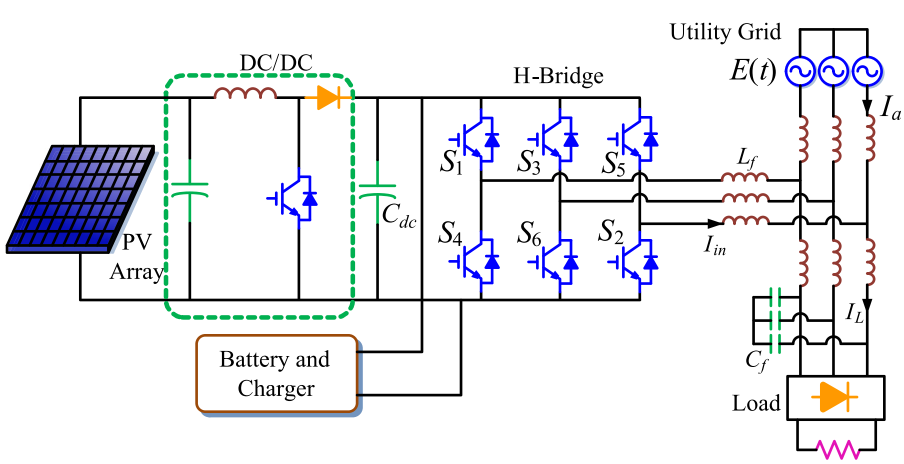


Fig. 56. Three-phase H-bridge MFGCI presented by Kim et al.

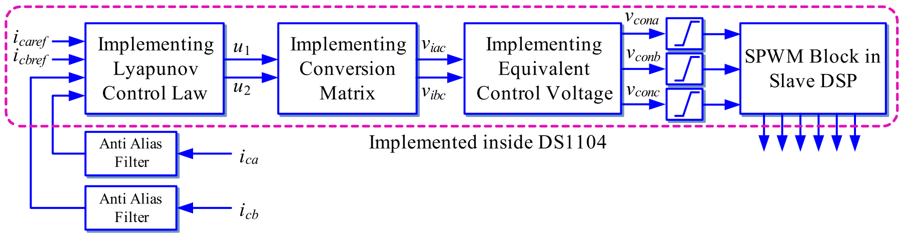


Fig. 59. Control scheme of the MFGCI investigated by Dasgupta et al.

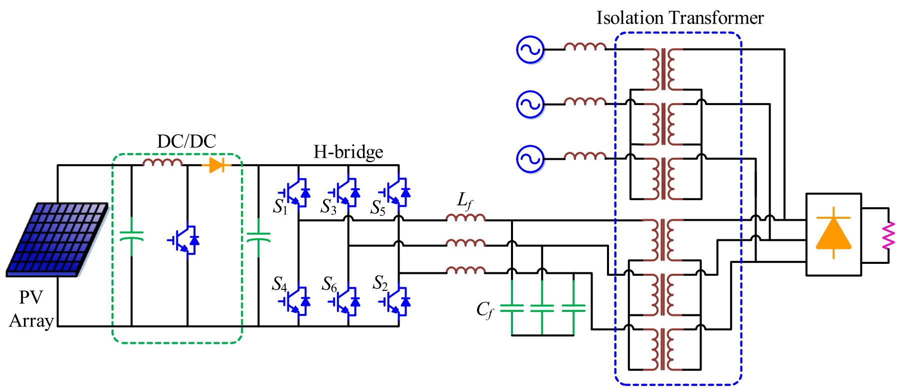


Fig. 60. Three-phase H-bridge topology of the MFGCI by Cheng et al.

Table 27
Parameters of the three-phase H-bridge topology by Cheng et al.

Dc-source	PV array
Capacity	5 kVA
Extra function	PFC and APF

Table 28
Parameters of the MFGCI presented by Naderi et al.

Dc source	DG, V_{dc} = 1000 V
Utility voltage	380 V
Passive components	R_s = 0.05 Ω, L_s = 1 mH, R_c = 0.1 Ω
Control strategy	PI control, hysteresis modulation
Extra functions	APF and RPI

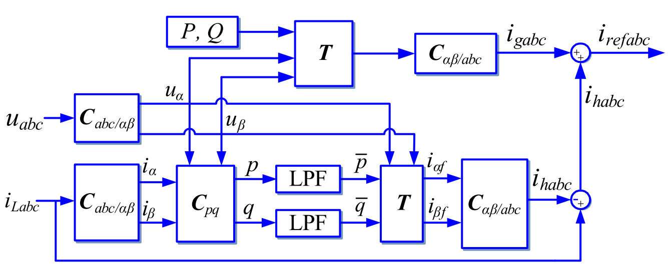


Fig. 61. Algorithm to generate reference current.

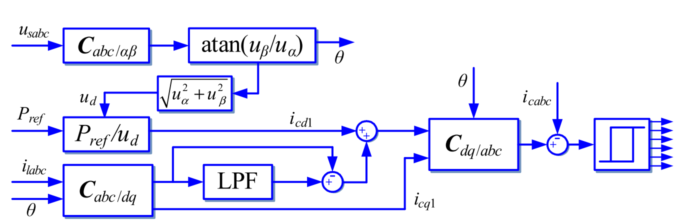


Fig. 63. Block diagram of the controller.

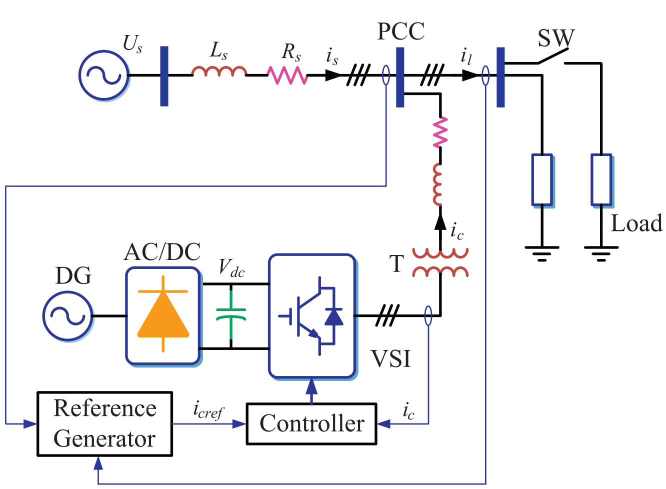


Fig. 62. Single-line diagram of the MFGCI and its control principle.

dual-synchronous rotating frames. Power generation tracking is achieved in the positive-sequence frame. On the other hand, the unbalance voltage correction is realized in the negative-sequence frame. It should be noted that a θ-shift is utilized to form the reference current in negative-sequence to compensate unbalance component of the utility voltage. Besides, the active power of the MFGCI is regulated by a PI controller. Additionally, a direction control is embedded. Thus, if $k_{dir}=-1$, the MFGCI can interface the DG to utility; whereas, the energy of utility can be fed to energy storage DG, such as batteries, when $k_{dir}=1$. Furthermore, a novel algorithm named as multi-variable filter is proposed to separate the positive- and negative-sequence components of the unbalance utility voltage, as proposed in Fig. 93(b).

Pinto et al. have given a MFGCI configuration as shown in Fig. 94, whose parameters are described in Table 41 [121]. Its control strategy is given in Fig. 95, from which it can be found that instantaneous power theory is employed to form the harmonic and unbalance current for compensation.

Although three-phase four-bridge topology may be a good choice for the MFGCI application in three-phase four-wire utility system, three-phase full-bridge topology may be also suitable for some consideration. Especially, the increasing cost due to 4 more IGBTs may be less than the benefit due to voltage and current reduce of IGBTs, compared with three-phase four-bridge structure. On the other hand, the bulk transformers in three-phase full-bridge structure can provide reliable and effective isolation, which is greatly suitable for some situations required high reliability. It should be note that the ac side of this topology can be decoupled, therefore three single-phase GCI can be totally independent and flexibly operate in parallel. Of cause, this topology can also be decoupled in dc side, which can connect three independent micro-sources to utility. It is particularly suitable for energy storage devices application. Because of the dc decoupling, three energy storage devices can be controlled independently, so the SOC of different energy storage devices can be easy to balance. Additionally, the dc voltage can be low, and the set-up DC/DC converter with high gain can be cancelled.

Table 29
Parameters of the single-phase full-bridge MFGCI presented by Mohod et al.

Dc source	Battery, the voltage of dc-link is $V_{dc}=800$ V
Capacity	150 kW
Utility voltage	Three-phase 415 V/50 Hz
Passive components	Micro-wind generator: 150 kW, 415 V, 50 Hz, 4 poles, $R_s=0.01$ Ω, $R_r=0.015$ Ω, $L_s=0.06$ H, $L_r=0.06$ H, wind velocity 5 m/s Battery: dc 800 V, cell capacity 500 Ah, type-lead acid Transformer: 1 kVA, Y–Y type, 415/800 V, 50 Hz Load: three-phase nonlinear load, $R=10$ Ω, $C=1$ μF
Power electronic devices	IGBT: rated voltage 1200 V, forward current 50 A, gate voltage ± 20 V, turn-on delay 70 ns, turn-off delay 400 ns, power dissipation 300 W
Control strategy	PI control, hysteresis modulation
Extra functions	APF

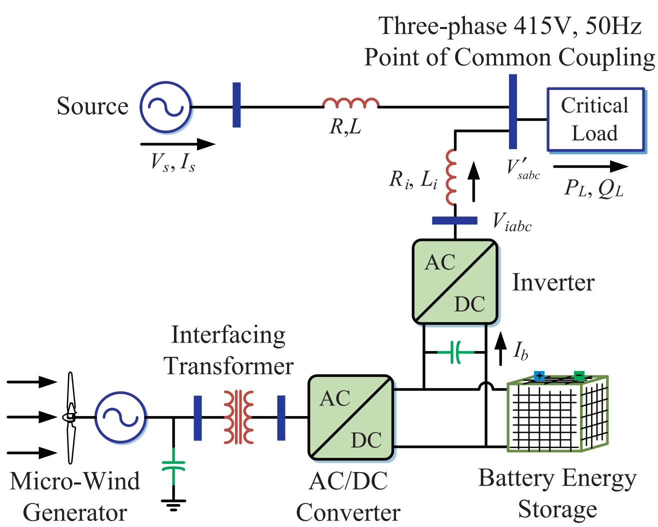


Fig. 64. Configuration of the MFGCI presented by Mohod et al.

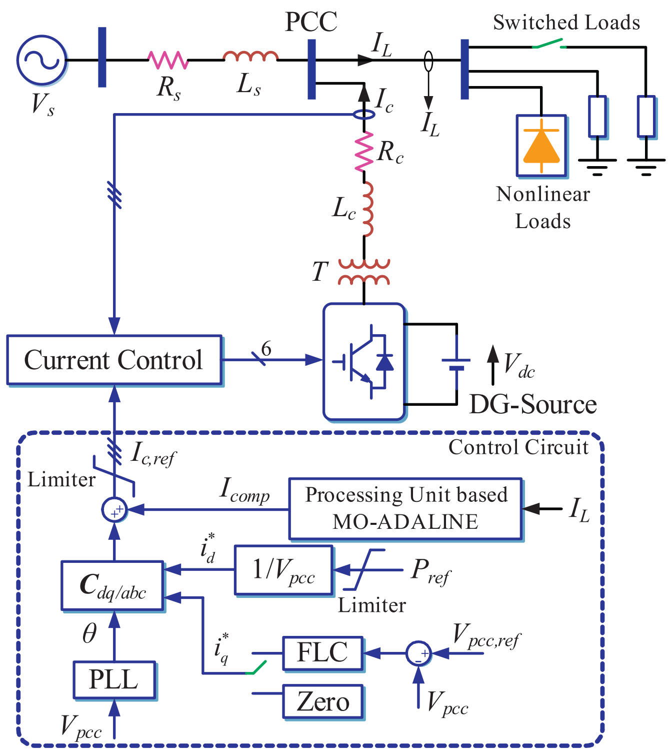


Fig. 66. Block diagram of the proposed MFGCI control system by Marei et al.

Table 30
Parameters of the three-phase H-bridge topology by Marei et al.

Dc-source	Micro-source, voltage of dc-bus $V_{dc}=500$ V
Voltage of utility grid	200 V (RMS value of line-voltage)/60 Hz
Passive components	$L_s=1$ mH, $R_s=0.07$ Ω, $L_c=1.6$ mH, $R=1$ Ω, $L=3$ mH, $R_b=0.1$ Ω, $L_b=1.68$ mH, $R_c=5$ Ω, $L_{dc}=3.5$ mH, $R_{dc}=1.5$~3.5 Ω
Control strategy	FLC control, PI control, SPWM modulation
Extra function	APF

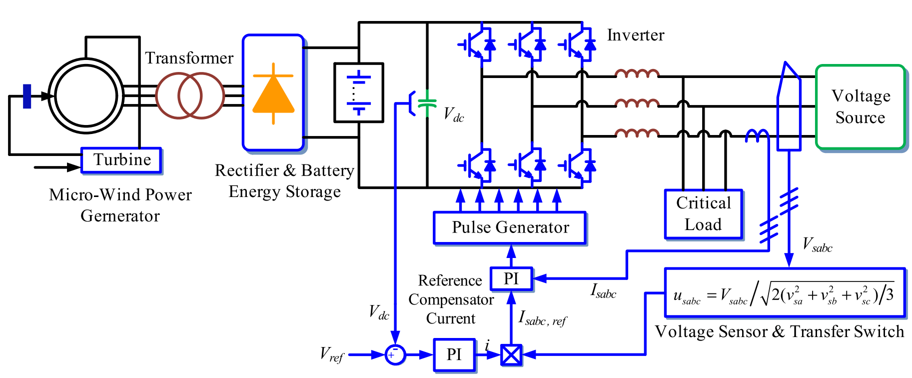


Fig. 65. Control scheme of the MFGCI studied by Mohod et al.

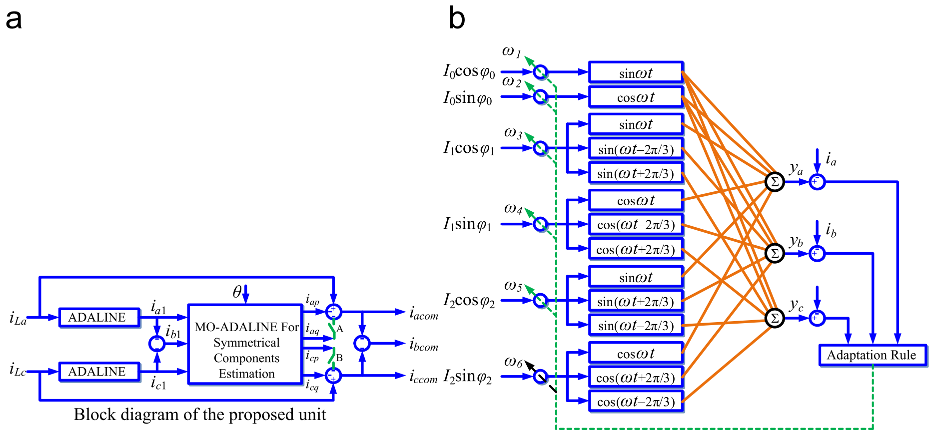


Fig. 67. Control diagram of the MFGCI configuration presented by Marei et al. (a) Schematic diagram of the control strategy and (b) block diagram of the detection approach using adaptive neurons.

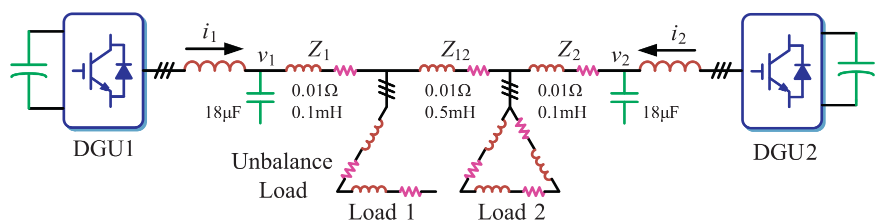


Fig. 68. MFGCI configuration presented by Cheng et al.

Table 31
Parameters of the three phase H-bridge topology by Cheng et al.

Dc-source	Micro-source, V_{dc}=380 V
Voltage of utility grid	220 V(RMS value of line-voltage)/60 Hz
Capacity	1 kVA
Switching frequency	20 kHz
Passive components	Two-phase unbalance load 46.6 Ω, three-phase balance load 280 Ω
Control strategy	Droop control, PI control, SPWM modulation
Extra function	Unbalance compensation

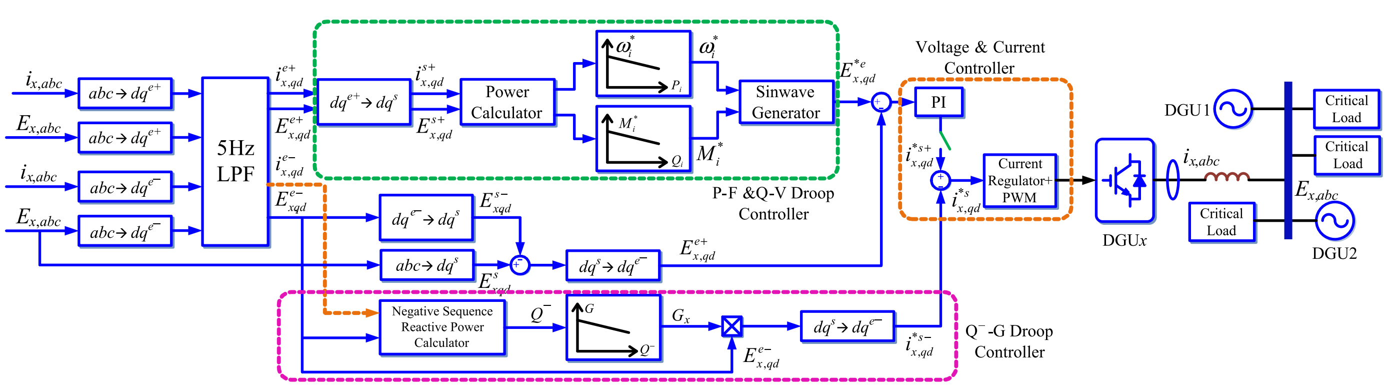


Fig. 69. Droop control strategy of the MFGCI configuration proposed by Cheng et al.

Majumder et al. give a MFGCI configuration using three-phase full-bridge structure, as explained in Fig. 96 [122,123]. In addition, an ac MG application with this kind of MFGCI is studied.

For each MFGCI, to prevent the total reference current, composed of power generation tracking and power quality compensation functionalities, exceeding its rated one, an algorithm to calculate the reference current is presented. When the rated apparent of MFGCI is larger than the demand of harmonic and unbalance loads, it takes

$$\begin{cases} P_{MG} = P_{comp,rated} - P_{Lav} < 0 \\ Q_{MG} = Q_{comp,rated} - Q_{Lav} < 0 \end{cases} \quad (11)$$

where P_{MG}/Q_{MG}, P_{Lav}/Q_{Lav}, and P_{comp}/Q_{comp}, are the active and reactive power supplied by the MG, the demanded of load, and supplied by MFGCI, respectively. Furthermore, the compensation

power supplied by the MFGCI can be expressed as

$$\begin{bmatrix} i_{comp,a} \\ i_{comp,b} \\ i_{comp,c} \end{bmatrix} = \begin{bmatrix} i_{NLa} \\ i_{NLb} \\ i_{NLc} \end{bmatrix} + \frac{1}{K} \begin{bmatrix} 3P_{MG}v_{pa} + \sqrt{3}Q_{MG}(v_{pb} - v_{pc}) \\ 3P_{MG}v_{pb} + \sqrt{3}Q_{MG}(v_{pc} - v_{pa}) \\ 3P_{MG}v_{pc} + \sqrt{3}Q_{MG}(v_{pa} - v_{pb}) \end{bmatrix} \tag{12}$$

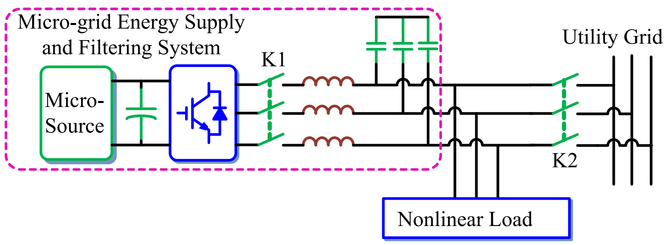


Fig. 70. The MFGCI configuration presented by Lv et al.

Table 32
Parameters of the three phase full bridge topology by Lv et al.

Dc-source	Micro-source, $V_{dc}=1000$ V
Voltage of utility grid	230 V(RMS value of phase-voltage)/50 Hz
Capacity	400 kVA
Switching frequency	12.8 kHz
Passive components	Buffer capacitor $C_{dc}=10$ mF; LC filter $L_f=0.2$ mH, $C_f=30$ μF
Control strategy	PI control, SPWM modulation
Extra function	APF

where $K = v_{pa}^2 + v_{pb}^2 + v_{pc}^2$ is the sum of square of each utility phase-voltage. When the rated apparent power of the MFGCI is less than the demand of loads, it takes

$$\begin{cases} P_{MG} = P_{Lav} - P_{comp} = P_{Lav} - \lambda_P P_{Lav} = P_{Lav}(1-\lambda_P) > 0 \\ Q_{MG} = Q_{Lav} - Q_{comp} = Q_{Lav} - \lambda_Q Q_{Lav} = Q_{Lav}(1-\lambda_Q) > 0 \end{cases} \tag{13}$$

where $\lambda_P \in (0, 1)$ and $\lambda_Q \in (0, 1)$ are compensation coefficients of the MFGCI. It is easy to found that the MG will supply part of harmonic and reactive current of the load, when the MFGCI cannot satisfy the demand of loads fully. In this constitution, the reference current of the MFGCI can be written as

$$\begin{bmatrix} i_{comp,a} \\ i_{comp,b} \\ i_{comp,c} \end{bmatrix} = \begin{bmatrix} i_{NLa} \\ i_{NLb} \\ i_{NLc} \end{bmatrix} - \frac{1}{K} \begin{bmatrix} 3P_{Lav}(1-\lambda_P)v_{pa} + \sqrt{3}Q_{MG}(1-\lambda_Q)(v_{pb} - v_{pc}) \\ 3P_{Lav}(1-\lambda_P)v_{pb} + \sqrt{3}Q_{MG}(1-\lambda_Q)(v_{pc} - v_{pa}) \\ 3P_{Lav}(1-\lambda_P)v_{pc} + \sqrt{3}Q_{MG}(1-\lambda_Q)(v_{pa} - v_{pb}) \end{bmatrix} \tag{14}$$

Table 33
Parameters of the single-phase full-bridge MFGCI presented by Mohamed and E.F. El Saadany.

Dc source	DG, $V_{dc}=600$ V
Utility voltage	110 V/60 Hz
Passive components	$L_s=1$ mH, $R_s=0.08$ Ω, $L=2.5$ mH, $R=1$ Ω; load L_1: 20 kW at a lagging power factor 0.9; load L_2: 30 kW at a lagging power factor 0.85; switching capacitor: 20 kVAR
Switching frequency	6.7 kHz
Control strategy	Hybrid linear with variable-structure control, SPWM
Extra functions	DVR

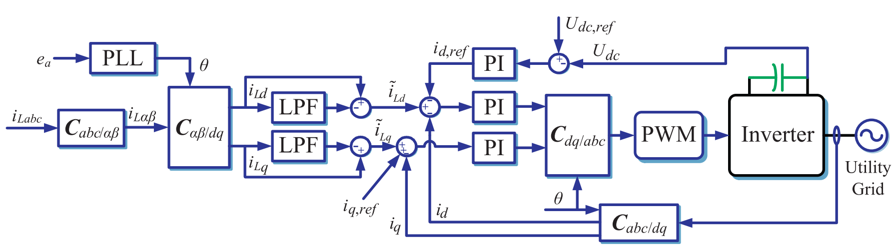


Fig. 71. Control strategy of the MFGCI configuration proposed by Lv et al.

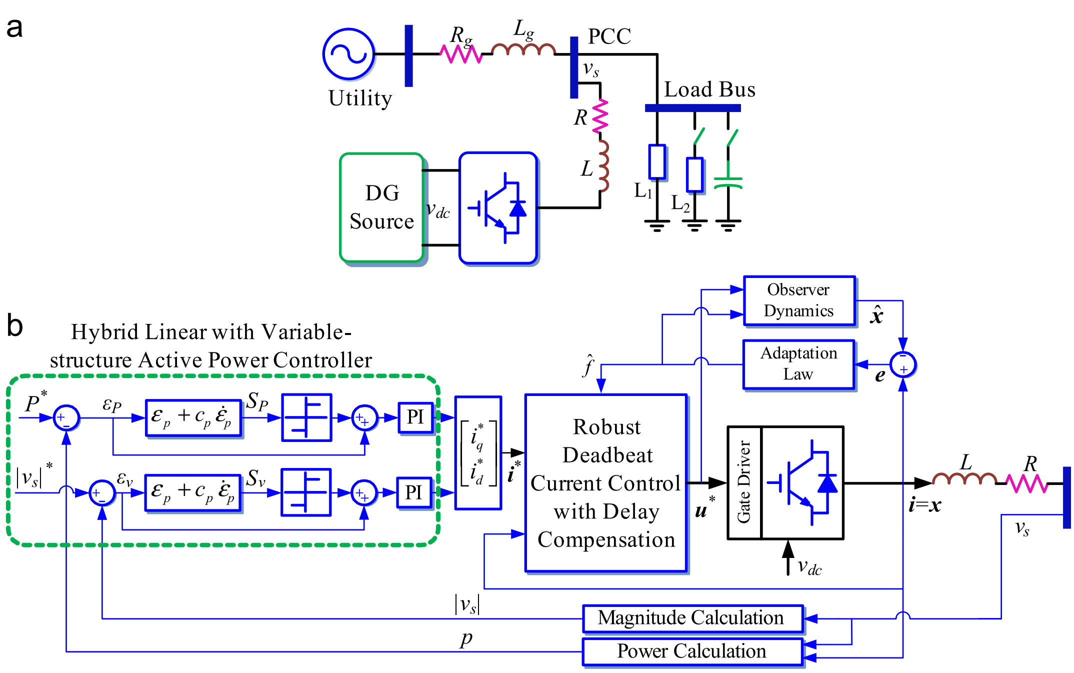


Fig. 72. Configuration of the MFGCI studied by Mohamed and El Saadany. (a) Overview diagram and (b) detailed block diagram of the MFGCI.

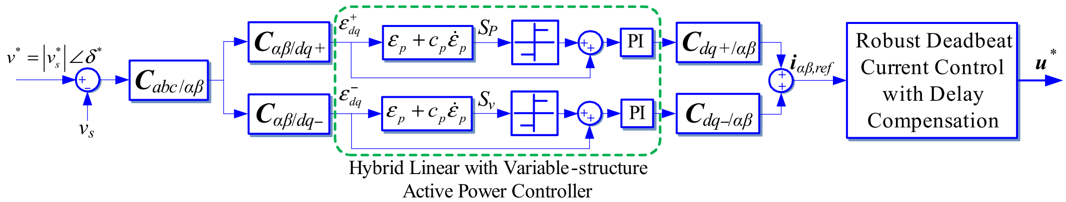


Fig. 73. Control strategy for unbalance voltage correction.

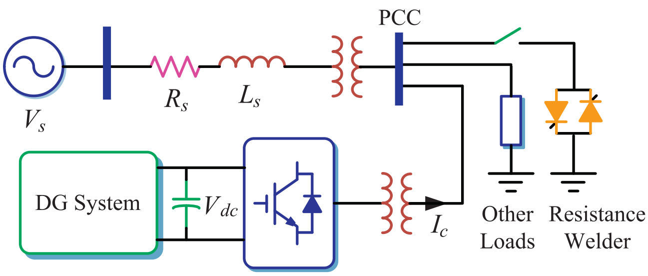


Fig. 74. Configuration of the MFGCI studied by Marei et al.

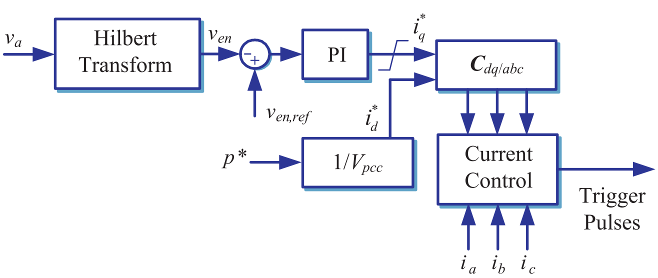


Fig. 75. Control strategy of the MFGCI presented by Marei et al.

Table 34
Parameters of the single-phase full-bridge MFGCI presented by Saitou and Shimizu.

Dc source	Battery, V_{dc}=600 V
Utility voltage	110 V/50 Hz
Passive components	L_s=1.2 mH
Switching frequency	15 kHz
Control strategy	PI, SPWM
Extra functions	RPI

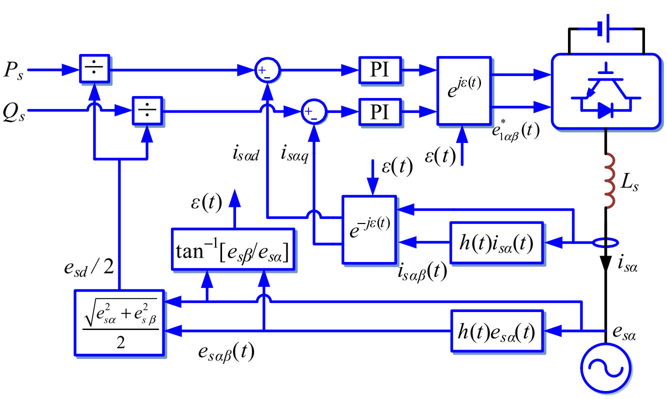


Fig. 76. Configuration of the MFGCI investigated by Saitou and Shimizu.

The control strategy of this configuration is depicted in Fig. 97. According to the reference current computation as mentioned above, a linear quadratic regulator (LQR) and the hysteresis modulation are employed to generate of the trigger pulses of the IGBTs.

In [112], Majumder et al. have noticed that there may be several MFGCIs in a MG, it is very important to exploit the coordination control of multiple MFGCIs. As a consequence, a coordination control strategy using communication lines is discussed in [112] as demonstrated in Fig. 98. However, this coordination control approach may be hardly suitable for some complex MGs, because the communication lines may be very long and hard to expand, the reliability and flexibility of the MGs are lowered, as well as some excellent features, for instance plug-and-play and hot-swap, cannot be achieved. Therefore, it is very necessary to study the coordination control strategy without communication lines.

The MFGCI configurations mentioned before can act as APF and compensate the harmonic and reactive current of the local load. However, the harmonic and reactive current can also be absorbed by passive filters. Although, the fast dynamic response and good robustness are the advantages of APF, it cannot avoid that the APF filters are expensive compared with passive filters. On the contrary, the system parameters of passive filters may be varied with the operation condition, but they are cheap and reliable. To fully utilize the advantages of active and passive filters, Chen et al. have given a DGS configuration including a MFGCI and passive filters, as exhibited in Fig. 99, whose parameters are given in Table 42 [17]. In this system, the MFGCI and the utility grid are the sources, for the power quality conditioners, the passive filters are installed at the terminals of loads; while the MFGCI is equipped at the PCC. The inductors of utility are split as L_s and L_t, while the impedances of loads are Z_{Li} (i=1, 2, …, 5). Note that the load 1, load 2, and load 3 are fed by passive filters in parallel, while the other loads are fed by passive filters in series.

The control strategy of the MFGCI is introduced in Fig. 100. The Fast Fourier Transform (FFT) is employed to detect the fundamental component of the voltage. Simultaneously, the compensation current of the equivalent load current i_{abc} is identified using instantaneous reactive power theory. It is worth nothing to note that a SPWM modulation is also used to generate the trigger pulses of voltage source converter (VSC). According to this control strategy, the PMSG can inject active, reactive, and harmonic current to the DGS. As a consequence, the utility just need absorb or supply fundamental active current. The power flow of this configuration is illustrated in Fig. 101.

So far, the previously mentioned MFGCIs mainly catch the extra compensation functionalities in parallel such as APF, PFC, and UPS and so on. To expand the extra functionalities of the MFGCIs, Han et al. have investigated a MFGCI configuration, as depicted in Fig. 102, whose parameters are listed in Table 43 [124]. This MFGCI can perform the power quality condition functionalities like an UPQC.

From the configuration in Fig. 102, it can be seen that the dc-source of this MFGCI is connected to a distributed generator (DG), which is different from an UPQC has the same topology. A schematic diagram of its control principle is depicted in Fig. 103. The conventional UPQC directly absorbs power to maintain the voltage of the dc-link, while the dc-link of the MFGCI is fed by RESs and/or energy storage devices. It should be noted that the series converter works just when the utility voltage is sag, swell, and/or unbalance; on the contrary, the parallel converter works all the time

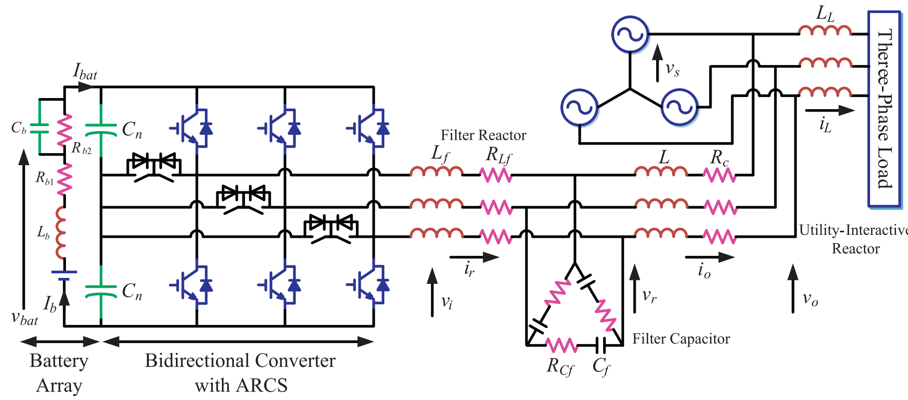


Fig. 77. Utility connected bi-directional soft-switching MFGCI presented by Chandhaket et al.

Table 35
Parameters of the MFGCI proposed by Chandhaket et al.

Dc-source	Micro-source, V_{dc}=440 V
Capacity	20 kVA
Voltage of utility grid	200 V (RMS value of line-voltage)/60 Hz
Sampling frequency	12 kHz
parameters	L_b=0.1 H, R_{b1}=0.05 Ω, R_{b2}=0.05 Ω, C_b=1 F, L_f=3 mH, R_{Lf}=0.05 Ω, C_r=55 μF, C_n=9.7 mF
Control strategy	PI, space vector pulse width modulation (SVPWM)
Extra function	PWM rectifier, APF

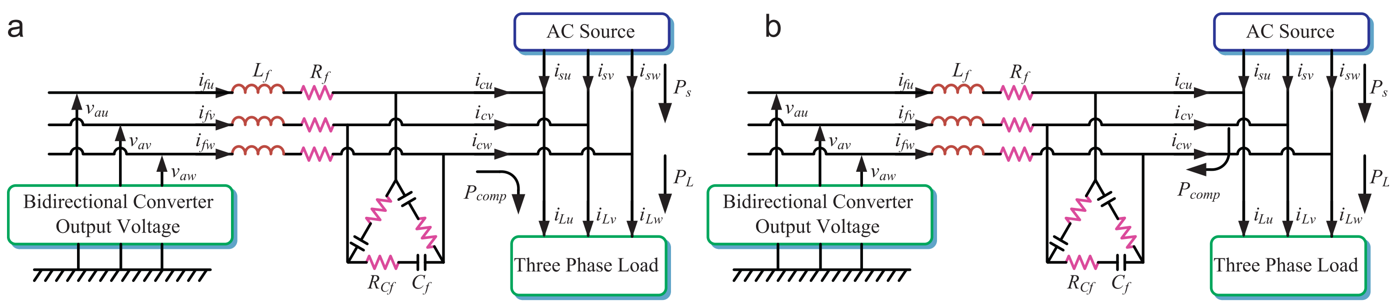


Fig. 78. Two operation modes of the MFGCI configuration presented by Chandhaket et al. (a) Energy supply (inverter) mode and (b) energy storage (rectifier) mode.

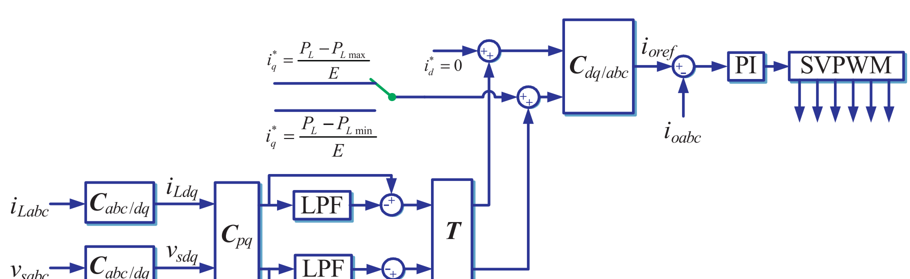


Fig. 79. Control strategy of the MFGCI configuration presented by Chandhaket et al.

as the interface to generate active power and compensate power quality issues.

Fig. 104 shows the configuration of the parallel converter, which is the same as conventional three-phase GCI. For the DG subsystem, the voltage of the DG is detected to control the terminal voltage of DG is stable, which is fed by a transformer and a diode rectifier. The PLL is employed to catch the phase of the positive-sequence utility voltage, which can avoid the disturbance from unbalance and distorted components of utility voltage. For the series converter, its output voltage and current are sampled to control the compensation voltage in series. The shunt converter samples its output current, the voltage and current of loads to supply the harmonic current to nonlinear load.

In detail, the control strategy of series converter is demonstrated in Fig. 105. The deviation between the standard and sampled utility voltage, namely V_{ref} and V_s, derive the reference voltage of converter V_F^*. Then a PI regulator is utilized to form the reference current I_{SF}^*. Due to the outer current loop, the modulation signal for PWM logic V_C^* is achieved to generate the trigger pulses of IGBTs.

The shunt converter has two operation modes, namely APF mode and UPS mode. In APF mode, the shunt converter acts as a current-controlled source, whose control diagram is introduced in Fig. 106. The detected positive-sequence voltage $v'_{s\alpha\beta}$ and load current $i_{L\alpha\beta}$ in $\alpha\beta$ frame can be utilized to calculate the instantaneous power p and q. It should be noted that the regulator of dc-

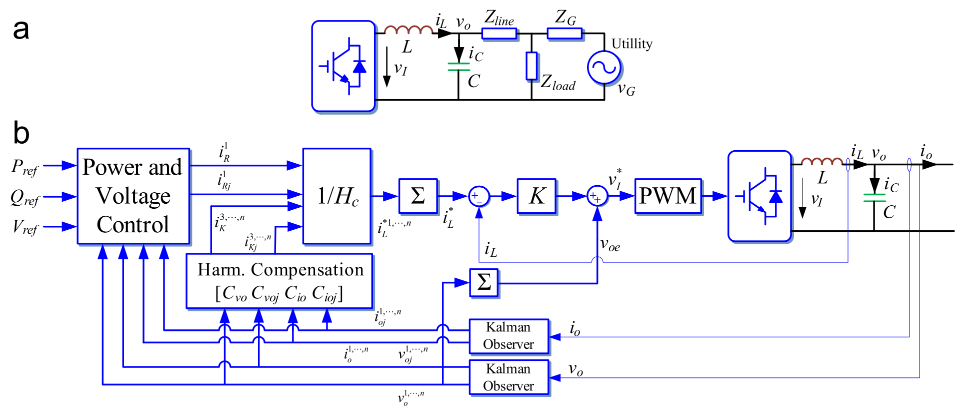


Fig. 80. Configuration of the MFGCI presented by Prodanovic et al. (a) Overall system and (b) system architecture in detail.

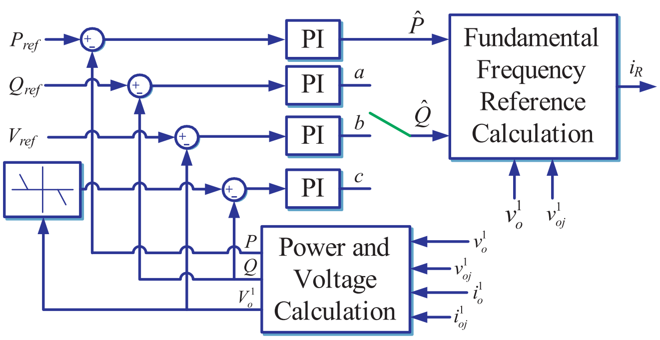


Fig. 81. Detailed block diagram for power and voltage control.

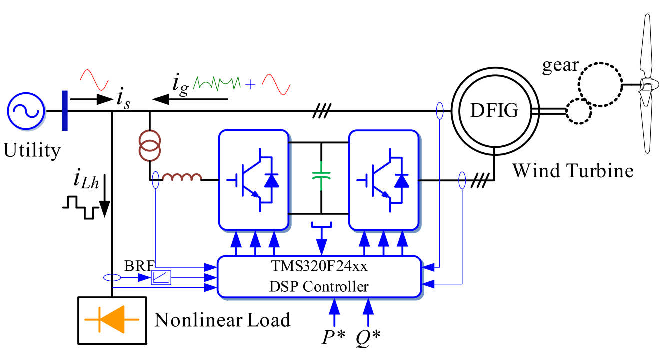


Fig. 82. Block diagram of the proposed method.

Table 36
Parameters of the three phase full bridge topology by Abolhassani et al.

Dc-source	DFIG
Capacity	7.5 kW
Voltage of utility grid	230 V/60 Hz
Sampling frequency	20 kHz
Extra function	APF

bus can be added to active power control loop, and instantaneous power theory is employed to form the reference current. The detailed block diagram of controller is explained in Fig. 107. Furthermore, a current regulator and a forward controller are employed to form the modulation signal. However, when the shunt converter works under UPS mode, it acts as a voltage-controlled source, as depicted in Fig. 107. Under such mode, an outer voltage loop and an inner current loop are utilized, which is simpler compared to APF mode. Associated with protection circuit, the modulation signal, and PWM logic, the trigger pulses of IGBTs are achieved.

Similarly, Li et al. also have researched a MFGCI configuration including three-phase four-bridge shunt and series converters, as shown in Fig. 108, whose parameters are described in Table 44 [125,126]. When the utility grid is interrupted, the shunt converter A acts as an UPS to supply the sensitive load. When the utility voltage is distorted, the series converter B can compensation the harmonic voltage components to satisfy sensitive load.

When the utility voltage is interrupted, the MFGCI acts as an UPS and generate a stable voltage. The brief and detailed control diagrams are exhibited in Fig. 109. It can be found that, the deviations of power angle and voltage amplitude are used to regulate the output active and reactive power of converter A, which yields its reference voltage in $\alpha\beta 0$ frame. Then complex controllers in positive-, negative-, and zero-sequence are employed to accurately track the reference voltage.

The control strategy of series converter is given in Fig. 110. From the overall block diagram in Fig. 110(a), it can be seen that the control strategy is comprised of an outer current loop and an inner voltage loop. A detailed description is available in Fig. 110(b). PI regulators in dq-axis and cross-decoupling terms are utilized in the outer current loop, while a PR controller is employed in 0-axis. The inner voltage loop is shown in Fig. 110(c). Similarly, PR controllers are implemented, where $1/K_{in}=V_{dc}/2$ is the amplification coefficient of the inverter.

It should be noted that the control strategy of shunt converter is given in Fig. 111 to keep the terminal voltage of load, when the utility voltage sags. Because there may be large current across shunt converter to damage the power electronic devices, a control approach named as flux-charge scheme is proposed for series converter. Due to the approach in Fig. 111, the series converter can be viewed as a virtual inductor to limit the possible over-current of shunt converter, which can ride-through the utility voltage sag effectively.

Wang et al. have described a UPQC-based MFGCI configuration as shown in Fig. 112, whose parameters are listed in Table 45 [127]. The MFGCI in Fig. 112(a) can be implemented to a micro-grid as shown in Fig. 112(b) to enhance its power quality at PCC. A detailed diagram of the MFGCI is shown in Fig. 112(c), as well as its control scheme is described in Fig. 113.

According to the control principle of the parallel converter as depicted in Fig. 113(a) and (b), PR controllers $G_{c\alpha\beta\gamma}(s)$ are utilized, in such a way that an excellent steady state feature can be obtained. Besides, the transfers $F_{i\alpha\beta\gamma}(s)=K_{f}s/(s+2\pi f_{hp})$, are employed to enhance the disturbance sensitivity of the MFGCI. Furthermore, $F_{i\alpha\beta\gamma}(s)=K_{ff}\, e^{-Td}$ is transfer delay function, where K_{ff} denotes the forward gain. Similarly, the control scheme of the series converter can be illustrated as shown in Fig. 113(c) and (d). It should be noted that a weighted currents feedback control approach is utilized to reduce the third-order LCL-filter model as a first-order one [128].

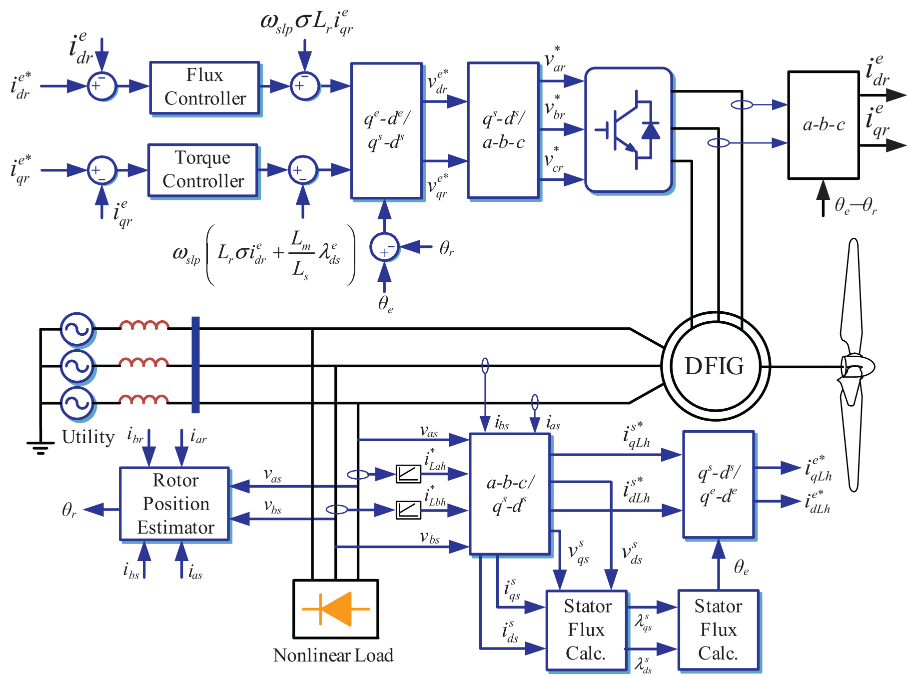


Fig. 83. Block diagram of the rotor side controller of the alternator/active filter for adjustable wind turbine.

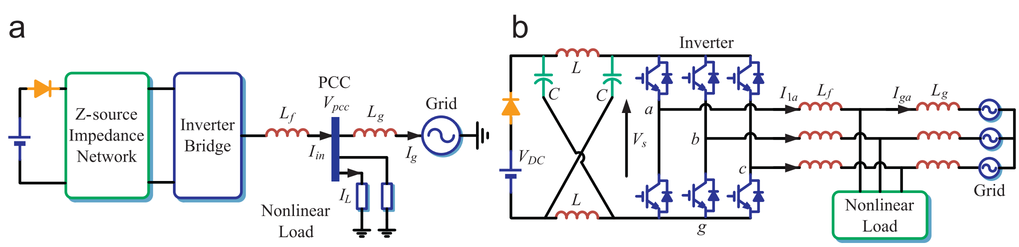


Fig. 84. Schematic and detailed diagram of the MFGCI presented by Gajanayake et al. (a) Overview diagram and (b) configuration of the MFGCI using ZSI in detail.

Table 37
Parameters of the single-phase full-bridge MFGCI presented by Gajanayake et al.

Dc source	The voltage of dc-link is V_{dc} = 60–100 V
Capacity	1 kVA
Utility voltage	RMS voltage of each phase 35 V
Passive components	L_f = 10 mH, L = 3.5 mH, C = 1500 μF, L_g = 1.6 mH
Control strategy	PR and PI control, SPWM modulation
Extra functions	APF

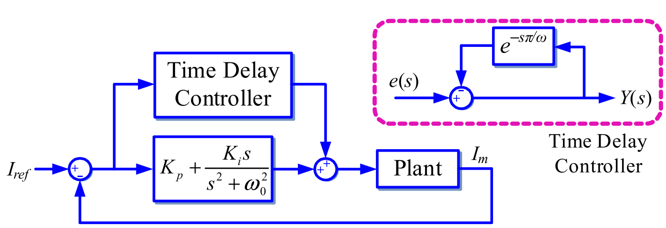


Fig. 85. Controller for ac side of the MFGCI.

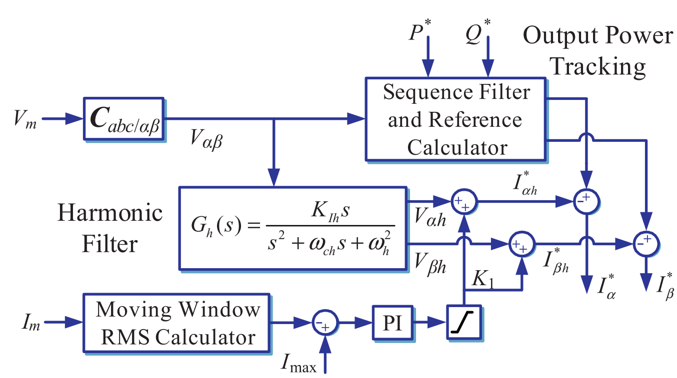


Fig. 86. Reference current generator for power quality improvement.

Yu et al. have given a similar MFGCI configuration, as demonstrated in Fig. 114 [129]. It can be found that, the MFGCI and MG share the dc-bus, while the parallel converter connects to ac-bus. It should be noted that the series converter embeds ac lines, which can compensate utility interruption.

The parallel converter is used to compensate the harmonic current of nonlinear load, as well as, the simplified equivalent circuit is exhibited in Fig. 115, while the control of parallel converter is shown in Fig. 116. A current loop is employed to track the fundamental and harmonic current components injected into utility. Because the amplitude of harmonic current and its order satisfy a hyperbolic function for diode rectifier load (and fifth and seventh components are major part), for convenient, a PR controller for the sixth order harmonic is employed to accurately compensate the fifth and seventh harmonic components.

Fig. 117 illustrates the equivalent circuit and the control strategy of the series converter. The series converter can compensate the voltage sag or swell, by the means of the outer voltage loop and the inner current loop. As a result, the voltage of the MG at PCC can satisfy standards.

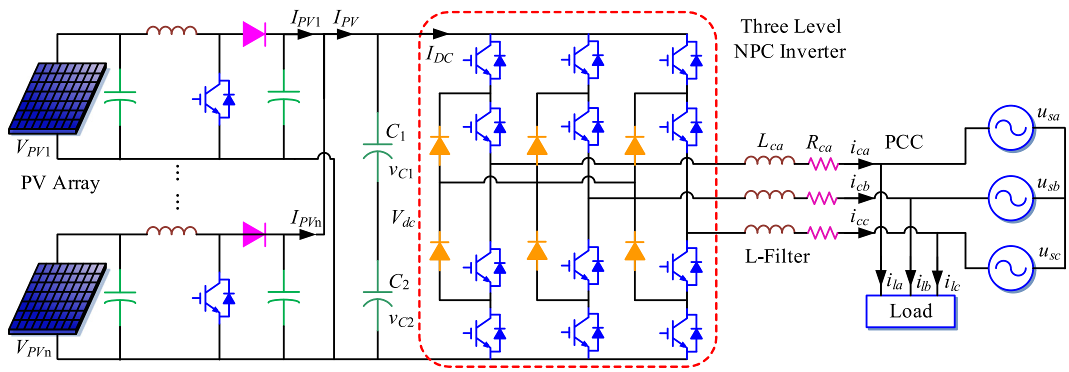


Fig. 87. Configuration of the MFGCI presented by Tsengenes and Adamidis.

Table 38
Parameters of the MFGCI presented by Tsengenes and Adamidis.

Dc source	PV array, v_{dcref}=1100 V
Utility voltage	230 V
Passive components	R_c=0.1 Ω, L_c=0.81 mH, C_1=C_2=4 mF
Control strategy	PI control, SVPWM modulation
Extra functions	APF

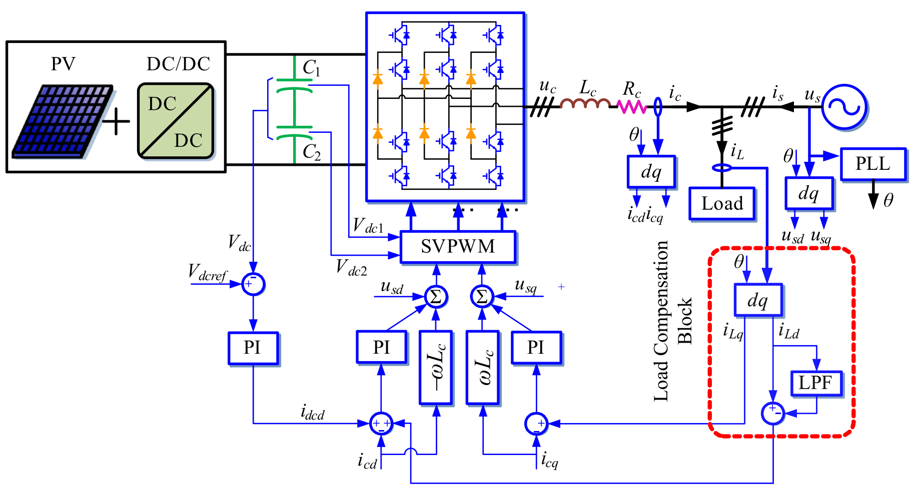


Fig. 88. Control strategy of the MFGCI proposed by Tsengenes and Adamidis.

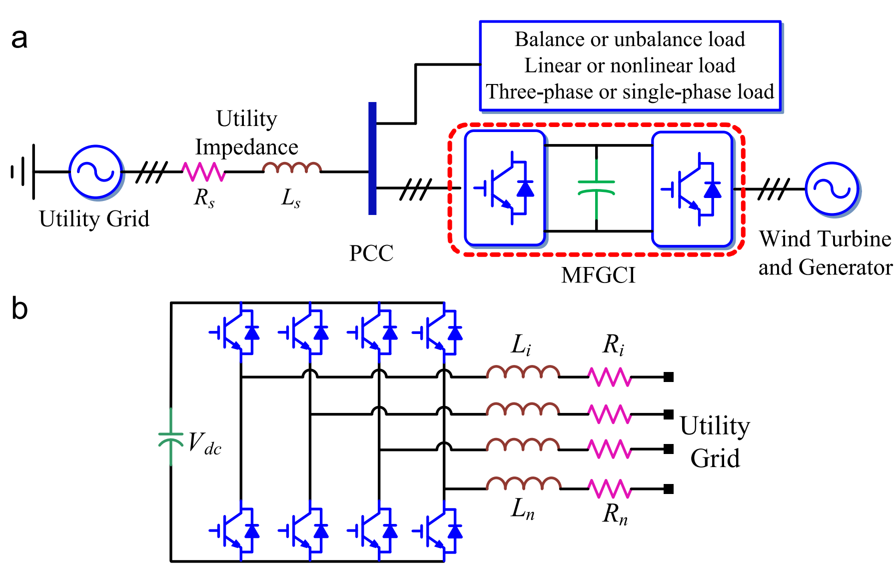


Fig. 89. Three-phase four-leg MFGCI presented by Sawant et al. (a) System configuration and (b) three-phase four-bridge converter.

Table 39
Parameters of the three-phase four-leg MFGCI proposed by Sawant et al.

Dc-source	Wind turbine, voltage of dc-bus V_{dc}=800 V
Voltage of utility grid	220 V/50 Hz
Switching frequency	10 kHz
Passive components	L_s=1.2 mH, R_s=10 mΩ, R_i=20 mΩ, L_i=2.4 mH (i=a, b, c), R_n=20 mΩ, L_n=30 mH
Control strategy	3D-SVPWM modulation
Extra function	APF

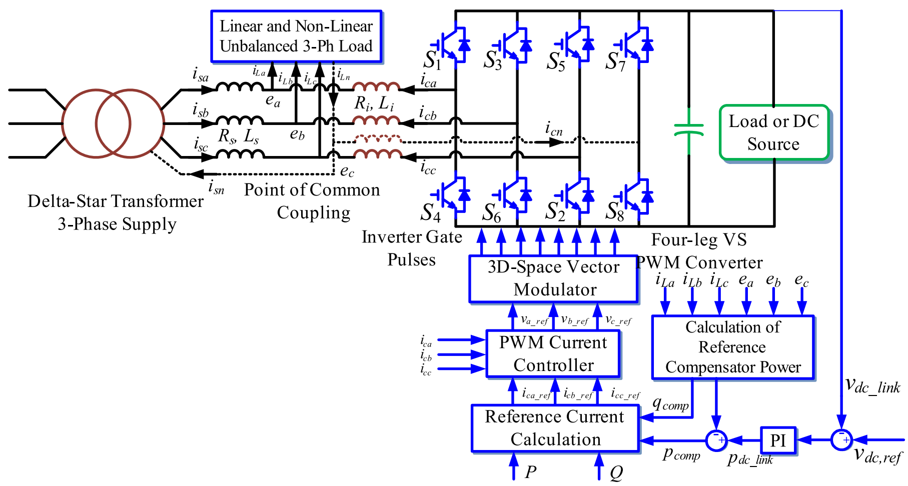


Fig. 90. Schematic block diagram of the MFGCI with four-leg voltage-source converter.

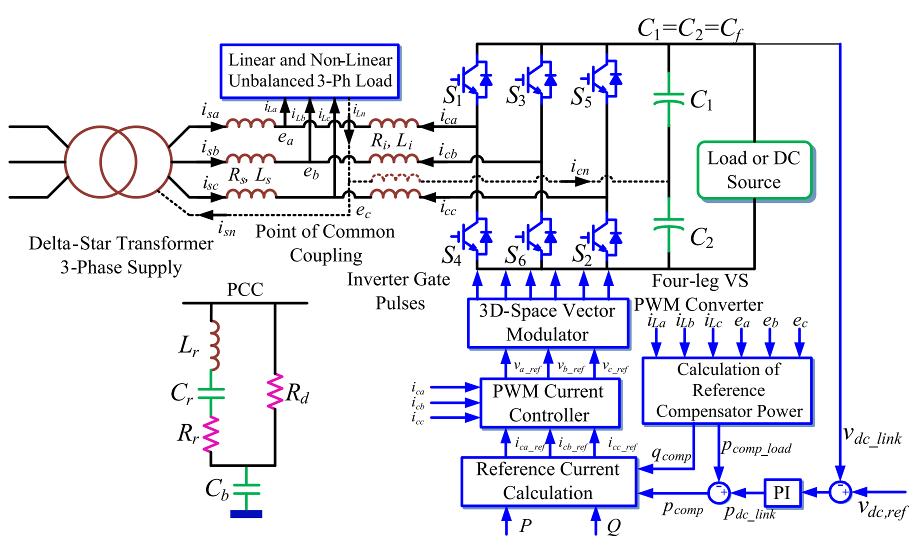


Fig. 91. The MFGCI configuration using split capacitor investigated by Sawant et al.

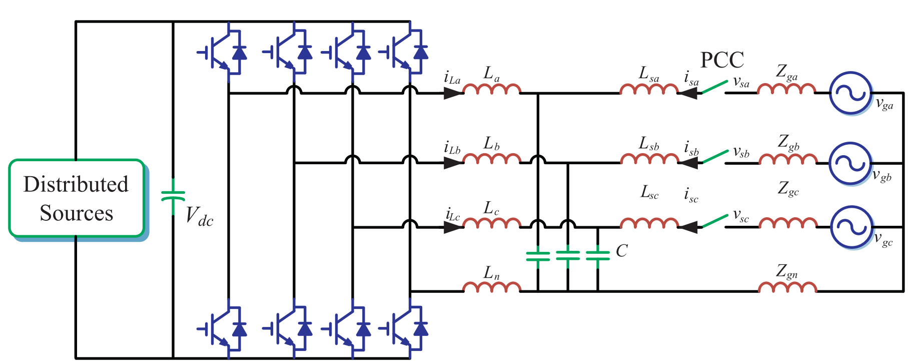


Fig. 92. Schematic diagram of the MFGCI.

Table 40
Parameters of the single-phase full-bridge MFGCI presented by Wang et al.

Dc source	PV array
Capacity	1 kW
Utility voltage	110 V/50 Hz
Passive components	L_1=5 mH, C_f=4 μF, L_f=2.5 mH; diode rectifier L=150 mH, R=35 Ω
Switching frequency	10 kHz
Control strategy	PI control, SPWM
Extra functions	APF

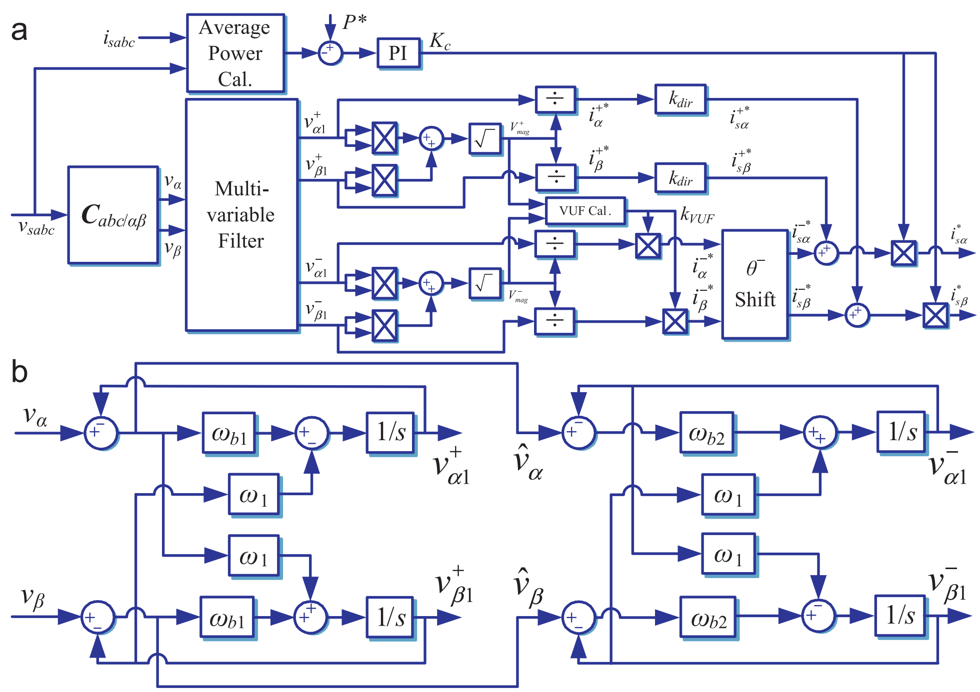


Fig. 93. Reference current generation for the MFGCI presented by Wang et al. (a) Block diagram of the control principle and (b) the novel algorithm for positive- and negative-sequence detection.

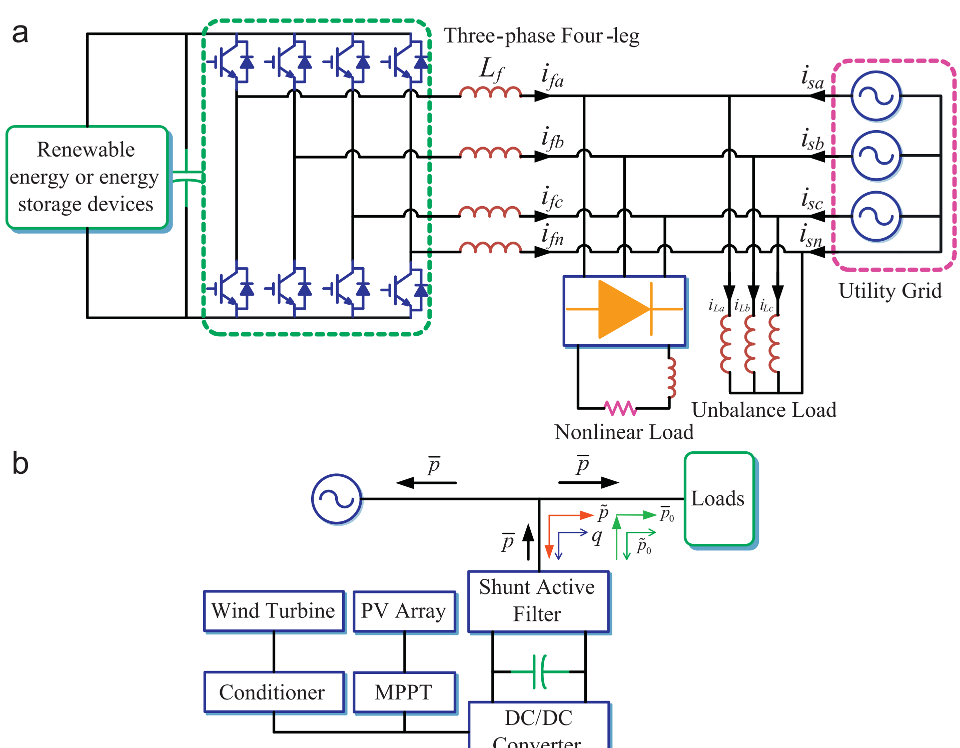


Fig. 94. Three-phase four-leg MFGCI configuration researched by Pinto et al. (a) System configuration and (b) interface system and p–q theory power components.

Table 41
Parameters of the three-phase four-leg MFGCI presented by Pinto et al.

Voltage of utility grid	75 V/50 Hz
Switching frequency	10 kHz
Passive components	Unbalance loads: 200 mH, 200 mH, 0 mH Nonlinear loads: 60 Ω, 68 mH
Power electronic devices	IGBT
Extra function	APF and unbalance compensation

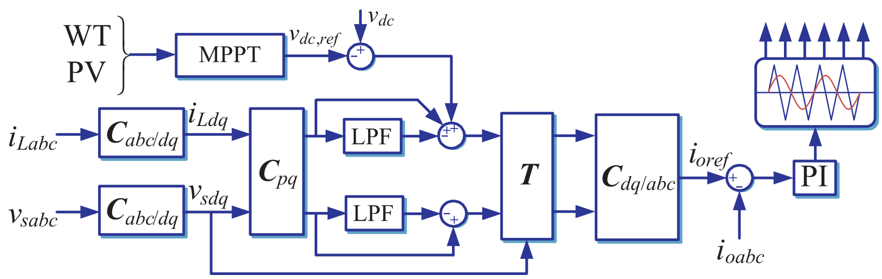


Fig. 95. Control strategy of the MFGCI configuration proposed by Pinto et al.

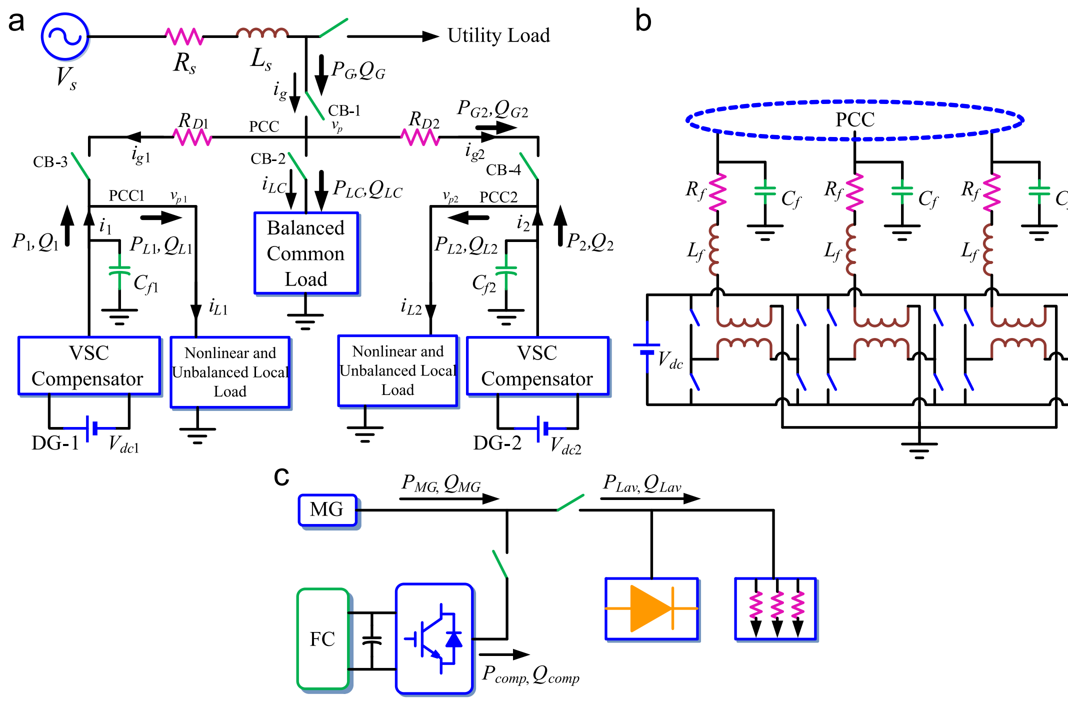


Fig. 96. MG and utility system under consideration by Majumder et al. (a) Micro-grid with two MFGCIs, (b) configuration of the MFGCI and (c) the power flow of the system.

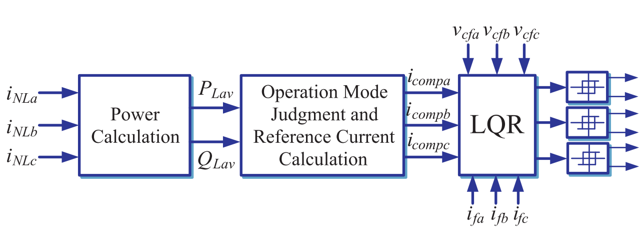


Fig. 97. Control strategy of the MFGCI topology presented by Majumder et al.

When the utility grid is interrupted, the MG transfers to islanded mode. Meanwhile the parallel converter acts as an UPS and supply reference voltage for other GCIs and loads in the MG to keep the MG stable.

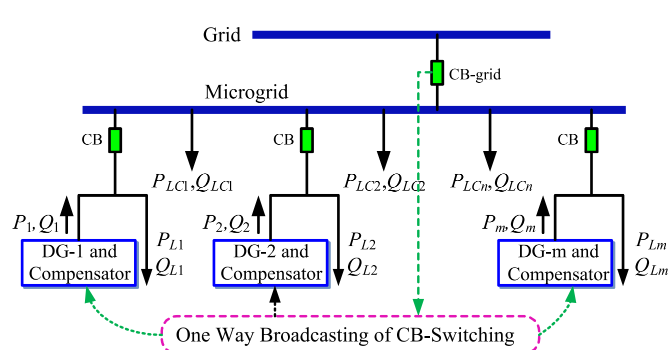


Fig. 98. A MG structure with several MFGCIs and loads.

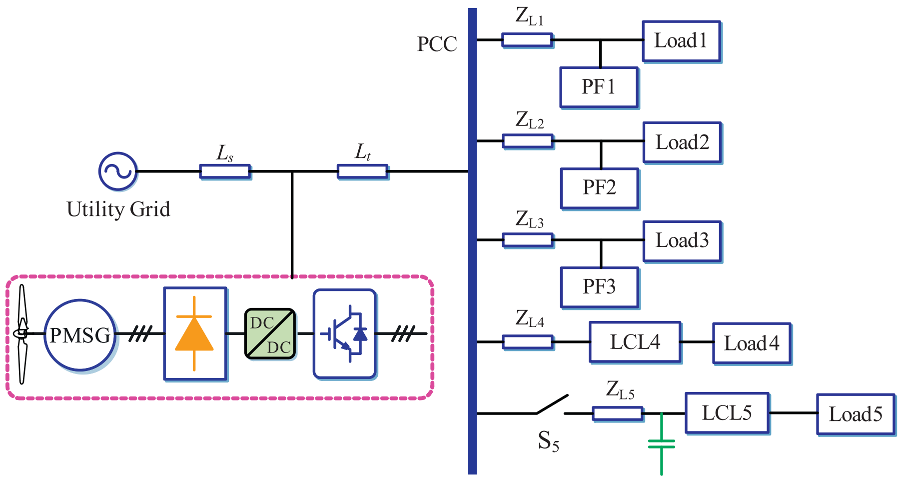


Fig. 99. Configuration of a DGS with MFGCI presented by Chen et al.

Table 42
Parameters of the system studied by Chen et al.

Dc-source	PMG (permanent magnet generator), voltage of dc-bus V_{dc}=960 V
Switching frequency	3.15 kHz
Passive components	Load 1 is a thyristor rectifier in three-phase, whose trigger angle is 58°. The active and reactive power of passive filter PF 1 are P=290 kW and Q=−457 kW
	Load 2 is a diode rectifier in single-phase. The active and reactive power of passive filter PF 2 are P=−134 kW and Q=−167 kW, whose unbalance coefficient is 8.2%
	Load 3 is a thyristor rectifier in three-phase, whose trigger angle is 10°. The active and reactive power of passive filter PF 3 are P=−110 kW and Q=−8 kW
	Load 4 is a diode rectifier in three-phase. The active and reactive power of passive filter LCL 4 are P=−60 kW and Q=−0.4 kW
	Load 5 is a diode rectifier in three-phase. The active and reactive power of passive filter LCL 5 are P=−30 kW and Q=75 kW
	The system inductors are L_s=0.01 mH and L_t=0.16 mH
Control strategy	SPWM modulation
Extra functions	APF, unbalance and harmonic current compensation using passive filters

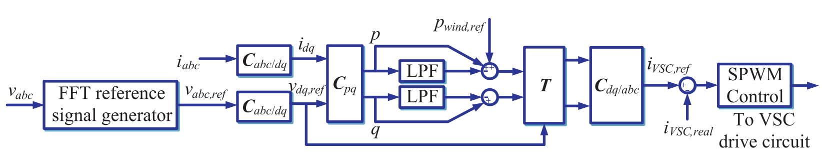


Fig. 100. Block diagram of the control system for the VSC with FFT for functional voltage extraction.

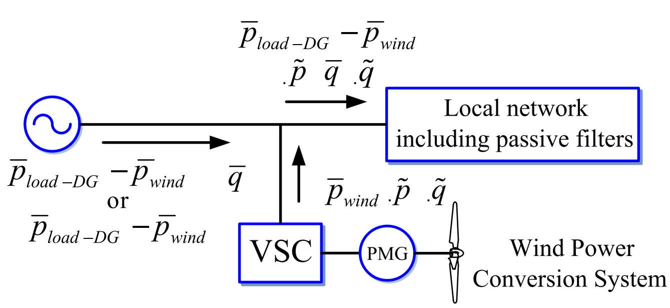


Fig. 101. Possible instantaneous power relation in the studied system.

6. Analysis and discussion

MFGCIs are special GCIs, whose control strategies can partly inherit the ones of conventional GCIs. MFGCIS can be classified as many categories according to different considerations, as exhibited in Fig. 118.

According to the utility, MFGCIs can be classified as depicted in Fig. 118(a). It can be seen that single-phase and three-phase utility application drawn more attention; whereas, there has no MFGCI for two-phase system application. However, two-phase utility grids are widely implemented in railway systems. Thus, this research point maybe encouraging in the following years.

From the view of modulation in Fig. 118(b), the control strategies of MFGCIs can be classified as three categories, namely hysteresis, SPWM, and SVPWM [130,131]. Among them, the hysteresis modulation has the advantage of fast dynamic response. However, the switching frequency is not constant in hysteresis modulation, and some improved hysteresis modulation approaches with constant switching frequency are very complex [132]. Therefore it may burden the filter and controller design. On the contrary, the SPWM modulation has gained common attention due to its constant switching frequency and flexible control approaches. For instance, PI control [133], PR control [134], weighted currents feedback control [128], deadbeat control [135], repetitive control [136,137], iterative learning control [138], and robust control [139] all can be implemented on SPWM modulation. However, the obvious drawback of SPWM modulation is the low efficiency of dc voltage. Besides, SVPWM is good modulation due to its high efficiency of dc voltage, which utilizes eight space voltage vectors to approximately emulate the rotating voltage vector. It also has the advantages of constant switching frequency and flexible control approaches. In general, the control approaches suitable for the SPWM can be implemented on

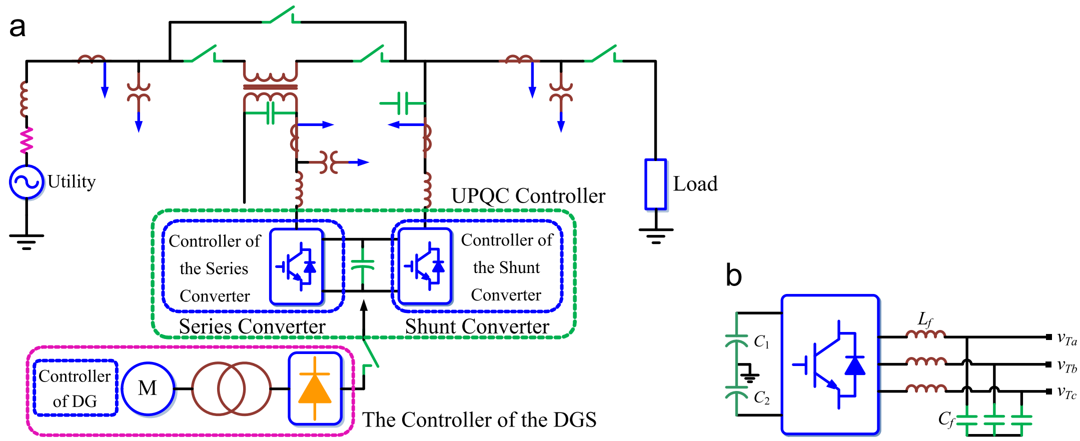


Fig. 102. Three-phase H-bridge MFGCI used as UPQC presented by Han et al. (a) Overview block diagram and (b) inverter stage of the MFGCI.

Table 43
Parameters of the MFGCI presented by Han et al.

Dc-source	DG, voltage of dc-bus $V_{dc}=700$ V
Voltage of utility grid	220 V/60 Hz
Switching frequency	10 kHz
Passive components	Buffer capacitor $C_1=C_2=6600$ μF
	Parallel converter, filter $L_f=600$ μH, $C_f=40$ μF, switching frequency 10 kHz
	Series converter, filter $L_f=600$ μH, $C_f=40$ μF, switching frequency 10 kHz, the rounding ratio of transformer 500:100, capacity 6 kVA
	Capacity of nonlinear load and linear load are 17.54 kVA and 3.27 kVA, respectively
	DG, capacity 30 kW, rounding ratio of transformer 380:500 V, voltage of diode rectifier 700 V
	Inductor of system $R=1$ mΩ, $L=0.01$ mH
Control strategy	PI control
Extra function	UPQC (APF, voltage sag/swell/interruption compensation)

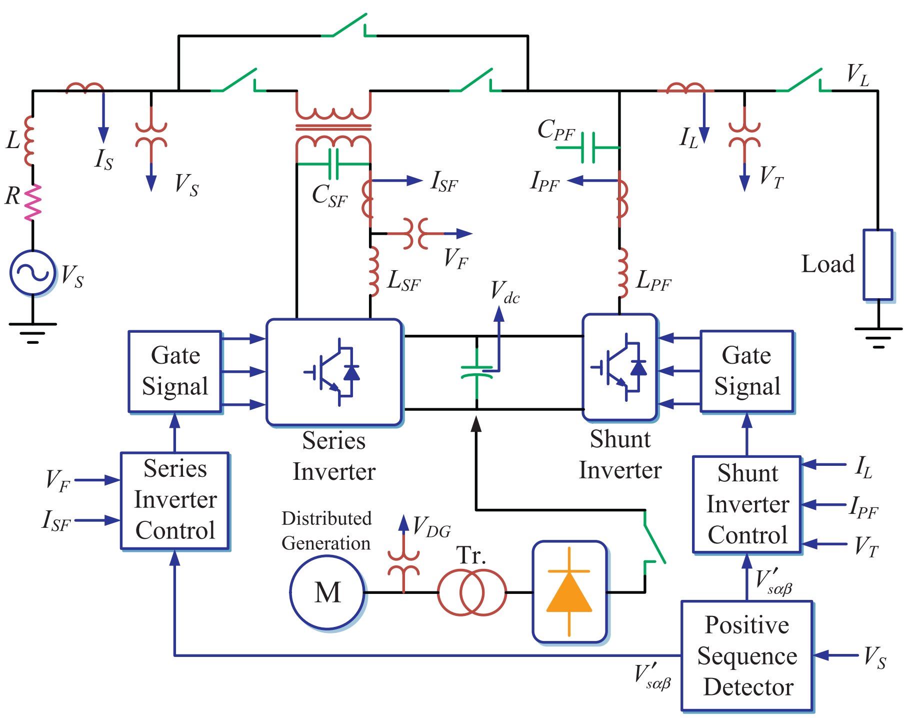


Fig. 103. Brief block diagram of the control strategy for the MFGCI configuration be Han et al.

SVPWM modulation. However, SVPWM modulation is more complicated to achieve on DSP than SPWM.

From the view of auxiliary functionalities of MFGCIs, they can be classified as illustrated in Fig. 118(c). Because the GCIs are usual CC-VSIs, the ancillary services of MFGCIs to enhance power quality on current issues can easily be embedded in. However, the functionalities for voltage issues are hardly achieved using the CC-VSIs GCIs. Thus, some special topologies are expected. As mentioned before, the MFGCIs can act as APF, RPI, PFC, unbalance compensation (UC), DVR, harmonic voltage compensation

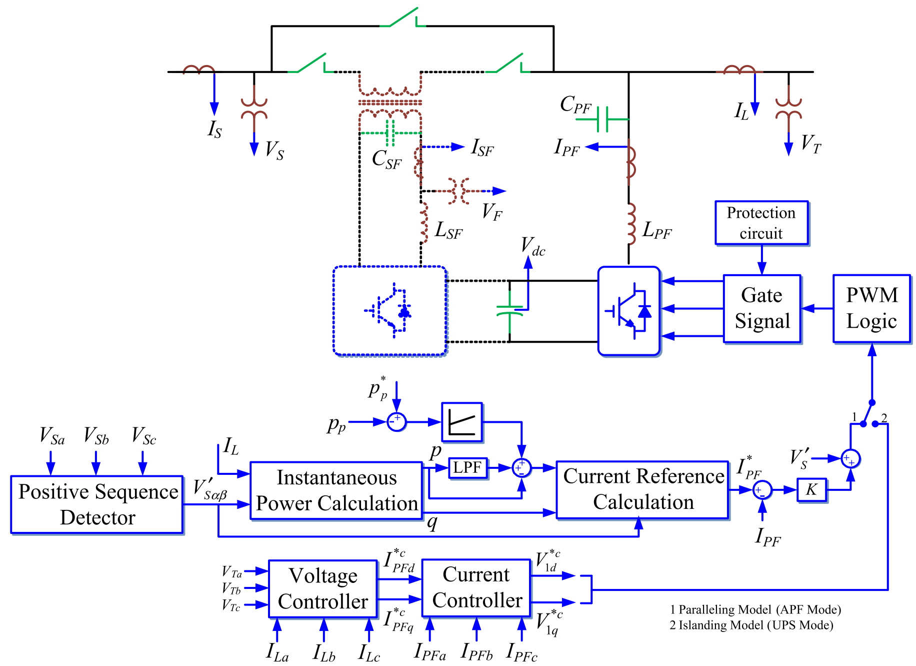


Fig. 104. Shunt inverter control block diagram.

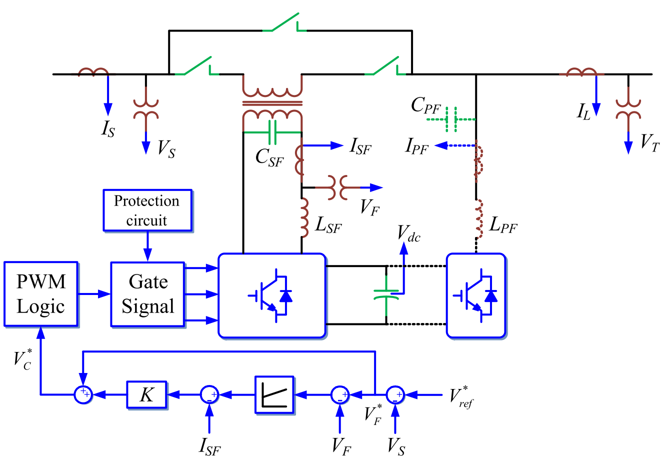


Fig. 105. Series inverter control block diagram.

(HVC), UPS, Voltage unbalance/interruption/sag/swell compensation (UISWC), UPQC and so on.

From the view of detection approaches of compensation components, MFGCIs can be classified as shown in Fig. 118(d). The auxiliary functionalities of MFGCIs are the essentially different from conventional GCIs, where the detection approaches of compensation components are a very important part of the control strategies of MFGCIs. A detail comparison of different approaches for compensation components detection is available in Table 46. These approaches are suitable for MFGCIs application in different conditions. The available approaches can be classified as two categories, namely frequency domain approaches and time domain approaches [141–143]. DFT-based algorithms are a typical frequency domain approaches, but these kinds of methods are complex and poor in dynamic response [144]. Therefore, the detection approaches in time domain gain more and more attention. These kinds of methods include FBD power theory method [145,146], instantaneous power theory (IP) method [147,148], i_d–i_q method [149], i_p–i_q method [147], projection method [147], adaptive filter (AF) method [150], Kalman filter method [151], neural network (NN) method [152] and so on. It should be noted that the previously mentioned MFGCIs mainly utilized instantaneous power theory to detect the harmonic and reactive current of load for compensating, because it has clear physical meaning and is easy implementation on DSP.

Additionally, from the view of the objective for control, the control strategies of MFGCIs can also be divided into two categories, namely direct current control and indirect current control [140]. The indirect current control can control the grid-connected current by the means of voltage control. Its dynamic response is fast, but it is sensitive to system parameters, and the control approaches are inflexible. Therefore, the direct current control is paid more expectation.

The MFGCI cannot only achieve power generation tracking, but also can complete the reactive, unbalance, and harmonic current compensation. To facilitate the algorithm of reference current generation, MFGCIs mainly take direct current control. However, from the view of modulation, all three kinds of modulation methods have been used, according to the history of modulation technology. Table 47 exhibits a detailed comparison of different MFGCIs topologies.

From Table 47, it can be found that, the control methods of available MFGCIs mainly utilize direct current PI control associated with SPWM modulation. As mentioned before, the hysteresis modulation has the drawbacks of varied switching frequency, which is not easy for filter design, and may lead to large current THD. In addition, the SVPWM modulation can enhance the efficiency of dc voltage, but it may burden the controller. As previously mentioned, this paper has investigated the available MFGCI topologies in capacity, switching frequency, auxiliary functionalities, and application aspects in detail. There are interesting conclusion can be drawn:

- Firstly, the available MFGCIs are mainly experimental prototypes, whose capacities are low, in general.

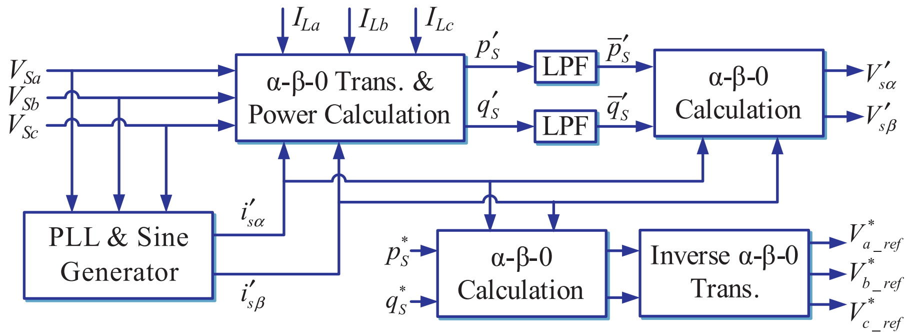


Fig. 106. Positive-sequence detector and voltage reference generator.

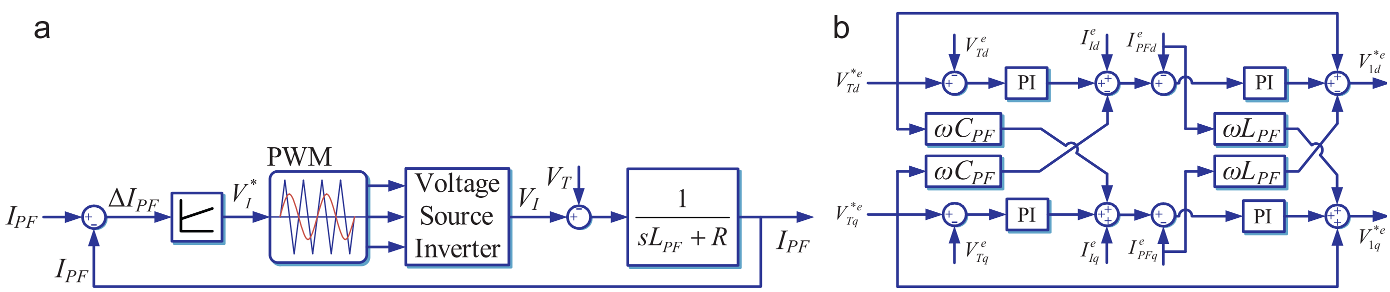


Fig. 107. Control strategy of the shunt inverter. (a) Overview of the control principle and (b) the voltage control of the shunt inverter.

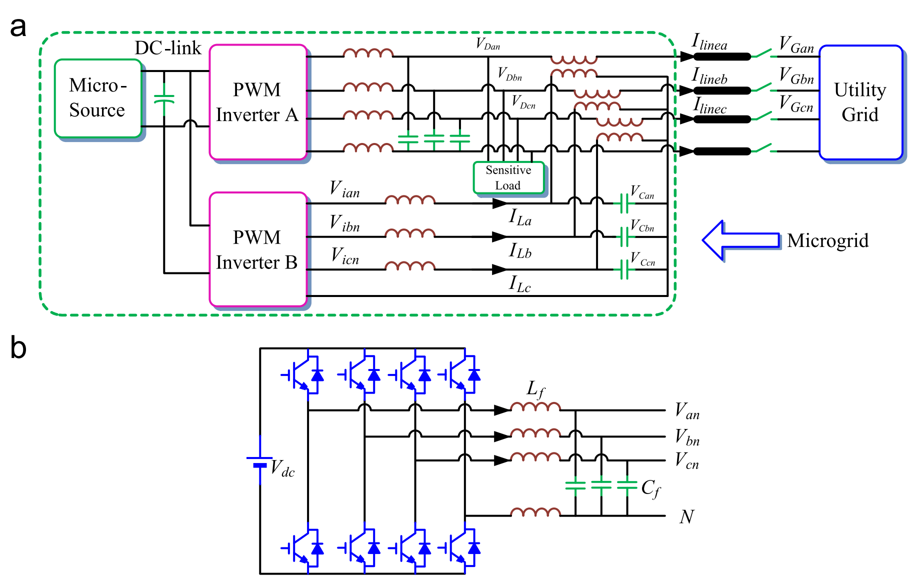


Fig. 108. Configuration of the MFGCI presented by Li et al. (a) Structure of the UPQC-based MFGCI and (b) power electronic topology of the shunt and series inverter.

Table 44
Parameters of the MFGCI topology by Li et al.

Dc-source	Micro-sources, voltage of dc-bus 700 V
Voltage of utility grid	100 V (amplitude of phase-voltage)/50 Hz
Switching frequency	10 kHz (sampling frequency, 5 kHz, controller dSPACE DS1103-TMS320F240)
Control strategy	PI control, proportional resonant control, SPWM modulation
Extra functions	Voltage interruption/sag/harmonic compensation

- Secondly, the auxiliary functionalities of MFGCIs still need exploit. The current compensation mainly focuses on harmonic, reactive, and unbalance components. Besides, the voltage compensation mainly focuses on voltage sag/swell/interruption. Harmonic and unbalance compensation of utility voltage need further investigation.
- Thirdly, the capacities of MFGCIs in single-phase are small, which are mainly implemented in PV grid-connected systems.

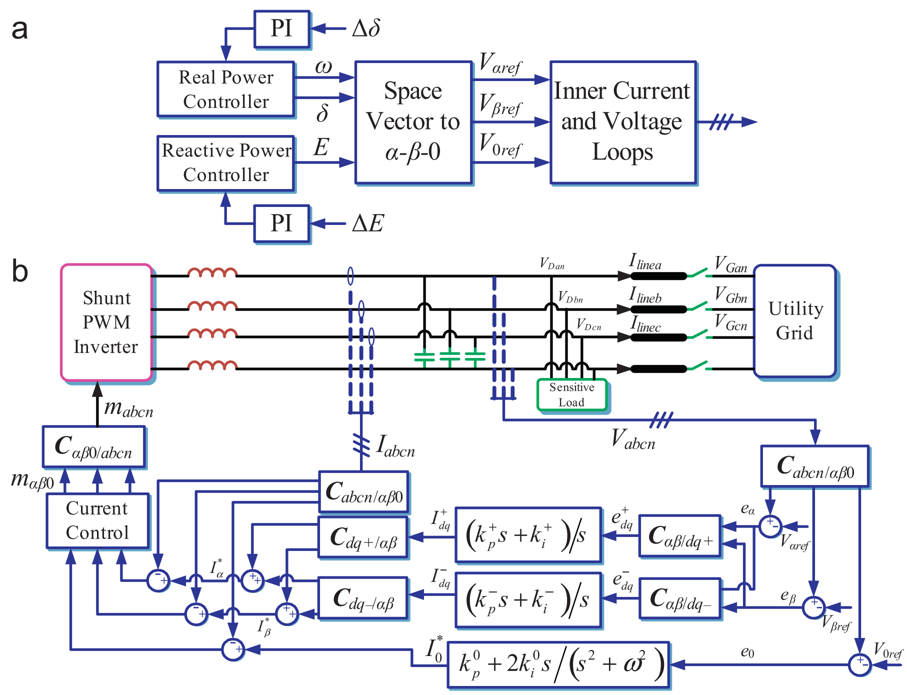


Fig. 109. Control scheme for shunt inverter A. (a) Overall control structure and (b) voltage control algorithm.

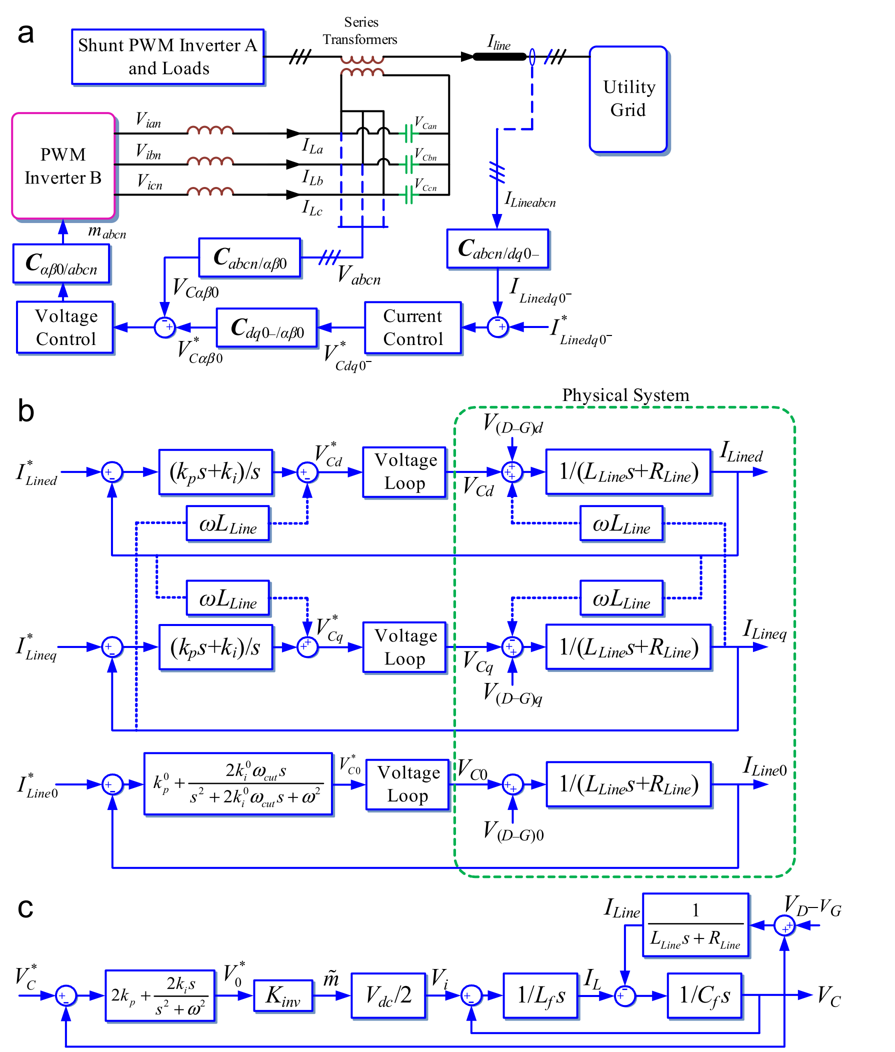


Fig. 110. Control scheme for series inverter B. (a) General representation, (b) outer current loop in the negative synchronous frame and (c) inner voltage loop.

However, the capacities of MFGCIs in three-phase are much larger usually, which are utilized in middle- and large-scale wind and solar plants.

- At last, the switching frequency of small capacity MFGCIs are much higher than the ones of large-capacity MFGCIs. Meanwhile, soft-switching approaches are important means to enhance the efficiency of MFGCIs.

As mentioned before, there have many topologies and control strategies of MFGCIs been well documented for different capacities, application fields, and auxiliary functionalities, as well as a new research field is exploited. However, the capacities of existing MFGCIs are generally small and the auxiliary functionalities are still not perfect. Besides, it is hard to say which topology is better than the others, and a further work on the topology theory of MFGCIs is essential necessary. There may be some work frames on MFGCIs researches as follows:

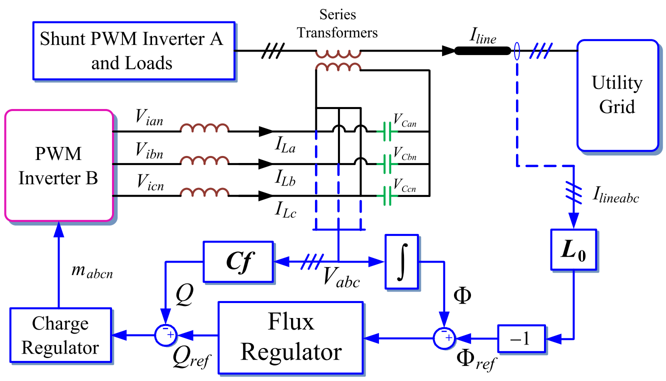


Fig. 111. Flux-charge control scheme for series inverter B.

1. New power electronic topologies of MFGCIs. It is important to build a uniform MFGCI configuration, which can compensate harmonic, reactive, and unbalance current in parallel, as well can compensate harmonic, unbalance, and sag/swell/interruption voltage at the same time. Besides, the dc voltage of micro-sources should be high enough to connect to DC/AC stages of existing MFGCIs. Therefore, a high set-up DC/DC stage may be needed, which will increase the cost and reduce the efficiency of the system. In summary, new power electronic topologies of MFGCIs should be an encouraging research field.
2. The application of MFGCIs for industrial power electric system. The capacity of existing MFGCIs is small, and it should promote the experimental prototype for industrial application. Simultaneously, some multi-level topologies, structures in parallel and/or series should be employed to enhance the current and voltage capacity of MFGCIs.
3. Soft-switching technology and efficiency enhancement. The power loss and heat are very important issues for the

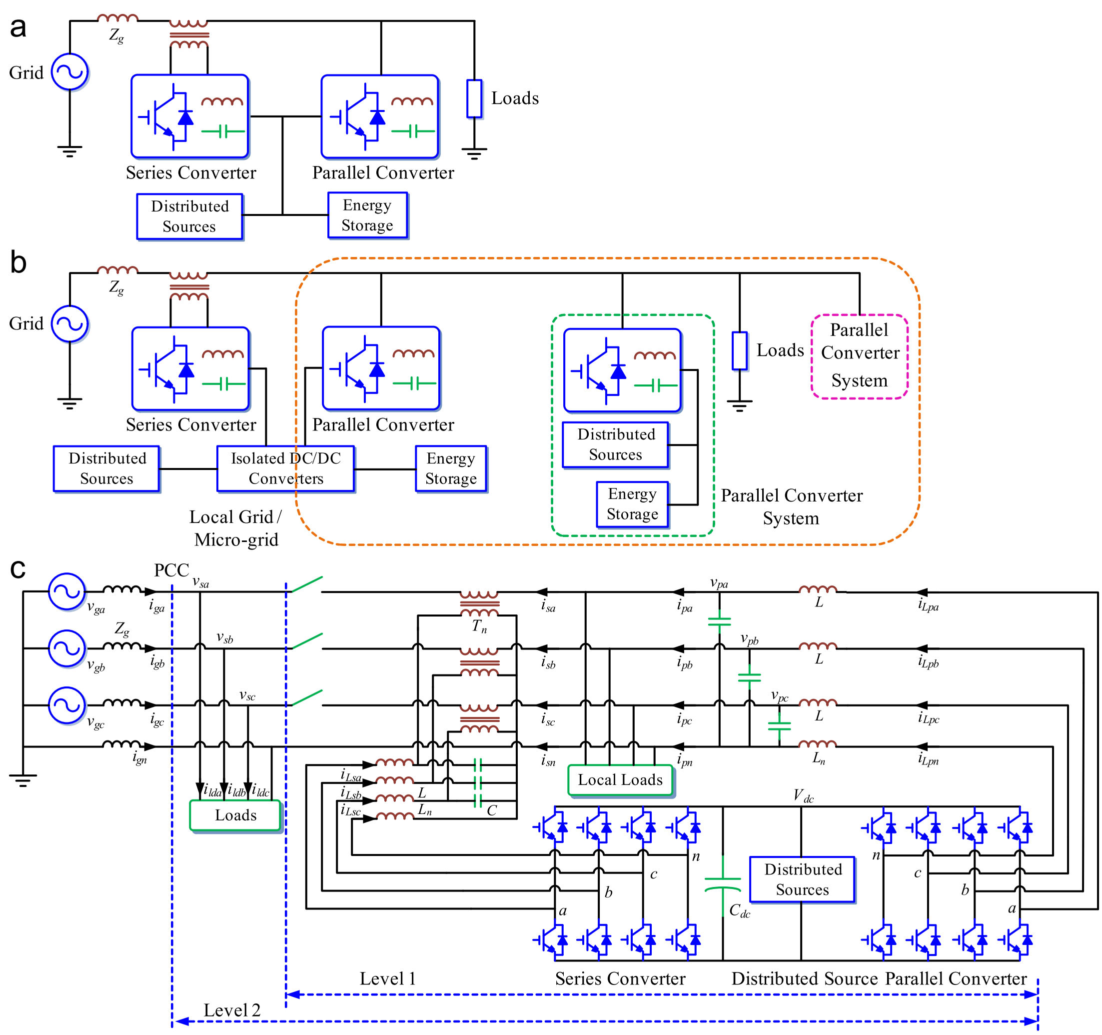


Fig. 112. Configuration of the MFGCI presented by Wang et al. (a) Basic schematic diagram, (b) a micro-grid consists of the MFGCI and (c) a detailed diagram of the MFGCI.

Table 45
Parameters of the single-phase full-bridge MFGCI presented by Wang et al.

Dc source	The voltage of dc-link is V_{dc}=750 V
Utility voltage	230 V/50 Hz
Passive components	Z_g=2 mH, L=1.8 mH, L_n=0.67 mH, C=4400 μF, L_g=1.6 mH, T_n=1:1
Switching frequency	16 kHz
Control strategy	PR and PI control, SPWM modulation
Extra functions	UPQC

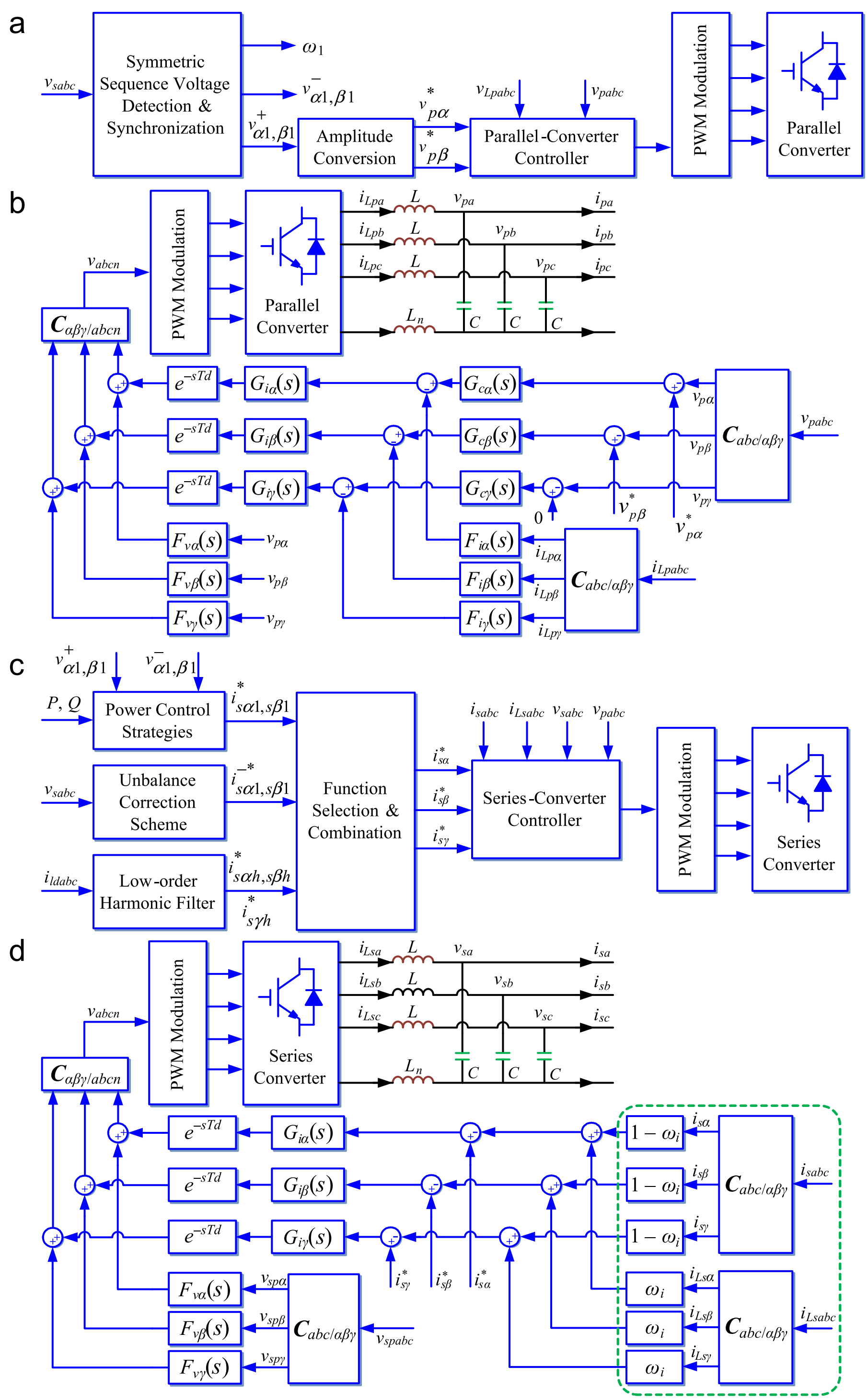


Fig. 113. Scheme diagram of the MFGCI presented by Wang et al. (a) Overview of the controller of parallel converter, (b) diagram of the controller of parallel converter in detail, (c) schematic diagram of the controller of series converter and (d) detailed block diagram of the controller of series converter.

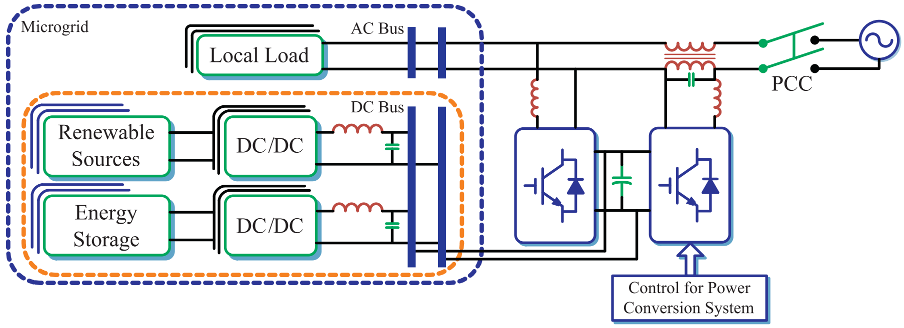


Fig. 114. MFGCI configuration presented by Yu et al.

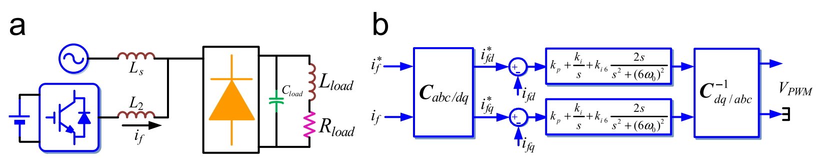


Fig. 115. Circuit model and control strategy of the MFGCI studied by Yu et al. (a) The equivalent circuit of the whole system under normal operation condition and (b) control scheme of MFGCI.

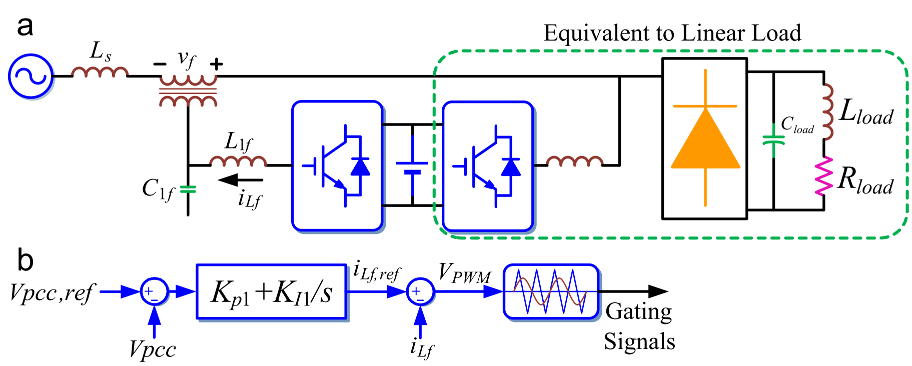


Fig. 116. Equivalent circuit of the whole system under EPS sag/swell condition and corresponding cascaded voltage. (a) Circuit model and (b) control principle.

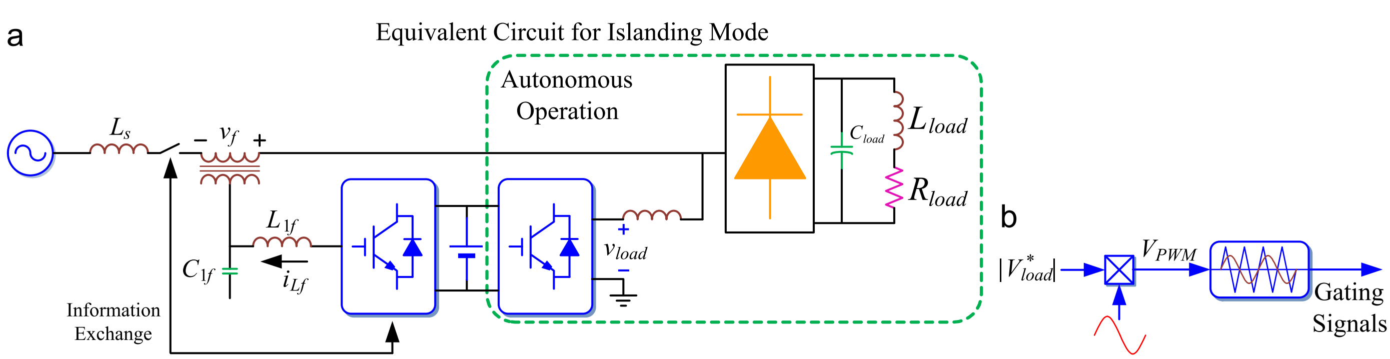


Fig. 117. Control scheme for the shunt connected converter. (a) The equivalent circuit and (b) the control scheme under islanded mode.

reliability and efficiency of a MFGCI. The soft-switching technology can greatly improve these features. However, the existing MFGCIs seldom consider such issues.

4. Novel control strategies should be exploited. As the development of control theory and technology, the control strategies of MFGCIs have covered hysteresis, SPWM, and SVPWM modulation; however, the commonly used approach is SPWM modulation with PI controller. To obtain better performance on steady and dynamic operation of MFGCIs, some advanced control strategies such as LQR, robust control, and feedback linearization control should be discussed. Besides, a DGS and MG may contain a lot of MFGCIs, so the coordination control of MFGCIs is a very significant scenario.
5. The stability of MFGCIs in a DGS or MG. There may be many MFGCIs and conventional GCIs in a DGS or MG, which might weaken the stability performance of DGS or MG to immunize

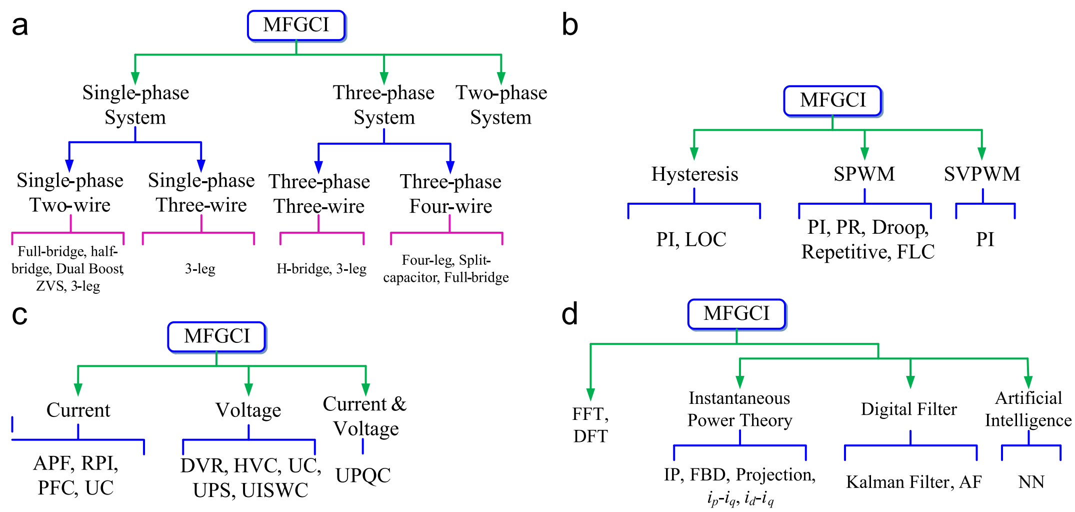


Fig. 118. Several categories of MFGCIs in different considerations. (a) Utility-based classification of MFGCIs, (b) classification of MFGCIs based on modulation and control approaches, (c) classification of MFGCIs based on auxiliary services and (d) classification of MFGCIs based on the methods of compensation components detection.

Table 46
Detailed comparisons of different approaches to detect compensation current.

Algorithm	Frequency domain	Time domain							
	DFT	IP	i_d–i_q	i_p–i_q	Projection	FBD	AF	Kalman	NN
Easy or not	×	√	√	√	√	√	×	×	×
Single-phase application or not	√	×	×	×	×	×	√	√	√
Need PLL or not	×	×	√	×	×	×	×	×	×

Table 47
Comparisons of multi-functional grid-inverter topologies.

Utility	Author	Topology	Current mode	Modulation/ control	Capacity	Switching frequency (kHz)	Extra functions	Application
Single-phase	Kuo et al. [56]	Full-bridge	Direct	SPWM/PI	≤1.5 kVA	20	APF	PV
	Wu et al. [57]	Full-bridge	Direct	SPWM/PI	≤1.5 kVA	20	APF	PV
	Wu et al. [62]	Full-bridge	Direct	SPWM/PI	1 kVA	19.45	APF, PFC	PV
	Sladic et al. [63]	Full-bridge	Direct	Hysteresis	–	15	APF	PV
	Calleja and Jimenez [65]	Full-bridge	Direct	Hysteresis	1 kVA	14.2	APF, RPI	PV
	Seo et al. [66]	Full-bridge	Direct	SPWM/PI	3 kVA	20	APF	PV
	Wu and Shen [67]	Full-bridge	Direct	SPWM/PI	1 kVA	25	APF	PV
	Wu et al. [68]	Half-bridge	Direct	SPWM/PI	≤1.5 kVA	20	APF	PV
	Patidar et al. [70]	Full-bridge	Direct	Hysteresis/PI	1.2 kVA	25	APF	PV
	Hirachi et al. [71]	Full-bridge	Direct	SPWM/PI	3 kVA	–	APF	PV
	Dasgupta et al. [72]	Full-bridge	Direct	SPWM/Lyapunov	–	10	APF	Micro-source
	Chiang et al. [73]	Full-bridge	Direct	SPWM/PI	≤1 kVA	–	APF, UPS	PV
	Bojoi et al. [74]	Full-bridge	Direct	SPWM/repetitive	4 kVA	10	APF, PFC	Micro-source
	Cirrincione et al. [76]	Full-bridge	Direct	SPWM/PR	–	15	APF	PV
	Macken et al. [77]	Full-bridge	Direct	SPWM/PI	1 kVA	–	APF	PV
	Hosseini et al. [78]	Two-boost	Indirect	SPWM/PI	≤3 kVA	20	DVR, PFC	PV
	Mastromauro et al. [79]	Full-bridge	Direct	SPWM/repetitive	1.2 kVA	20	DVR, HVC	PV
	Dasgupta et al. [82]	Full-bridge	Indirect	SPWM/repetitive	–	10	DVR, HVC	PV
	Lin and Yang [83]	Three-leg	Direct	SPWM/PI	1.5 kVA	20	UPQC	PV
	Kuo. [85]	Three-leg	Direct	SPWM/PI	1 kVA	18	APF	PV
	Souza et al. [86]	HB ZVS	Direct	SPWM/PI	1 kVA	100/10	APF	PV
Three-phase	Wu et al. [89]	H-bridge	Direct	SPWM/PI	1.1 kVA	20	APF	PV
	He et al. [91]	Full-bridge	Direct	SPWM/repetitive	5 kVA	–	APF	Micro-source
	Yu et al. [93]	H-bridge	Direct	SPWM/PI	10 kVA	–	APF, RPI	Micro-source
	Kim et al. [94]	H-bridge	Direct	Hysteresis	–	20	APF	PV
	Dasgupta et al. [95]	H-bridge	Direct	SPWM/Lyapunov	75 VA	–	APF	Micro-source
	Cheng et al. [97]	H-bridge	–	–	5 kVA	–	PFC, UPS	PV
	Naderi et al. [98]	H-bridge	Direct	Hysteresis	–	–	APF, RPI	Micro-source
		H-bridge	Direct	Hysteresis	150 kVA	–	APF	Battery

Table 47 (*continued*)

Utility	Author	Topology	Current mode	Modulation/ control	Capacity	Switching frequency (kHz)	Extra functions	Application
	Mohod and Aware [99]							
	Marei et al. [100]	H-bridge	Direct	SPWM/FLC, PI	–	–	APF	Micro-source
	Cheng et al. [102]	H-bridge	Direct	SPWM/droop control	1 kVA	20	UC	Micro-source
	Lv et al. [103]	H-bridge	Direct	SPWM/PI	400 kVA	12.8	APF	Micro-source
	Mohamed and Saadany [105]	H-bridge	Indirect	SPWM/VSC	–	6.7	DVR	Micro-source
	Saitou and Shimizu [107]	H-bridge	Direct	SPWM/PI	–	15	RPI	Battery
	Chandhaket et al. [108]	H-bridge	Direct	SPWM/PI	20 kVA	–	PWM rectifier, APF	Battery
	Abolhassani et al. [112]	H-bridge	Direct	SPWM/PI	7.5 kVA	–	APF	DFIG
	Gajanayake et al. [115]	ZVI	Direct	SVPWM/PI	1 kVA	–	APF	Micro-source
	Tsengenes and Adamidis [116]	Three-level NPC	Direct	SVPWM/PI	–	–	APF	PV
	Sawant and Chandorkar [117]	Four-bridge	Direct	3D-SVPWM	–	10	APF, UC	PMSG
	Wang et al. [119]	Four-bridge	Direct	SPWM/PI	1 kVA	10	APF	PV
	Pinto et al. [121]	Four-bridge	Direct	–	–	–	APF, UC	Micro-source
	Majumder et al. [122]	Full-bridge	Direct	Hysteresis/LQR	–	–	APF, UC	Micro-source
	Chen et al. [17]	H-bridge	Direct	SPWM/PI	–	3.15	APF, UC	PMSG
	Han et al. [124]	H-bridge	Direct	SPWM/PI	30 kVA	10	APF, ISWC	WT
	Li et al. [125]	Four-bridge	Direct	SPWM/PI	–	10	ISWC	Micro-source
	Wang et al. [127]	Four-bridge	Direct	SPWM/PI, PR	–	16	UPQC	Micro-source
	Yu and Khambadkone [129]	Four-bridge	Direct	SPWM/PI	–	–	ISWC, APF	Micro-source

disturbance. How to analyze, judge, and control the stability of DGS or MG need further work.

7. Conclusion

Recently, GCIs have caught common attention as important components of DGSs and MGs, due to the deeply research on DGS and MG to make better use of RESs. To enhance the cost-effective of GCIs and the power quality of DGSs and MGs, a new and encouraging field on MFGCIs is exploited. In this paper, a comprehensive review on the topologies and control strategies of MFGCIs are achieved. Additionally, detailed analysis, comparison, and discussion on the existing MFGCIs are investigated. Besides, some interesting frames for further work are summarized. It is expected that this review will be a helpful reference on MFGCIs for the researchers, engineers, manufacturers, and users concerning GCIs.

Acknowledgments

The financial support from National Natural Science Foundation of China (No.50907060) and China Postdoctoral Science Foundation funded project (20090451438) are gratefully acknowledged.

References

[1] Andersson G, Donalek P, Farmer R, Hatziargyriou N, Kamwa I, Kundur P, Martins N, Paserba J, Pourbeik P, Sanchez Gasca J, Schulz R, Stankovic A, Taylor C, Vittal V. Causes of the 2003 major grid blackouts in North America Europe, and recommended means to improve system dynamic performance. IEEE Transactions on Power Systems 2005;20(4):1922–8.
[2] Chen QQ, Yin XG, You DH, Hou H, Tong GY, Wang B, Liu H. Review on blackout process in China Southern area main power grid in 2008 snow disaster. In: Proceedings of the IEEE power and energy society general meeting. Calgary, Alberta, Canada; 26–30 July, 2009. p. 1–8.
[3] Su S, Li YH, Duan XZ. Self-organized criticality of power system faults and its application in adaptation to extreme climate. Chinese Science Bulletin 2009;54(7):1251–9.
[4] Rahman S. Green power: what is it and where can we find it? IEEE Power and Energy Magazine 2003;1(1):30–7.
[5] Beér JM. Low carbon emission electricity generating technology options. 〈http://web.mit.edu/mitei/docs/seminars/iap10/low-carbon.pdf〉 [26.12.2010].
[6] Dugan RC, McDermott TE. Distributed generation. IEEE Industry Applications Magazine 2002;8(2):19–25.
[7] Carley S. Distributed generation: an empirical analysis of primary motivators. Energy Policy 2009;37(5):1648–59.
[8] Amor MB, Lesage P, Pineau PO, Samson R. Can distributed generation offer substantial benefits in a Northeastern American context? A case study of small-scale renewable technologies using a life cycle methodology Renewable and Sustainable Energy Reviews 2010;14(9):2885–95.
[9] Lasseter RH. Microgrids and distributed generation. Journal of Energy Engineering 2007;133(3):144–9.
[10] Kroposki B, Lasseter R, Ise T, Morozumi S, Papathanassiou S, Hatziargyriou N. Making microgrids work. IEEE Power and Energy Magazine 2008;6(3):40–53.
[11] Huang JY, Jiang CW, Xu R. A review on distributed energy resources and MicroGrid. Renewable and Sustainable Energy Reviews 2008;12(9):2472–83.
[12] Lidula NWA, Rajapakse AD. Microgrids research: a review of experimental microgrids and test systems. Renewable and Sustainable Energy Reviews 2011;15(1):186–202.
[13] Ustun TS, Ozansoy C, Zayegh A. Recent developments in microgrids and example cases around the world—a review. Renewable and Sustainable Energy Reviews 2011;15(8):4030–41.
[14] Zeng Z, Yang H, Zhao R. Study on small signal stability of microgrids: a review and a new approach. Renewable and Sustainable Energy Reviews 2011;15(9):4818–28.
[15] Blaabjerg F, Zhe C, Kjaer SB. Power electronics as efficient interface in dispersed power generation systems. IEEE Transactions on Power Electronics 2004;19(5):1184–94.
[16] Xue YS, Chang LC, Sren BK, Bordonau J, Shimizu T. Topologies of single-phase inverters for small distributed power generators: an overview. IEEE Transactions on Power Electronics 2004;19(5):1305–14.
[17] Chen Z, Blaabjerg F, Pedersen JK. A multi-functional power electronic converter in distributed generation power systems. In: Proceedings of the IEEE annual power electronics specialists conference. Recife, Brazil; 12–18 June, 2005. p. 1738–44.
[18] Jardan RK, Nagy I. Power quality conditioning in distributed generation systems. In: Proceedings of the IEEE power electronics and motion control conference. Shanghai, China; 14–16 August 2006. p. 1–5.

[19] Belenguer E, Beltran H, Aparicio N. Distributed generation power inverters as shunt active power filters for losses minimization in the distribution network. In: Proceedings of the European conference on power electronics and applications. Aalborg, Denmark; 2–5 September, 2007. p. 1–10.
[20] Macken KJP. Control of inverter-based distributed generation used to provide premium power quality. In: Proceedings of the IEEE power electronics specialists conference. Aachen, Germany; 20–25 June, 2004. p. 3188–94.
[21] Joos G, Ooi BT, McGillis D, Galiana FD, Marceau R. The potential of distributed generation to provide ancillary services. In: Proceedings of the IEEE power engineering society summer meeting. Seattle (WA), United states; 16–20 July, 2000. p. 1762–7.
[22] Triggianese M, Liccardo F, Marino P. Ancillary services performed by distributed generation in grid integration. In: Proceedings of the international conference on clean electrical power. Capri, Italy; 21–23 May, 2007. p. 164–70.
[23] Tsengenes G, Adamidis G. Investigation of the behavior of a three phase grid-connected photovoltaic system to control active and reactive power. Electric Power Systems Research 2011;81(1):177–84.
[24] Takigawa K, Okada N, Kuwabara N, Kitamura A, Yamamoto F. Development and performance test of smart power conditioner for value-added PV application. Solar Energy Materials and Solar Cells 2003;75(3–4):547–55.
[25] Albuquerque FL, Moraes AJ, Guimaraes GC, Sanhueza SMR, Vaz AR. Photovoltaic solar system connected to the electric power grid operating as active power generator and reactive power compensator. Solar Energy 2010;84(7):1310–7.
[26] Khadem SK, Basu M, Conlon MF. Power quality in grid connected renewable energy systems role of custom power devices. In: Proceedings of the international conference on renewable energy and power quality (ICREPQ). Granada, Spain; 23–25 March, 2010. p. 1–6.
[27] Chakraborty S, Kramer B, Kroposki B. A review of power electronics interfaces for distributed energy systems towards achieving low-cost modular design. Renewable and Sustainable Energy Reviews 2009;13(9):2323–35.
[28] Kroposki B, Pink C, DeBlasio R, Thomas H, Simo X, Es M, Sen PK. Benefits of power electronic interfaces for distributed energy systems. IEEE Transactions on Energy Conversion 2010;25(3):901–8.
[29] Kirubakaran A, Jain S, Nema RK. A review on fuel cell technologies and power electronic interface. Renewable and Sustainable Energy Reviews 2009;13 (9):2430–40.
[30] Zhao B, Yu Q, Sun W. Extended-phase-shift control of isolated bi-directional DC–DC converter for power distribution in microgrid. IEEE Transactions on Power Electronics; in press.
[31] Du Y, Lukic S, Jacobson B, Huang A. Review of high power isolated bi-directional DC-DC converters for PHEV/EV DC charging infrastructure. In: Proceedings of the IEEE energy conversion congress and exposition (ECCE). Phoenix (AZ); 17–22 September, 2011. p. 553–60.
[32] Du Y, Zhou X, Bai S, Lukic S, Huang A. Review of non-isolated bi-directional DC–DC converters for plug-in hybrid electric vehicle charge station application at municipal parking decks. In: Proceedings of the IEEE applied power electronics conference and exposition. Palm Springs (CA), United States; 21–25 Febraury, 2010. p. 1145–51.
[33] Cobben JFG, Kling WL, Myrzik JMA. Power quality aspects of a future micro grid. In: Proceedings of the IEEE international conference on future power systems. Amsterdam, Netherlands; 18 November 2005. p. 1–5.
[34] Jonasson I, Soder L. Power quality on ships—a questionnaire evaluation concerning island power system. In: Proceedings of the IEEE power engineering society transmission and distribution conference. Vancouver, BC, Canada; 15–19 July, 2001. p. 216–21.
[35] Enslin JHR, Heskes PJM. Harmonic interaction between a large number of distributed power inverters and the distribution network. IEEE Transactions on Power Electronics 2004;19(6):1586–93.
[36] Bollen MH, Hassan F. Integration of distributed generation in the power system. Wiley-IEEE Press; 2011.
[37] Salim RH, Oleskovicz M, Ramos RA. Power quality of distributed generation systems as affected by electromechanical oscillations—definitions and possible solutions. IET Generation, Transmission and Distribution 2011;5(11):1114–23.
[38] Li G, Zhang Z, Li X, Wang S, Zhou M. A methodology for power quality evaluation in distribution network with distributed generation. In: Proceedings of the IEEE international conference on critical infrastructure. Beijing, China; 20–22 September, 2010. p. 1–6.
[39] Salarvand A, Mirzaeian B, Moallem M. Obtaining a quantitative index for power quality evaluation in competitive electricity market. IET Generation, Transmission and Distribution 2010;4(7):810–23.
[40] Driesen J, Green T, Van Craenenbroeck T, Belmans R. The development of power quality markets. In: Proceedings of the IEEE power engineering society transmission and distribution conference. New York (NY), United states; 27–31 January, 2002. p. 262–7.
[41] Hu JB, Zhang W, Wang HS, He YK, Xu L. Proportional integral plus multi-frequency resonant current controller for grid-connected voltage source converter under imbalanced and distorted supply voltage conditions. Journal of Zhejiang University—Science A 2009;10(10):1532–40.
[42] Rodriguez P, Timbus AV, Teodorescu R, Liserre M, Blaabjerg F. Flexible active power control of distributed power generation systems during grid faults. IEEE Transactions on Industrial Electronics 2007;54(5):2583–92.
[43] Roscoe AJ, Finney SJ, Burt GM. Tradeoffs between AC power quality and DC bus ripple for 3-phase 3-wire inverter-connected devices within microgrids. IEEE Transactions on Power Electronics 2011;26(3):674–88.
[44] Hu Y, Chen Z, Excell P. Power quality improvement of unbalanced power system with distributed generation units. In: Proceedings of the IEEE international conference on electric utility deregulation and restructuring and power technologies. Weihai, Shandong, China; 6–9 July, 2011. p. 417–23.
[45] Peng FZ, Akagi H, Nabae A. A new approach to harmonic compensation in power systems—a combined system of shunt passive and series active filters. IEEE Transactions on Industry Applications 1990;26(6):983–90.
[46] Akagi H, Fujita H, Wada K. Shunt active filter based on voltage detection for harmonic termination of a radial power distribution line. IEEE Transactions on Industry Applications 1999;35(3):638–45.
[47] Fujita H, Akagi H. Voltage-regulation performance of a shunt active filter intended for installation on a power distribution system. IEEE Transactions on Power Electronics 2007;22(3):1046–53.
[48] Lee TL, Li JC, Cheng PT. Discrete frequency tuning active filter for power system harmonics. IEEE Transactions on Power Electronics 2009;24 (5):1209–17.
[49] Ghosh A, Ledwich G. Compensation of distribution system voltage using DVR. IEEE Transactions on Power Delivery 2002;17(4):1030–6.
[50] Mahdianpoor FM, Hooshmand RA, Ataei M. A new approach to multi-functional dynamic voltage restorer implementation for emergency control in distribution systems. IEEE Transactions on Power Delivery 2011;26 (2):882–90.
[51] Arulampalam A, Barnes M, Jenkins N, Ekanayake JB. Power quality and stability improvement of a wind farm using STATCOM supported with hybrid battery energy storage. IEE Proceedings—Generation, Transmission and Distribution 2006;153(6):701–10.
[52] Lowenstein MZ. Improving power factor in the presence of harmonics using low-voltage tuned filters. IEEE Transactions on Industry Applications 1993;29(3):528–35.
[53] Bansal RC. Automatic reactive-power control of isolated wind-diesel hybrid power systems. IEEE Transactions on Industrial Electronics 2006;53 (4):1116–26.
[54] Ke Z, Jiang W, Lv Z, Luo A, Kang Z. A micro-grid reactive voltage collaborative control system configuring DSTATCOM. In: Proceedings of the IEEE mechanic automation and control engineering. Inner Mongolia, China; 15–17 July, 2011. p. 1887–90.
[55] Sannino A, Svensson J, Larsson T. Power-electronic solutions to power quality problems. Electric Power Systems Research 2003;66(1):71–82.
[56] Kuo Y, Liang T, Chen J. Novel maximum-power-point-tracking controller for photovoltaic energy conversion system. IEEE Transactions on Industrial Electronics 2001;48(3):594–601.
[57] Wu TF, Nei HS, Shen CL, Li GF. A single-phase two-wire grid-connection PV inverter with active power filtering and nonlinear inductance consideration. In: Proceedings of the IEEE applied power electronics conference and exposition. Anaheim, California; 22–26 February, 2004. p. 1566–71.
[58] Wu TF, Nei HH, Shen CL, Chen TM. A single-phase inverter system for PV power injection and active power filtering with nonlinear inductor consideration. IEEE Transactions on Industry Applications 2005;41(4):1075–83.
[59] Esram T, Chapman PL. Comparison of photovoltaic array maximum power point tracking techniques. IEEE Transactions on Energy Conversion 2007;22 (2):439–49.
[60] Esram T, Kimball JW, Krein PT, Chapman PL, Midya P. Dynamic maximum power point tracking of photovoltaic arrays using ripple correlation control. IEEE Transactions on Power Electronics 2006;21(5):1282–90.
[61] Salas V, Olias E, Barrado A, Lazaro A. Review of the maximum power point tracking algorithms for stand-alone photovoltaic systems. Solar Energy Materials and Solar Cells 2006;90(11):1555–78.
[62] Wu TF, Chang CH, Chen YK. A multi-function photovoltaic power supply system with grid-connection and power factor correction features. In: Proceedings of the IEEE power electronics specialists conference. Galway, Ireland; 18–23 June, 2000. p. 1185–90.
[63] Sladic S, Bariic B, Sokovic M. Cost-effective power converter for thin film solar cell technology and improved power quality. Journal of Materials Processing Technology 2008;201(1–3):786–90.
[64] Kirawanich P, O'Connell RM. Fuzzy logic control of an active power line conditioner. IEEE Transactions on Power Electronics 2004;19(6):1574–85.
[65] Calleja H, Jimenez H. Performance of a grid connected PV system used as active filter. Energy Conversion and Management 2004;45(15–16):2417–28.
[66] Seo HR, Jang SJ, Kim GH, Park M, Yu IK. Hardware based performance analysis of a multi-function single-phase PV-AF system. In: Proceedings of the IEEE energy conversion congress and exposition. San Jose, California, USA; 20–24 September, 2009. p. 2213–7.
[67] Wu Y, Shen C. Implementation of a DC power system with PV grid-connection and active power filtering. In: Proceedings of the IEEE power electronics for distributed generation systems. Hefei, China; 16–18 June 2010. p. 116–21.
[68] Wu TF, Nien HS, Hui HM, Shen CL. PV power injection and active power filtering with amplitude-clamping and amplitude-scaling algorithms. IEEE Transactions on Industry Applications 2007;43(3):731–41.
[69] Wu TF, Nien HS, Shen CL, Hsieh HM Chen YM. A half-bridge 1Φ2W PV inverter system with active power filtering and real power injection. In: Proceedings of the IEEE applied power electronics conference and exposition. Austin (TX), USA; March 6–10, 2005. p. 428–34.
[70] Patidar RD, Singh SP, Khatod DK. Single-phase single-stage grid-interactive photovoltaic system with active filter functions. In: Proceedings of the IEEE power and energy society general meeting. Minneapolis (MN), USA; 25–29 July, 2010. p. 1–7.

[71] Hirachi K, Mii T, Nakashiba T, Laknath KGD, Nakaoka M. Utility-interactive multi-functional bidirectional converter for solar photovoltaic power conditioner with energy storage batteries. In: Proceedings of the IEEE industrial electronics, control, and instrumentation. Taiwan, China; August 5–10, 1996. p. 1693–8.
[72] Dasgupta S, Sahoo SK, Panda SK. Single-phase inverter control techniques for interfacing renewable energy sources with microgrid—part I: parallel-connected inverter topology with active and reactive power flow control along with grid current shaping. IEEE Transactions on Power Electronics 2011;26(3):717–31.
[73] Chiang SJ, Chang KT, Yen CY. Residential photovoltaic energy storage system. IEEE Transactions on Industrial Electronics 1998;45(3):385–94.
[74] Bojoi RI, Limongi LR, Roiu D, Tenconi A. Enhanced power quality control strategy for single-phase inverters in distributed generation systems. IEEE Transactions on Power Electronics 2011;26(3):798–806.
[75] Limongi LR, Bojoi R, Tenconi A, Clotea L. Single-phase inverter with power quality features for distributed generation systems. In: Proceedings of the IEEE conference on optimization of electrical and electronic equipment. Brasov; May 22–24, 2008. p. 313–8.
[76] Cirrincione M, Pucci M, Vitale G. A single-phase DG generation unit with shunt active power filter capability by adaptive neural filtering. In: Proceedings of the IEEE industrial electronics conference. Paris, France; 6–10 November, 2006. p. 4373–80.
[77] Macken KJP, Vanthournout K, Van den Keybus J, Deconinck G, Belmans RJM. Distributed control of renewable generation units with integrated active filter. IEEE Transactions on Power Electronics 2004;19(5):1353–60.
[78] Hosseini SH, Danyali S, Goharrizi AY. Single stage single phase series-grid connected PV system for voltage compensation and power supply. In: Proceedings of the IEEE power and energy society general meeting. Calgary, Alberta, Canada; 26–30 July, 2009. p. 1–7.
[79] Mastromauro RA, Liserre M, Dell'Aquila A. PV system power quality enhancement by means of a voltage controlled shunt-converter. In: Proceedings of the IEEE power electronics specialists conference. Rhodes, Greece; 15–19 June, 2008. p. 2358–63.
[80] Mastromauro RA, Liserre M, Dell'Aquila A. Single-phase grid-connected photovoltaic systems with power quality conditioner functionality. In: Proceedings of the IEEE European conference on power electronics and applications. Aalborg, Denmark; 2–5 September, 2007. p. 1–11.
[81] Vasquez JC, Mastromauro RA, Guerrero JM, Liserre M. Voltage support provided by a droop-controlled multifunctional inverter. IEEE Transactions on Industrial Electronics 2009;56(11):4510–9.
[82] Dasgupta S, Sahoo SK, Panda SK, Amaratunga GAJ. Single-phase inverter-control techniques for interfacing renewable energy sources with microgrid—part II: series-connected inverter topology to mitigate voltage-related problems along with active power flow control. IEEE Transactions on Power Electronics 2011;26(3):732–46.
[83] Lin BR, Yang TY. Implementation of active power filter with asymmetrical inverter legs for harmonic and reactive power compensation. Electric Power Systems Research 2005;73(2):227–37.
[84] Geibel D, Degner T, Hardt C, Antchev M, Krusteva A. Improvement of power quality and reliability with multifunctional PV-inverters in distributed energy systems. In: Proceedings of the IEEE international conference on electrical power quality and utilisation. Lodz, Poland; 15–17 September, 2009. p. 1–6.
[85] Kuo YC, Liang TJ, Chen JF. A high-efficiency single-phase three-wire photovoltaic energy conversion system. IEEE Transactions on Industrial Electronics 2003;50(1):116–22.
[86] De Souza KCA, Dos Santos WM, Martins DC. A single-phase grid-connected PV system with active power filter. International Journal of Circuits, Systems and Signal 2008;2(1):50–5.
[87] De Souza KCA, Dos Santos WM, Martins DC. Optimization of the ferrite core volume in a single-phase grid-connected PV system with active and reactive power control. In: Proceedings of the conference on IEEE industrial electronics society. Arizona, USA; 7–10 November, 2010. p. 2803–10.
[88] De Souza KCA, Martins DC. A single-phase active power filter based in a two stages grid-connected PV system. In: Proceedings of the IEEE power electronics and motion control conference. Poznan, Poland; 1–3 September, 2008. p. 1951–6.
[89] Wu TF, Shen CL, Chang CH, Chiu J. 1Φ3W grid-connection PV power inverter with partial active power filter. IEEE Transactions on Aerospace and Electronic Systems 2003;39(2):635–46.
[90] Wu TF, Shen CL, Nei HS. A 1Φ3W grid-connection PV power inverter with APF based on nonlinear programming and FZPD algorithm. In: Proceedings of the applied power electronics conference and exposition. Miami Beach, Florida, USA; February 9-–13, 2003. p. 546–52.
[91] He JW, Munir MS, Li YW. Opportunities for power quality improvement through DG-grid interfacing converters. In: Proceedings of the IEEE power electronics conference. Sapporo, Japan; June 21–24 2010. p. 1657–64.
[92] He JW, Li YW, Munir MS. A flexible harmonic control approach through voltage-controlled DG — grid interfacing converters. IEEE Transactions on Industrial Electronics 2012;59(1):444–55.
[93] Yu H, Pan J, Xiang A. A multi-function grid-connected PV system with reactive power compensation for the grid. Solar Energy 2005;79(1):101–6.
[94] Kim S, Gwonjong Y, Jinsoo S. A bifunctional utility connected photovoltaic system with power factor correction and UPS facility. In: Proceedings of the IEEE photovoltaic specialists conference. Washington, DC, USA; 13–17 May, 1996. p. 1363–8.
[95] Dasgupta S, Mohan SN, Sahoo SK, Panda SK. A Lyapunov function based current controller to control active and reactive power flow in a three phase grid connected PV inverter under generalized grid voltage conditions. In: Proceedings of the IEEE international conference on power electronics and ECCE Asia. Jeju, Korea; May 30–June 3, 2011. p. 1110–7.
[96] Dasgupta S, Mohan SN, Sahoo SK, Panda SK. Derivation of instantaneous current references for three phase PV inverter connected to grid with active and reactive power flow control. In: Proceedings of the IEEE international conference on power electronics and ECCE Asia. Jeju, Korea; May 30–June 3, 2011. p. 1228–35.
[97] Cheng L, Cheung R, Leung KH. Advanced photovoltaic inverter with additional active power line conditioning capability. In: Proceedings of the IEEE power electronics specialists conference. St. Louis, Missouri; June 22–27, 1997. p. 279–83.
[98] Naderi S, Pouresmaeil E, Gao WD. The frequency-independent control method for distributed generation systems. Applied Energy, in press.
[99] Mohod SW, Aware MV. Micro wind power generator with battery energy storage for critical load. IEEE Systems Journal 2012;6(1):118–25.
[100] Marei MI, El-Saadany EF, Salama MMA. A novel control algorithm for the DG interface to mitigate power quality problems. IEEE Transactions on Power Delivery 2004;19(3):1384–92.
[101] Marei MI, El-Saadany EF, Salama MMA. A flexible DG interface based on a new RLS algorithm for power quality improvement. IEEE Systems Journal 2011;6(1):68–75.
[102] Cheng PT, Chen CA, Lee TL, Kuo SY. A cooperative imbalance compensation method for distributed-generation interface converters. IEEE Transactions on Industry Applications 2009;45(2):805–15.
[103] Lv Z, Luo A, Wu C, Shuai Z, Kang Z. A research of microgrid energy supply and filtering system based on inverter multiplexing. In: Proceedings of the IEEE international conference on sustainable power generation and supply. Nanjing, China; 6–7 April, 2009. p. 1–7.
[104] Luo S, Luo A, Lv Z, Shen Y, Guo L, Jiang W. Power quality active control research of building integrated photovoltaic. In Proceedings of the IEEE power electronics for distributed generation systems. Hefei, China; June 16–18, 2010. p. 796–801.
[105] Mohamed ARIM, El Saadany EF. A control scheme for PWM voltage-source distributed-generation inverters for fast load-voltage regulation and effective mitigation of unbalanced voltage disturbances. IEEE Transactions on Industrial Electronics 2008;55(5):2072–84.
[106] Marei MI, Abdel Galil TK, El Saadany EF, Salama MMA. Hilbert transform based control algorithm of the DG interface for voltage flicker mitigation. IEEE Transactions on Power Delivery 2005;20(2):1129–33.
[107] Saitou M, Shimizu T. Generalized theory of instantaneous active and reactive powers in single-phase circuits based on Hilbert transform. In: Proceedings of the IEEE annual power electronics specialists conference. Cairns, Australia; 23–27 June, 2002. p. 1419–24.
[108] Chandhaket S, Yoshida M, Eiji H, Nakamura M, Konishi Y, Nakaoka M. Multi-functional digitally-controlled bidirectional interactive three-phase soft-switching PWM converter with resonant snubbers. In: Proceedings of the IEEE annual power electronics specialists conference. Vancouver, BC, Canada; June 17–21, 2001. p. 589–93.
[109] Yamamoto H, Inaba CY, Hiraki E, Nakaoka M. Multifunctional digitally-controlled bidirectional three-phase soft-switching PWM converter. In: Proceedings of the international conference on power electronics and variable speed drives. London, UK; 18–19 September, 2000. p. 86–90.
[110] Prodanovic M, De Brabandere K, Van Den Keybus J, Green T, Driesen J. Harmonic and reactive power compensation as ancillary services in inverter-based distributed generation. IET Generation, Transmission and Distribution 2007;1(3):432–8.
[111] Pogaku N, Green TC. Harmonic mitigation throughout a distribution system: a distributed-generator-based solution. IEE Proceedings: Generation, Transmission and Distribution 2006;153(3):350–8.
[112] Abolhassani MT, Enjeti P, Toliyat H. Integrated doubly fed electric alternator active filter (IDEA), a viable power quality solution, for wind energy conversion systems. IEEE Transactions on Energy Conversion 2008;23(2):642–50.
[113] Todeschini G, Emanuel AE. Transient response of a wind Energy conversion system used as active filter. IEEE Transactions on Energy Conversion 2011;26(2):522–31.
[114] Chen Z. Compensation schemes for a SCR converter in variable speed wind power systems. IEEE Transactions on Power Delivery 2004;19(2):813–21.
[115] Gajanayake CJ, Vilathgamuwa DM, Poh CL, Teodorescu R, Blaabjerg F. Z-source-inverter-based flexible distributed generation system solution for grid power quality improvement. IEEE Transactions on Energy Conversion 2009;24(3):695–704.
[116] Tsengenes G, Adamidis G. A multi-function grid connected PV system with three level NPC inverter and voltage oriented control. Solar Energy 2011;85(11):2595–610.
[117] Sawant RR, Chandorkar MC. A multifunctional four-leg grid-connected compensator. IEEE Transactions on Industry Applications 2009;45(1):249–59.
[118] Sawant RR, Chandorkar MC. Methods for multi-functional converter control in three-phase four-wire systems. IET Power Electronics 2009;2(1):52–66.

[119] Wang F, Duarte JL, Hendrix M. Control of grid-interfacing inverters with integrated voltage unbalance correction. In: Proceedings of the IEEE power electronics specialists conference. Rodes, Greece; 15–19 June 2008. p. 310–6.
[120] Wang F, Duarte JL, Hendrix MAM. Pliant active and reactive power control for grid-interactive converters under unbalanced voltage dips. IEEE Transactions on Power Electronics 2011;26(5):1511–21.
[121] Pinto JG, Pregitzer R, Monteiro LFC, Afonso JL. 3-Phase 4-wire shunt active power filter with renewable energy interface. In: Proceedings of international conference on renewable energies and power quality. Seville, Spain; 28–30 March, 2007. p. 1–6.
[122] Majumder R, Ghosh A, Ledwich G, Zare F. Load sharing and power quality enhanced operation of a distributed microgrid. IET Renewable Power Generation 2009;3(2):109–19.
[123] Shahnia F, Majumder R, Ghosh A, Ledwich G, Zare F. Operation and control of a hybrid microgrid containing unbalanced and nonlinear loads. Electric Power Systems Research 2010;80(8):954–65.
[124] Han B, Bae B, Kim H, Baek S. Combined operation of unified power-quality conditioner with distributed generation. IEEE Transactions on Power Delivery 2006;21(1):330–8.
[125] Li YW, Vilathgamuwa DM, Loh PC. Microgrid power quality enhancement using a three-phase four-wire grid-interfacing compensator. IEEE Transactions on Industry Applications 2005;41(6):1707–19.
[126] Li YW, Vilathgamuwa DM, Loh PC. A grid-interfacing power quality compensator for three-phase three-wire microgrid applications. IEEE Transactions on Power Electronics 2006;21(4):1021–31.
[127] Wang F, Duarte JL, Hendrix MAM. Grid-interfacing converter systems with enhanced voltage quality for microgrid application—concept and implementation. IEEE Transactions on Power Electronics 2011;26(12):3501–13.
[128] Shen G, Xu D, Cao L, Zhu X. An improved control strategy for grid-connected voltage source inverters with an LCL filter. IEEE Transactions on Power Electronics 2008;23(4):1899–906.
[129] Yu XX, Khambadkone AM. Multi-functional power CONVERTER building block to facilitate the connection of micro-grid. In: Proceedings of the IEEE workshop on control and modeling for power electronics. Zurich, Switzerland; 17–20 August, 2008. p. 1–6.
[130] Zhou K, Wang D. Relationship between space-vector modulation and three-phase carrier-based PWM: a comprehensive analysis. IEEE Transactions on Industrial Electronics 2002;49(1):186–96.
[131] Zeng QR, Chang LC. An advanced SVPWM-based predictive current controller for three-phase inverters in distributed generation systems. IEEE Transactions on Industrial Electronics 2008;55(3):1235–46.
[132] Kang BJ, Liaw CM. Robust hysteresis current-controlled PWM scheme with fixed switching frequency. IEE Proceedings—Electric Power Applications 2001;148(6):503–12.
[133] Dannehl J, Fuchs FW, Th XF, Gersen PB. PI state space current control of grid-connected PWM converters with LCL filters. IEEE Transactions on Power Electronics 2010;25(9):2320–30.
[134] Zmood DN, Holmes DG. Stationary frame current regulation of PWM inverters with zero steady-state error. IEEE Transactions on Power Electronics 2003;18(3):814–22.
[135] Qi C, Yang Y, Suo J. Deadbeat decoupling control of three-phase photovoltaic grid-connected inverters. In: Proceedings of the IEEE international conference on mechatronics and automation. Changchun, Jilin, China; 9–12 August, 2009. p. 3843–8.
[136] Moreno JC, Huerta JME, Gil RG, Gonzalez SA. A robust predictive current control for three-phase grid-connected inverters. IEEE Transactions on Industrial Electronics 2009;56(6):1993–2004.
[137] Miranda H, Teodorescu R, Rodriguez P, Helle L. Model predictive current control for high-power grid-connected converters with output LCL filter. In: Proceedings of the annual conference of IEEE on industrial electronics. Porto, Portugal; 3–5 November, 2009. p. 633–8.
[138] Dasgupta S, Sahoo SK, Panda SK. Design of a spatial iterative learning controller for single phase series connected PV module inverter for grid voltage compensation. In: Proceedings of the IEEE international power electronics conference. Sapporo, Japan; 21–24 June, 2010. p. 1980–7.
[139] Hornik T, Zhong QC. H_∞ repetitive voltage control of grid-connected inverters with a frequency adaptive mechanism,. IET Power Electronics 2010;3(6):925–35.
[140] Guo X, Wu W, Gu H. Modeling and simulation of direct output current control for LCL-interfaced grid-connected inverters with parallel passive damping. Simulation Modelling Practice and Theory 2010;18(7):946–56.
[141] Asiminoael L, Blaabjerg F, Hansen S. Detection is key—harmonic detection methods for active power filter applications. IEEE Industry Applications Magazine 2007;13(4):22–33.
[142] Rechka S, Ngandui E, Xu J, Sicard P. Performance evaluation of harmonics detection methods applied to harmonics compensation in presence of common power quality problems. Mathematics and Computers in Simulation 2003;63(3–5):363–75.
[143] Montero MIM, Cadaval ER, Gonzalez FB. Comparison of control strategies for shunt active power filters in three-phase four-wire systems. IEEE Transactions on Power Electronics 2007;22(1):229–36.
[144] Solomon OM. The use of DFT windows in signal-to-noise ratio and harmonic distortion computations. IEEE Transactions on Instrumentation and Measurement 1994;43(2):194–9.
[145] Morsi WG, El Hawary ME. Defining power components in nonsinusoidal unbalanced polyphase systems: the issues. IEEE Transactions on Power Delivery 2007;22(4):2428–38.
[146] Depenbrock M. The FBD-method, a generally applicable tool for analyzing power relations. IEEE Transactions on Power Systems 1993;8(2):381–7.
[147] Akagi H, Watanabe EH, Aredes M. Instantaneous power theory and applications to power conditioning. Hoboken, New Jersey: John Wiley and Sons, Inc.; 2007.
[148] Furuhashi T, Okuma S, Uchikawa Y. A study on the theory of instantaneous reactive power. IEEE Transactions on Industrial Electronics 1990;37(1):86–90.
[149] Srianthumrong S, Fujita H, Akagi H. Stability analysis of a series active filter integrated with a double-series diode rectifier. IEEE Transactions on Power Electronics 2002;17(1):117–24.
[150] Pereira RR, Da Silva CH, Da Silva LEB, Lambert-Torres G, Pinto JOP. New strategies for application of adaptive filters in active power filters. IEEE Transactions on Industry Applications 2011;47(3):1136–41.
[151] Rechka S, Ngandui E, Xu J, Sicard P. Analysis of harmonic detection algorithms and their application to active power filters for harmonics compensation and resonance damping. Canadian Journal of Electrical and Computer Engineering 2003;28(1):41–51.
[152] Han Y, Mansoor G, Yao L, Zhou, Chen C. Design and experimental investigation of a three-phase APF based on feed-forward plus feedback control. WSEAS Transactions on Power Systems 2008;2(3):15–20.